NASA CONTRACTOR REPORT

NASA CR-1510

A PROCEDURE FOR ASSESSING AIRCRAFT TURBULENCE-PENETRATION PERFORMANCE

by Richard F. Porter, James P. Loomis, and Alfred C. Robinson

Prepared by
BATTELLE MEMORIAL INSTITUTE
Columbus, Ohio
for

NATIONAL AERONAUTICS AND SPACE ADMINISTRATION • WASHINGTON, D. C. • MARCH 1970

A PROCEDURE FOR ASSESSING AIRCRAFT TURBULENCE-PENETRATION PERFORMANCE

By Richard F. Porter, James P. Loomis,
and Alfred C. Robinson

Prepared under Contract No. NASw-1737 by
BATTELLE MEMORIAL INSTITUTE
Columbus, Ohio

for

NATIONAL AERONAUTICS AND SPACE ADMINISTRATION

For sale by the Clearinghouse for Federal Scientific and Technical Information
Springfield, Virginia 22151 – Price $3.00

Abstract

A concept of a numerical rating for turbulence penetration performance is suggested which goes beyond exclusive consideration of structural loads. This performance rating is taken as the combined probability, at any instant of time, that the state vector defining the aircraft's perturbation behavior will lie in an undesirable region as defined by a constraint envelope representing the multiple hazards surrounding the trim point.

An investigation and evaluation of an elementary form of the general concept is made, with the constraints being limited to those which may be drawn in a two-dimensional space defined by angle-of-attack and airspeed excursions. The constraints are buffet, positive and negative load factor, minimum control speed, maximum dynamic pressure, and maximum Mach number.

The effort is confined to the class of large subsonic jet transports in cruise configuration; and, while limited to longitudinal rigid body motion, includes all three basic aircraft degrees of freedom as well as closed loop elevator and throttle control. Conventional power spectral density techniques are employed to consider the combined effects of uncorrelated vertical and head-on isotropic turbulence.

As presently formulated, the criterion rating is found to be most sensitive to such gross parameters as wing loading, altitude, and trim speed; and to be relatively insensitive to considerable variation in aircraft size. It is demonstrated that the criterion rating concept has potential utility as a rational basis for the selection of turbulence penetration speeds, and in estimating the influence of various longitudinal control schemes.

Acknowledgement

The authors wish to acknowledge the valuable contributions provided them by Mr. Norman H. Fischer of the Battelle staff. His efforts provided numerous useful and practical approaches to the extensive computer programming tasks conducted in connection with the research effort.

The authors also wish to express their appreciation to Mr. Richard Wasicko of NASA Headquarters. His guidance during the conduct of the program was very helpful. Specifically, he provided many useful inputs relating to the presentation of results as contained in this report.

Table of Contents

Table of Contents
(continued)

List of Figures

List of Figures
(continued)

A PROCEDURE FOR ASSESSING AIRCRAFT TURBULENCE-PENETRATION PERFORMANCE

by

Richard F. Porter, James P. Loomis,
and Alfred C. Robinson

Prepared under Contract No. NASW-1737 for the
National Aeronautics and Space Administration
Washington, D. C.

Introduction

This report covers a research effort relating to the development and analysis of a procedure for quantitatively evaluating the behavior of an aircraft when encountering atmospheric turbulence. This research is predicated on a general performance concept that goes beyond the traditional focus on structural loads. The procedure developed is a simplified replica of this general concept, and draws upon the current state of the art in analysis techniques and computational hardware. In this particular case, the analysis efforts were limited to large transport aircraft in the cruising flight regime. It is believed that the search for a meaningful performance concept for flight in turbulence is justified by certain historical trends and recent events.

The interest in airplane behavior in turbulence extends back to aviation's earliest days. The studies by Hunsaker[1] and Wilson[2], published in 1915, were among the first works in this area. These studies were broad in nature, and examined the general behavior of aircraft in gusts. The interest in this subject lapsed, and was not renewed again for nearly 15 years. The renewed interest was stimulated by the growing emphasis in the United States in the late 1920's and early 1930's on developing efficient transport aircraft. From that period on, almost without exception, research and development work relating to turbulence was directed at the determination of gust loads and structural design criteria.

The prediction of gust-induced loads posed a requirement to estimate the maximum expected gust velocity. The pioneering efforts in this area were performed by Rhode and Lundquist[3] of NACA in 1931. The structural design

criteria in use today are still largely predicated on their basic concepts. The most recent modifications to their procedure involve the computation of "derived equivalent gust velocity", as defined by Pratt and Walker[4], and reported in 1954.

As aircraft became larger and more flexible, the "discrete-gust concept" came under serious question. However, advances in generalized harmonic analysis and random process theory opened the way to the use of power spectral density techniques to describe the stochastic nature of atmospheric turbulence and, therefore, turbulence-induced loads. The work of Press, Meadows, and Hadlock[5] in this field, reported in 1956, was classic. In subsequent years, substantial progress has been made in developing an advanced methodology for determining the gust-induced flight-loads environment.

Events of the early 1960's sharply emphasized the need for a reassessment of aircraft behavior in turbulence. Several serious incidents and accidents involving both civil and military jet transports were experienced during flight through turbulence. An element common to all of these was an apparent loss of control followed by recovery attempts with varying degrees of success. The phrase "jet-upset" was commonly applied to these cases. At the operational level, efforts by such people as Soderlind[6] of Northwest Airlines focused much-needed attention on such factors as pilot cues in turbulence, flight instrument limitations, pilot control techniques, flight control effectiveness at high speeds, turbulence-penetration speeds, and pilot physiological limitations. Together, industry and government rapidly responded with corrective measures. These included revised penetration speeds, pilot seat restraints, improved attitude instrumentation, control system modifications, and recommended piloting procedures. In the way of a more comprehensive response, several research programs [7,8,9,10,11] involving in-flight and simulation work were initiated. The success of these collective efforts is indicated by the decrease in such incidents in the last few years.

By exercising hindsight, the historical events discussed above suggested some pertinent needs for the design and operation of future aircraft. First, and most obvious, was the need to identify and comprehend the various aircraft-behavior phenomena in turbulence which are either undesirable or hazardous. Not so obvious, but possibly of greater importance, was the need for a quantitative approach for assessing the combined effect of these phenomena as functions of aircraft characteristics, flight condition, and the control criteria employed. An obvious benefit involves improved flight safety. A secondary benefit is that of providing a tool which might help in bridging the gap between the research and operational segments of the aviation community. It was towards these ends that this research program was conducted.

Quantitative Performance Concept

In planning this research program, it was recognized that any general performance concept for flight through turbulence should ideally embrace all of the real-world factors involved. To begin with, the concept should take cognizance of the stochastic nature of the turbulence environment and the nonlinear characteristics of the aircraft upon which it acts. It should be sensitive to the important effects of aircraft characteristics, flight condition, and closed-loop control schemes on airplane behavior. Further, it should properly account for the true nature of threats and hazards. The aircraft's response exists in a multi-dimensional space defined by many state variables. Certain regions in this state space, if encountered, lead to irreversible catastrophic consequences (e.g., exceeding airframe ultimate strength). In other regions, potential hazards exist. That is, reversible catastrophic trends may develop. The threat here is probabalistic in that the consequences depend on how quickly and effectively the situation is dealt with (e.g., stall followed by dive). Any quantitative measure of performance should logically deal with the overall likelihood of undesirable and/or hazardous events occurring.

The performance concept described above is quite rigorous. It was recognized that much of the knowledge required to develop this concept is not currently available. On the other hand, there is a substantial pool of knowledge which has never been assimilated in this direction. Further, analysis techniques and computational hardware advancements in this past decade represent strong tools which have not yet been applied to their full capacity. With these resources available, it appeared both practical and timely that an initial step be made in the direction of developing a general performance concept for flight in turbulence.

The objective of this research program was to develop and exercise a simplified version of the general concept described above. The related purposes were to demonstrate the possible applicability of the concept and point the way towards needed refinements and/or extensions. The following guidelines were set forth with respect to this endeavor.

(1) Aircraft and Control System - The analysis would be limited to the vehicle's longitudinal dynamics, with the vehicle represented as a rigid, linear element. Its aerodynamic characteristics would be roughly consistent with the non-dimensionalized characteristics of a first-generation jet transport. Variations would be allowed in such factors as aircraft physical size, wing loading, trim flight condition, and control feedback parameters used.

(2) Turbulence Environment - The turbulence environment would be depicted by either of two power spectra. Combined vertical and head-on gusts of an isotropic and uncorrelated nature would be used.

(3) Turbulence-Penetration Constraints - Lacking better definitions, the situations to be avoided in flight through turbulence would be represented by constraint surfaces for such factors as buffet, positive and negative load factors, minimum control speed, and maximum dynamic pressure. These particular constraints would be described in the two-dimensional state space defined by angle of attack and velocity, and all matters dealing with aircraft response and performance would be considered in that space.

(4) Turbulence-Penetration Performance - The constraints mentioned above would, in the angle-of-attack/velocity state space, yield a closed constraint envelope. The performance criteria for judging flight through turbulence would relate to the likelihood of passing outside this envelope.

In addition to using the simplified procedure to analyze performance variations as functions of the many variables involved, attempts would be made to identify parameters against which performance would uniquely correlate.

Procedural Model Development

Figure 1 depicts the important elements of the procedural model which was developed to investigate the turbulence performance concept. It illustrates that the aircraft's response is a function both of the dynamics of the aircraft and control system, and the nature of the turbulence environment. In turn, the response together with the constraints and performance criteria determine the performance in turbulence. Using the guidelines described earlier, it was necessary to develop the necessary analytical models and computational programs for evaluating the procedure. These are described in the remainder of this report section.

Analytical Models

The detailed description of the development of analytical models is given in the Appendices to this report. They are described only to a limited depth here.

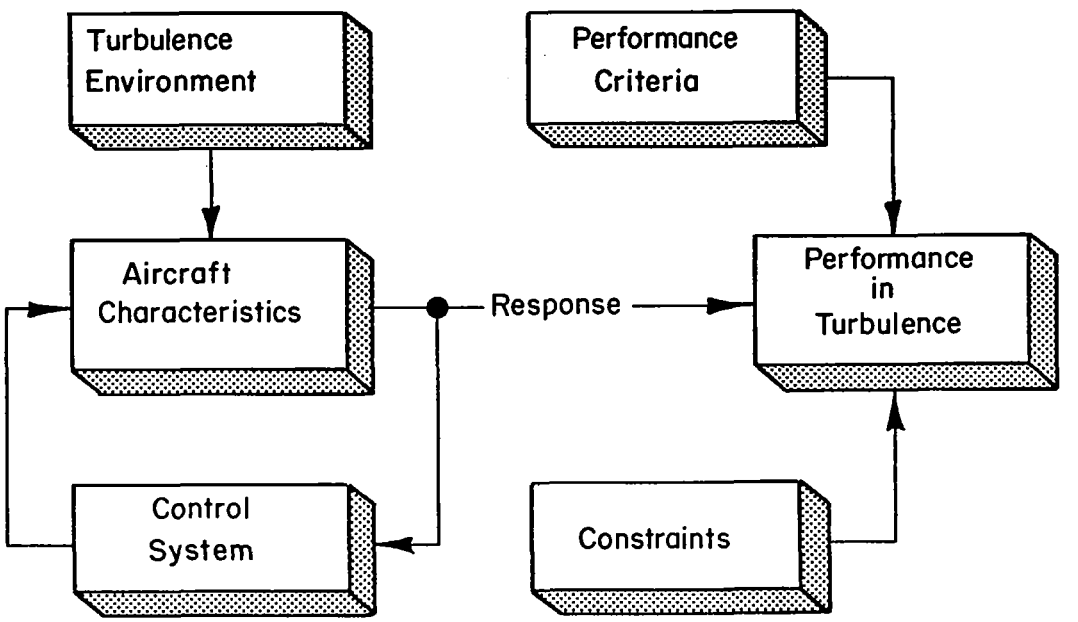

FIGURE I. ELEMENTS OF A PROCEDURAL MODEL RELATING TO A TURBULENCE PERFORMANCE CONCEPT.

Aircraft and Control System

As described in Appendix A, standard techniques were used to derive the equations describing the aircraft and control system dynamic behavior. The features and assumptions in this development include the seven described below:

(1) Three degree-of-freedom longitudinal rigid-body modes of motion were considered.

(2) The equations were linearized about a level-flight equilibrium condition.

(3) Atmospheric density was assumed to be an exponential function of altitude.

(4) The control system involved pure gain feedbacks with no equalization, and sensor and actuator dynamics were ignored.

(5) Both longitudinal and vertical gust velocity components were included.

(6) The lag in vertical gust penetration between the wing and horizontal tail was represented as an effective aerodynamic pitching rate.

(7) The aerodynamic lag in lift growth on the wing following gust penetration (Kussner Function) was included in approximate form; the unsteady aerodynamic effects of aircraft motion (Wagner Function) were ignored.

Eight linear differential equations were developed to represent the aircraft and its control system. These included the dynamic equations representing the two translational and one rotational degrees of freedom. A kinematic equation was included which related the time rate of change of altitude to both the aircraft's climb rate in the air mass and the instantaneous vertical gust velocity. A second-order lag was used to represent the engine's thrust response to throttle deflections. The following three closed-loop control functions were developed:

(1) A simple elevator control system with control effected by various combinations of velocity error, angle of attack error, longitudinal acceleration, pitch rate, and pitch attitude error.

(2) An autothrottle system with control effected by various combinations of velocity error, longitudinal acceleration, altitude error, and climb rate.

(3) An altitude control system which operated into the elevator system. Pitch attitude commands were generated as functions of both altitude error and climb rate.

α = angle of attack, rad

δ_e = tailplane incidence, rad

δ_{t_2} = pressure correction factor

θ = pitch attitude, rad

ρ = atmospheric density, slugs/ft^3

Physical Characteristics

The primary physical characteristic parameters of interest are wing mean aerodynamic chord length ($\bar{c}$), wing area (S), pitching moment of inertia (I_{yy}), and aircraft gross weight (W).

In an attempt to simplify the problem somewhat, it is assumed that while the aircraft's size would be allowed to vary, its basic geometry would remain fixed. Here geometry is construed to include such factors as fuselage slenderness ratio, wing aspect ratio, wing sweep, and the general attachment position of the wing to the fuselage. Having assumed this, other assumptions can be made with fair accuracy. First, given various aircraft physical sizes, wing area will vary proportionally with the square of the mean aerodynamic chord length. That is,

$$S = K_1 \bar{c}^2 \tag{B-1}$$

Second, the aircraft's radius of gyration (r) about the center of gravity will vary approximately linearly with mean aerodynamic chord length. Thus,

$$r = K_2 \bar{c} \tag{B-2}$$

This latter assumption is made recognizing that the distribution of airframe mass is far more influential in determining r than are the masses of fuel and payload which vary as gross weight varies.

Pitching moment of inertia is a function of radius of gyration, gross weight, and the gravitational constant (g), as follows:

$$I_{yy} = r^2 \frac{W}{g} \tag{B-3}$$

Combining (B-2) and (B-3) to eliminate r gives

$$I_{yy} = K_2^2 \bar{c}^2 \frac{W}{g} \tag{B-4}$$

A reference aircraft is chosen to evaluate the proportionality constants, K_1 and K_2. It is one of the first-generation type, four engine, turbojet-powered transports with a mean aerodynamic chord length of 20 feet and a wing area of 2400 square feet. A reasonable mid-range value for this aircraft's radius of gyration is 27 feet. Using these values in equations (B-1) and (B-2), the values of K_1 and K_2 are found to be 6.0 and 1.35, respectively. Thus, equations (B-1) and (B-4) can be rewritten as

$$S = 6\bar{c}^2 \tag{B-5}$$

$$I_{yy} = 22.6\ W \tag{B-6}$$

It is convenient to specify the aircraft's wing loading (W/S) as a parameter, instead of the W and S individually. Equations (B-5) and (B-6) can be combined to yield

$$I_{yy} = 135.6\bar{c}^2 \left(\frac{W}{S}\right) \tag{B-6a}$$

Based on the foregoing material, the process of fully describing the aircraft's physical characteristics can be viewed as a three-step process;

(1) Size the aircraft by selecting $\bar{c}$,

(2) Specify the wing loading $\left(\frac{W}{S}\right)$, and

(3) Calculate the pitching moment of inertia (I_{yy}).

Aerodynamic Characteristics

The longitudinal aerodynamic characteristics are of interest in this study and include the lift, drag, and pitching moment coefficients and derivatives. The nondimensionalized characteristics of the reference aircraft mentioned earlier will be used. These are, to a good order of approximation, applicable to an aircraft with the same geometrical configuration, even though it may differ in physical size. The aerodynamic characteristics presented in the following paragraphs are limited to the configuration with flaps and

landing gear retracted. Also, unlike the derivations in Appendix A, they involve values as measured from a zero angle-of-attack condition, and not the trim flight angle-of-attack.

Lift Characteristics

The equation below illustrates the dependence of lift coefficient (C_L) on aircraft angle of attack (α), and tailplane incidence (δ_e).

$$C_L = C_{L_o} + C_{L_\alpha} \cdot \alpha + C_{L_{\delta_e}} (\delta_e - \delta_{e_{ref}}) \qquad \text{(B-7)}$$

Here, $\delta_{e_{ref}}$ is a reference tailplane incidence of -4 degrees. Static airframe elasticity, and compressibility effects on C_L are accounted for by the fact that C_{L_o}, C_{L_α}, and $C_{L_{\delta_e}}$ are, in turn functions of flight Mach number (M), and flight altitude (h).

Figures B-1 through B-3 present the values of C_{L_o}, C_{L_α}, and $C_{L_{\delta_e}}$, respectively, as a function of Mach number and several flight altitudes.

Figure B-4 shows the aircraft's buffet boundary limit representing the limit C_L value as a function of Mach number. The dashed curve is a section of an ellipse approximating the boundary and will be used in generating the vehicle's flight envelopes, presented later in this Appendix, and the turbulence-penetration-constraint boundaries, discussed in Appendix C.

Drag Characteristics

The drag coefficient can be expressed in terms of incompressible drag, $(C_D)_L$ which varies with lift, and the drag rise due to Mach number, $(C_D)_M$.

$$C_D = (C_D)_L + (C_D)_M \qquad \text{(B-8)}$$

Figures B-5 and B-6 shows the variations of $(C_D)_L$ and $(C_D)_M$ with respect to C_L and M, respectively.

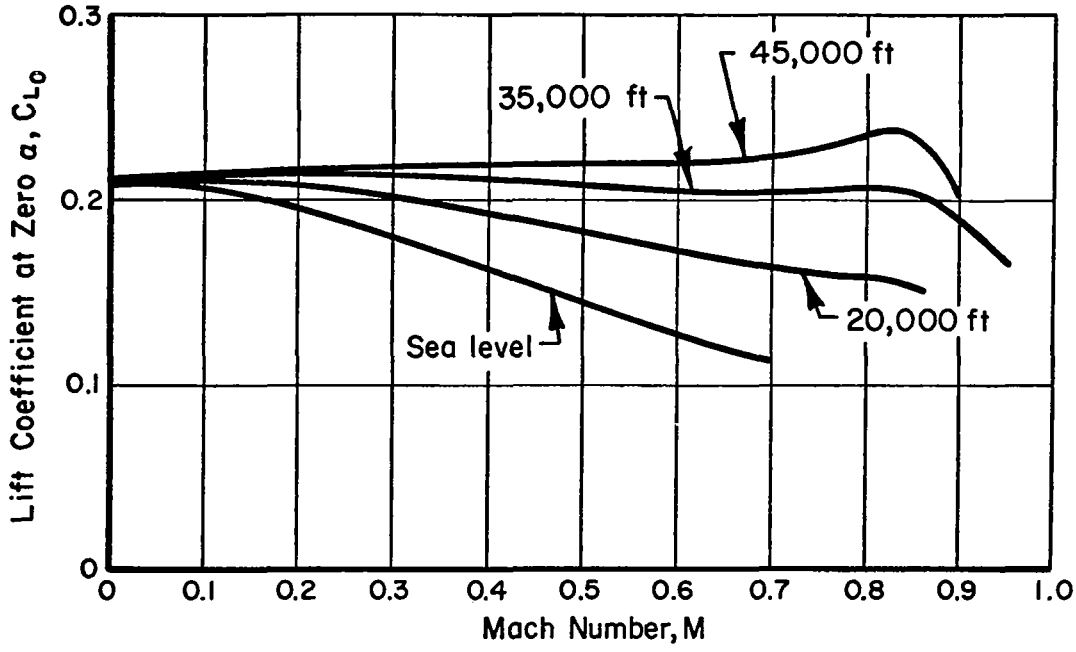

FIGURE B-I. VARIATION OF C_{L_0} WITH MACH NUMBER AND ALTITUDE

In addition to the basic drag coefficient, its rate of change relative to changes in both angle of attack and Mach number are of interest in studying the aircraft's dynamic response. The first of these derivatives, $\frac{\partial}{\partial\alpha}(C_D)_L$, is given by the following expression.

$$\frac{\partial}{\partial\alpha}(C_D)_L = \frac{\partial}{\partial C_L}(C_D)_L \cdot C_{L_\alpha} \tag{B-9}$$

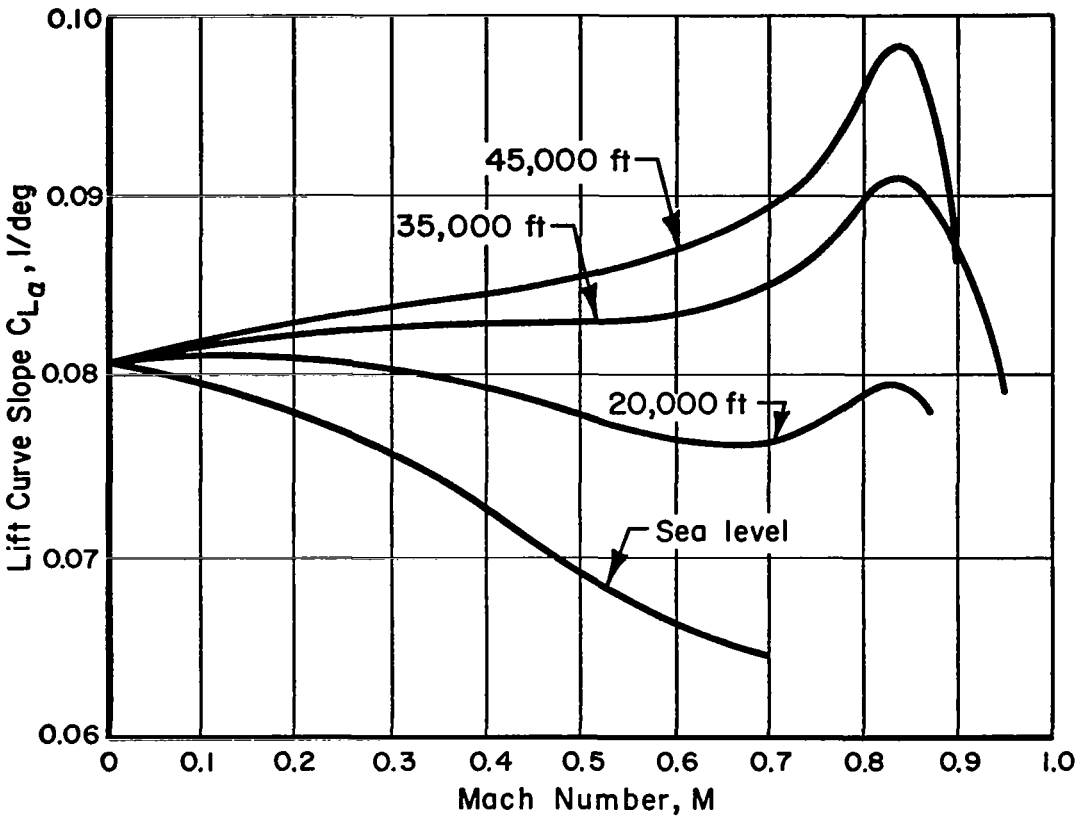

FIGURE B-2. VARIATION OF C_{L_α} WITH MACH NUMBER AND ALTITUDE

The data in Figure B-5 are used to obtain the characteristics of $\frac{\partial}{\partial\alpha}(C_D)_L$ for various values of C_L and C_{L_α}. The derivative $\frac{\partial}{\partial M}(C_D)_M$ is evaluated from the data presented in Figure B-6.

Figures B-7 and B-8 provide data on the derivatives $\frac{\partial}{\partial\alpha}(C_D)_L$ and $\frac{\partial}{\partial M}(C_D)_M$, respectively.

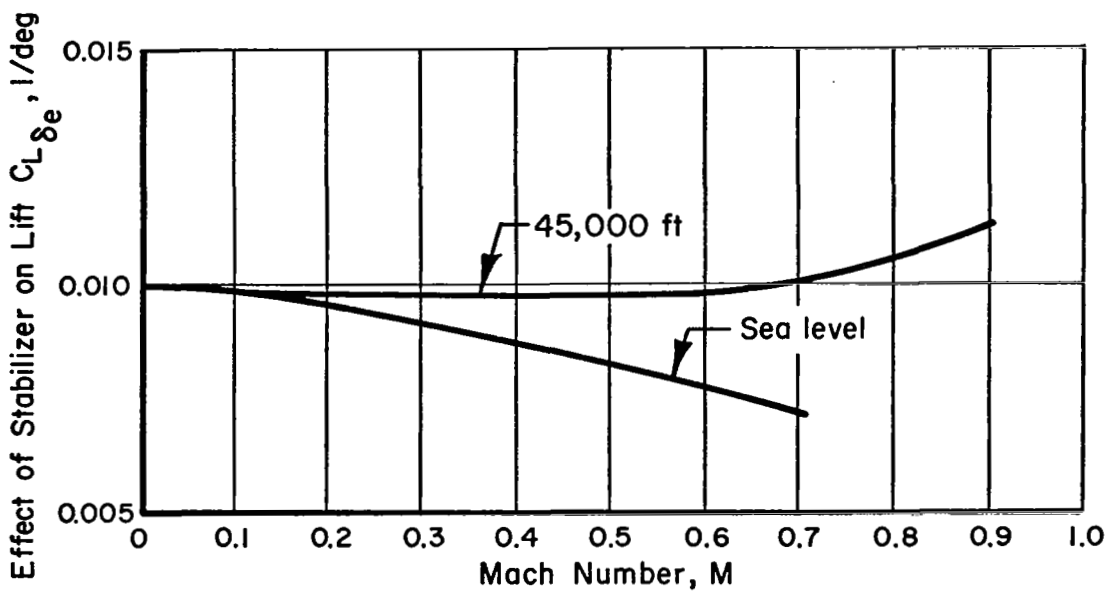

FIGURE B-3. VARIATION OF $C_{L_{\delta e}}$ WITH MACH NUMBER AND ALTITUDE

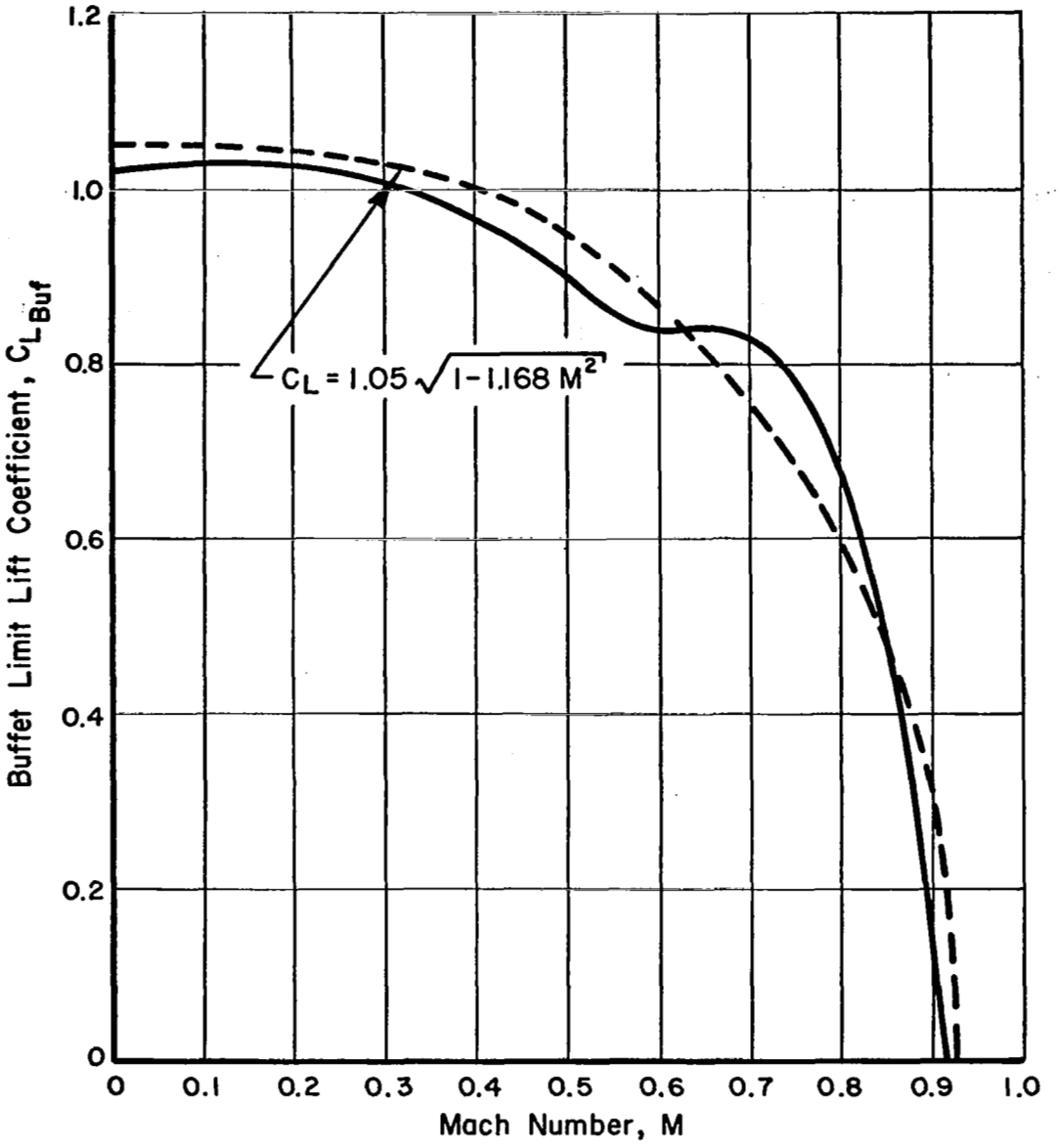

FIGURE B-4. BUFFET LIMIT LIFT COEFFICIENT VERSUS MACH NUMBER

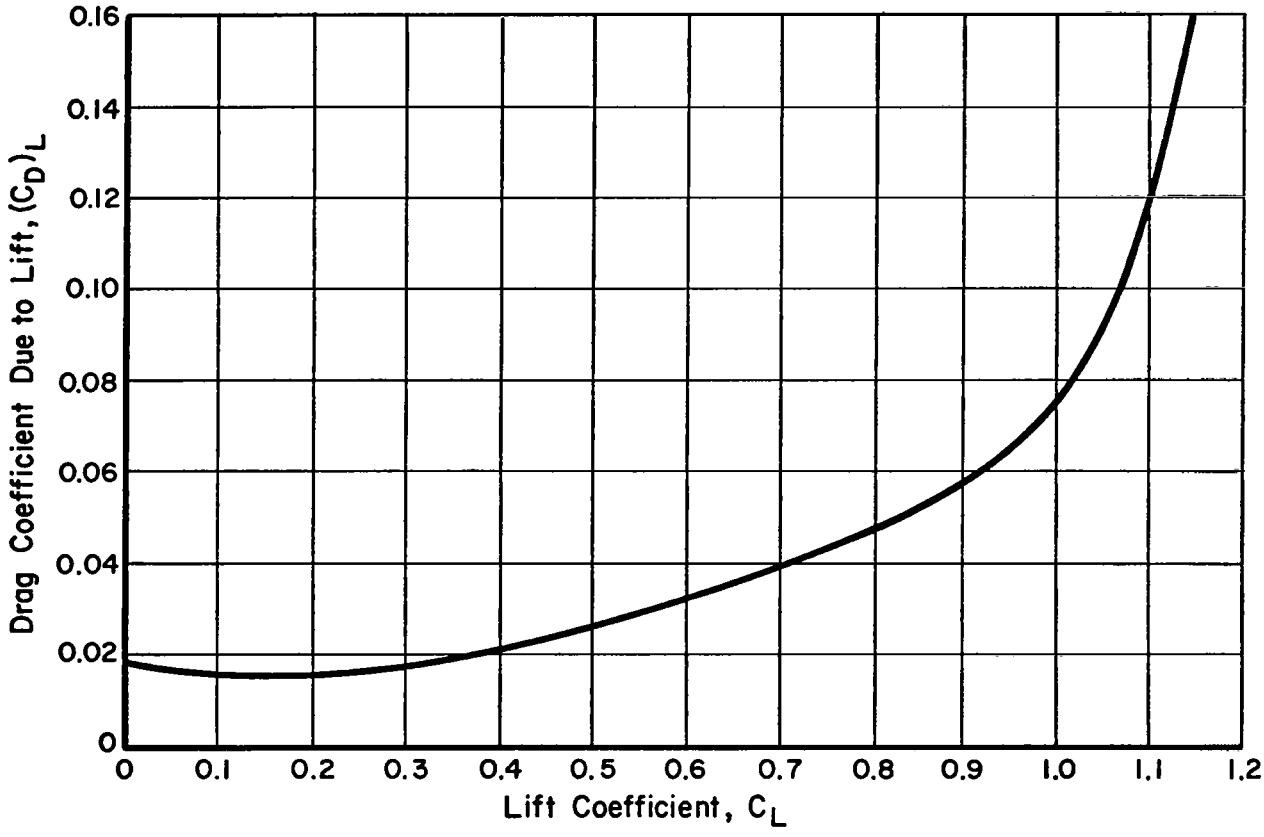

FIGURE B-5. DRAG COEFFICIENT DUE TO LIFT

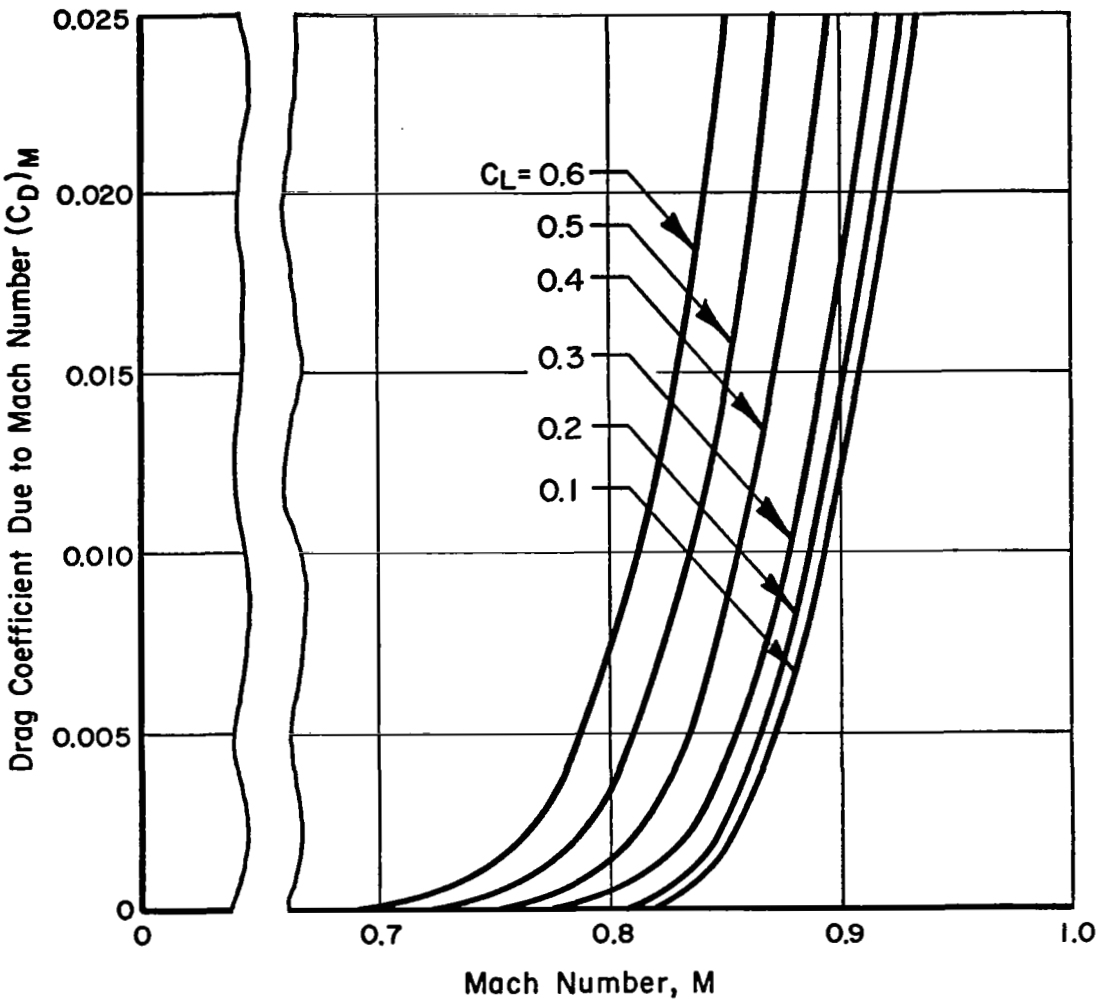

FIGURE B-6. DRAG COEFFICIENT DUE TO MACH NUMBER

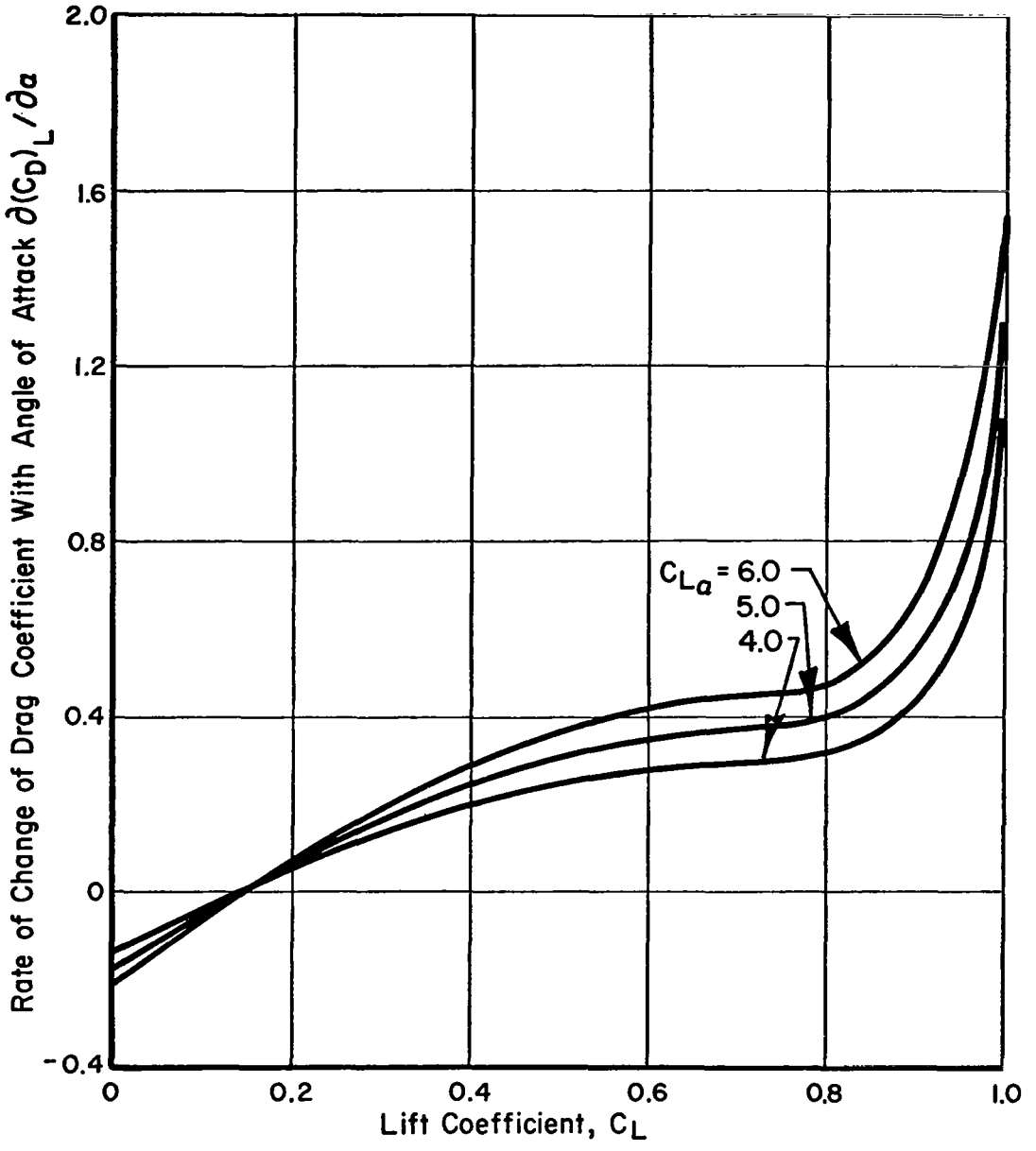

FIGURE B-7 VARIATION OF $\partial(C_D)_L/\partial\alpha$ WITH LIFT COEFFICIENT AND LIFT CURVE SLOPE

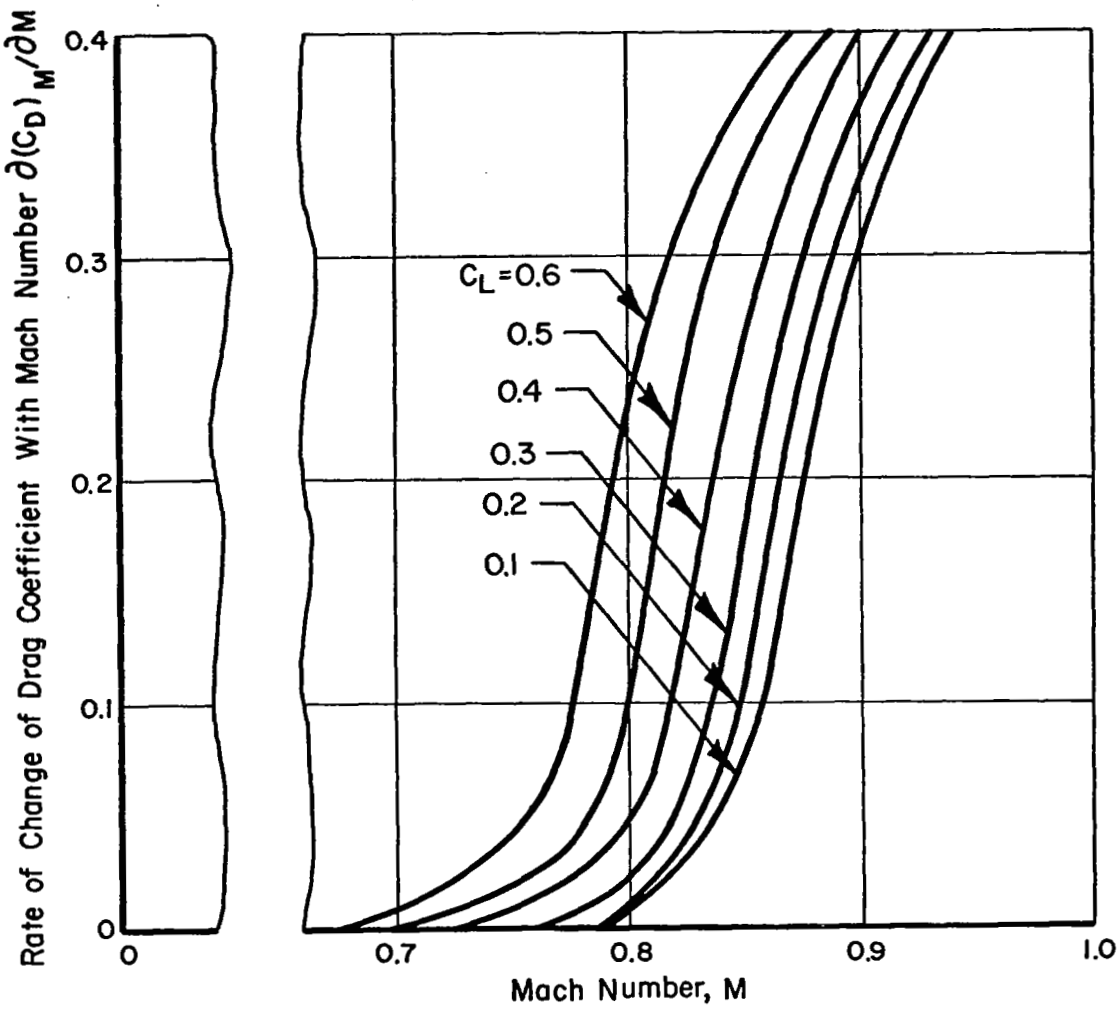

FIGURE B-8. VARIATION OF $\partial (C_D)_M / \partial M$ WITH LIFT COEFFICIENT AND MACH NUMBER

Pitching Moment Characteristics

An expression for the pitching moment coefficient is given as

$$C_m = C_{m_o} + \left(C_{m_\alpha}\right)_{ref} \cdot \alpha + C_{m_{\delta_e}} (\delta_e - \delta_{e_{ref}}) + C_{m_{X_{cg}}} (X_{cg} - X_{cg_{ref}})$$

$$+ \frac{\partial\left(C_{m_\alpha}\right)_{ref}}{\partial X_{cg}} (X_{cg} - X_{cg_{ref}}) \alpha + \frac{\partial Cm}{\partial(\bar{c}\dot{\alpha}/2V)} \dot{\alpha} + \frac{\partial Cm}{\partial(\bar{c}\dot{\theta}/2V)} \dot{\theta} \qquad \text{(B-10)}$$

In this equation, X_{cg} is the ratio of the center of gravity distance forward of the 0.25 MAC position, to the length of the mean aerodynamic chord. Thus, $X_{cg_{ref}} = 0.25$. The value of $(C_{m_\alpha})_{ref}$ is referenced to the condition where X_{cg} equals $X_{cg_{ref}}$. The effects of airframe static elasticity and compressibility on C_m are reflected in the derivatives of Equation (B-10), all of which vary with flight Mach number and altitude.

Figures B-9 through B-13 give the characteristics of C_{m_o}, $(C_{m_\alpha})_{ref}$, $C_{m_{\delta_e}}$, $C_{m_{X_{cg}}}$, and $\frac{\partial(C_{m_\alpha})_{ref}}{\partial X_{cg}}$ as a function of M and h.

Figures B-14 and B-15 present data on the variation of C_m with angle of attack rate ($\dot{\alpha}$) and pitching rate ($\dot{\theta}$).

Propulsion Characteristics

In this study involving aircraft dynamic response in turbulence, no specific attempt is made to characterize the thrust capacity of the vehicle's engines. That is, having selected a vehicle configuration and flight condition, it is assumed that the necessary thrust for level flight is available. For equilibrium flight, the following two expressions are applicable:

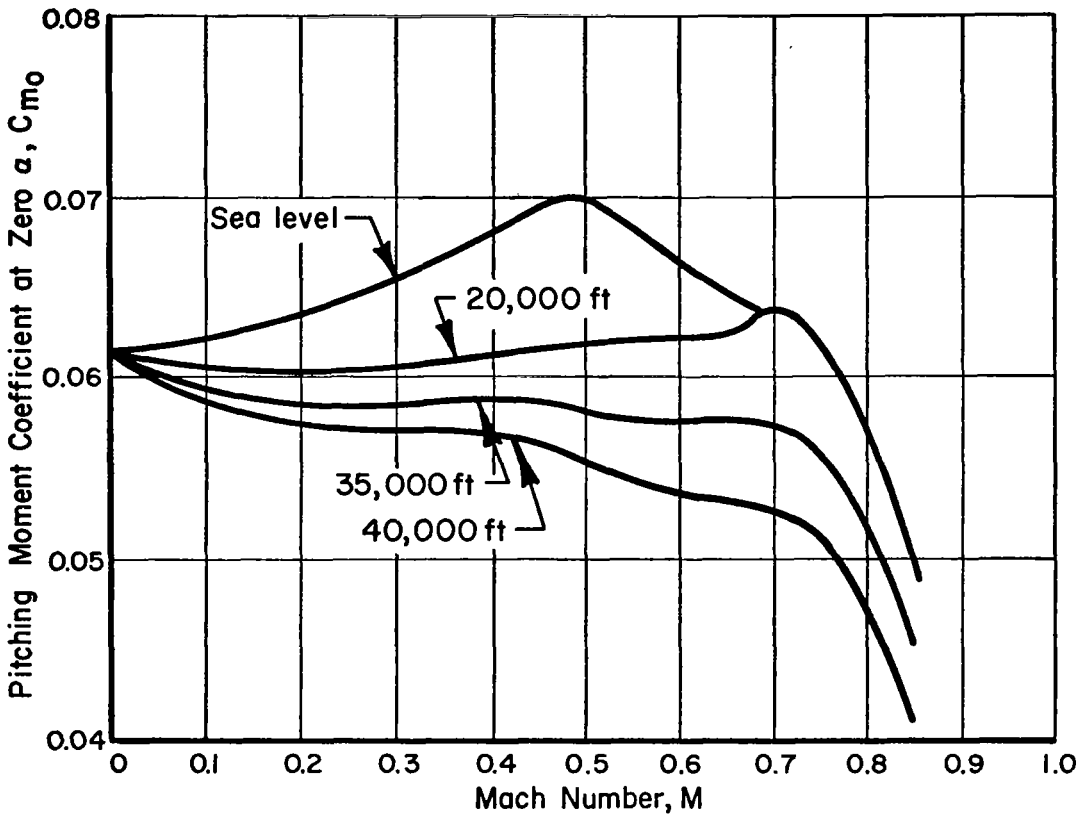

FIGURE B-9. VARIATION OF C_{m_0} WITH MACH NUMBER AND ALTITUDE

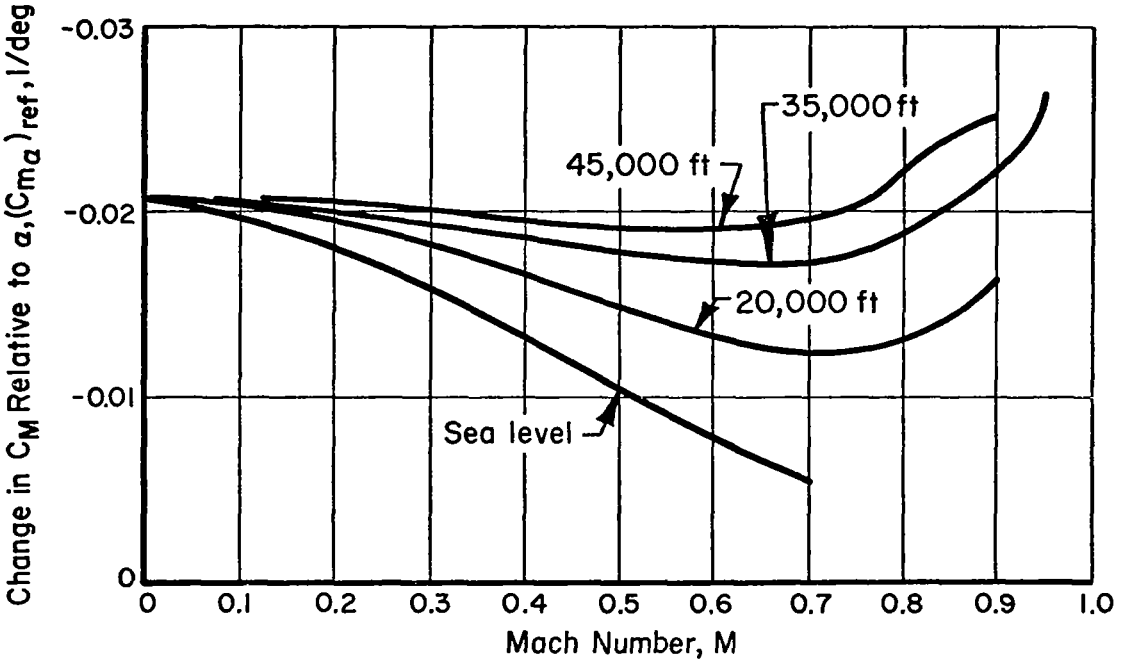

FIGURE B-10. VARIATION OF $(C_{m_\alpha})_{ref}$ WITH MACH NUMBER AND ALTITUDE

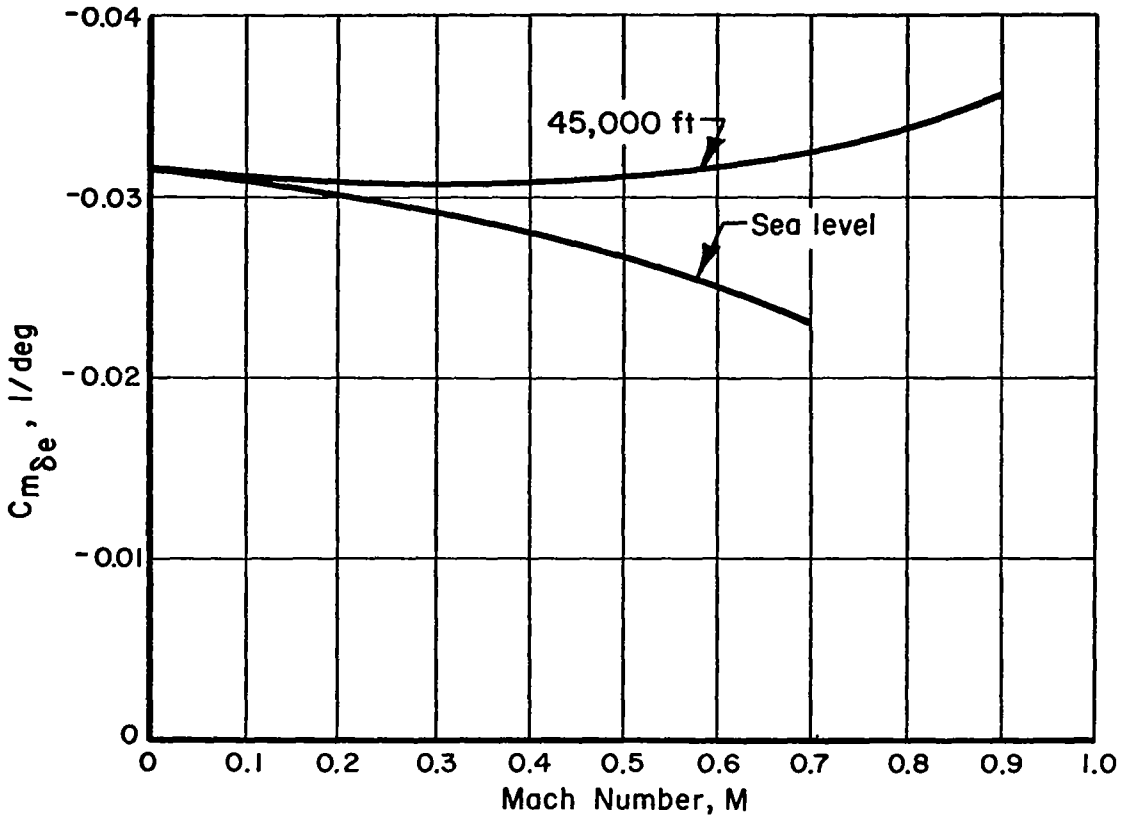

FIGURE B-11. VARIATION OF $C_{m_{\delta e}}$ WITH MACH NUMBER AND ALTITUDE

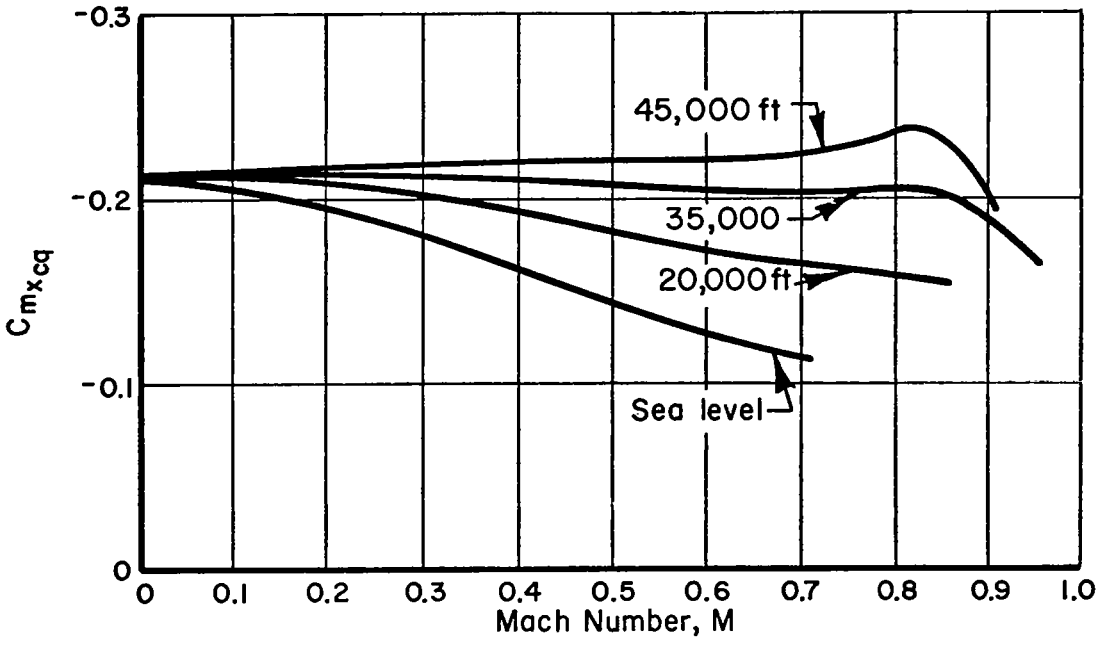

FIGURE B-12. VARIATION OF $C_{m_{xcq}}$ WITH MACH NUMBER AND ALTITUDE

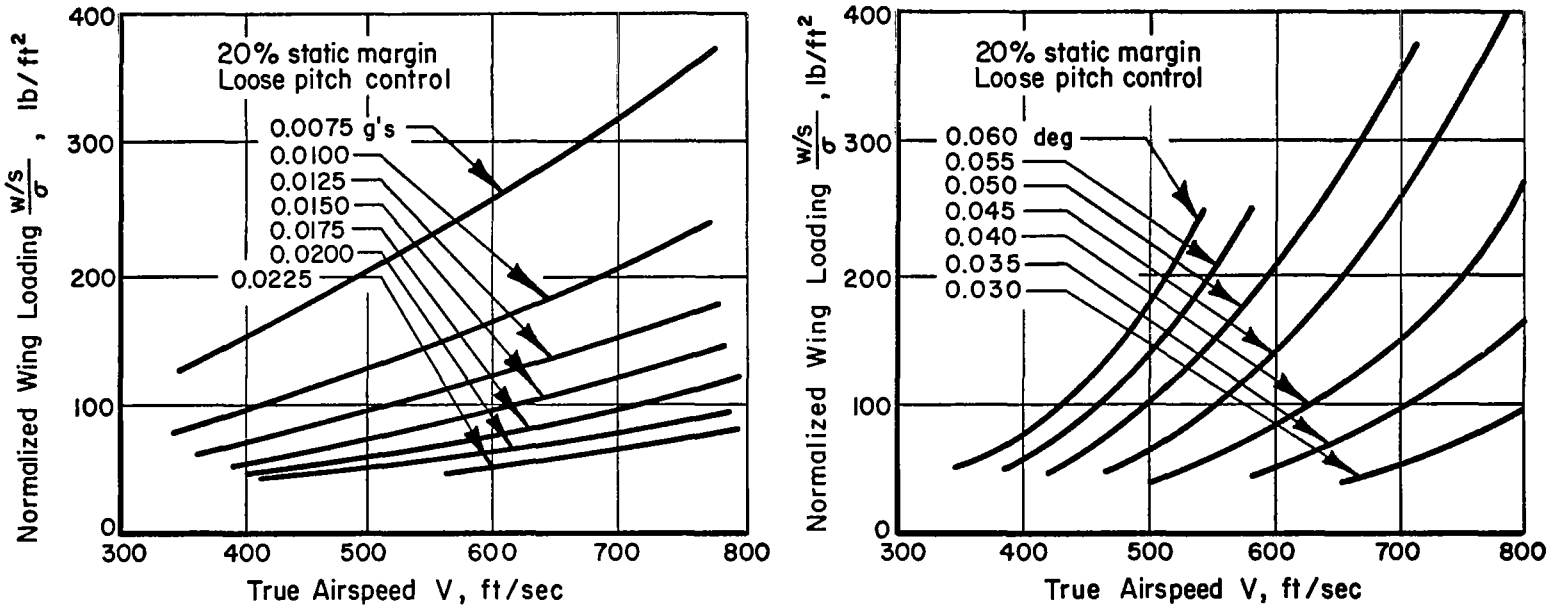

(a) Contours of constant RMS load factor

(b) Contours of constant RMS angle of attack

FIGURE 9. GENERALIZED RESPONSES TO UNIT TURBULENCE INTENSITIES IN FEET/SECOND.

Idealized Aircraft Performance

As developed in Appendix D, the aircraft's turbulence penetration performance involves a determination of the likelihood that defined constraint boundaries will be exceeded in a particular turbulence encounter. In order to make this determination, the aircraft responses and constraint envelope must be defined for each case of interest. The details of computing the constraint envelope, for any given case, are presented in Appendix C.

In the preceding subsection of this report, dealing with aircraft response, an idealized aircraft response model was described. Its use permitted an assessment of aircraft response in terms of a minimum number of influential parameters. Additionally, the determination that aircraft size effects were minimal allowed for analyzing response in terms of only velocity and mass parameter. Fortunately, with one exception, it was possible to uniquely define the constraint envelope for a given case in terms of these same two parameters. The exception is the dynamic pressure placard limit which obviously depends explicitly on altitude for a given true airspeed. Since this particular constraint is only significant at the lower-altitude, high-speed portion of the flight envelope, the constraint boundaries for given values of velocity and mass parameter were computed at sufficiently high altitude to preclude the dynamic pressure limit from becoming a governing constraint. The boundaries and envelopes thus obtained were then assumed to apply freely to all cases with identical parameter values.

Basic Performance Characteristics

For a given constraint envelope, the exceedance probability is a function of the variances in angle of attack and velocity responses which in turn are a function of the rms turbulence intensity. Whereas the aircraft response results discussed in the previous section were linear functions of the turbulence intensity, the exceedance probability results are related in a highly nonlinear way to the turbulence magnitude as illustrated in Figure 10.

Also shown in Figure 10 is the mean time between crossings of the closest constraint boundary, also a highly nonlinear function of turbulence intensity. This quantity, as outlined in Appendix D, is computed from the second moments of the angle of attack and velocity spectra and their cross spectrum.

It should be noted here that the turbulence intensity, as used in this investigation, is the true turbulence intensity as defined by the area under the complete power spectrum. As pointed out in Reference 11, some investigators have used a truncated spectrum to define the rms turbulence values, resulting in a smaller numberical value. During 15 traverses of a thunderstrom, as reported in Reference 11, truncated spectra values ranged from 6.1 to 16 ft/sec, whereas the true rms turbulence intensity for at least one of these was estimated to be 32.33 ft/sec.

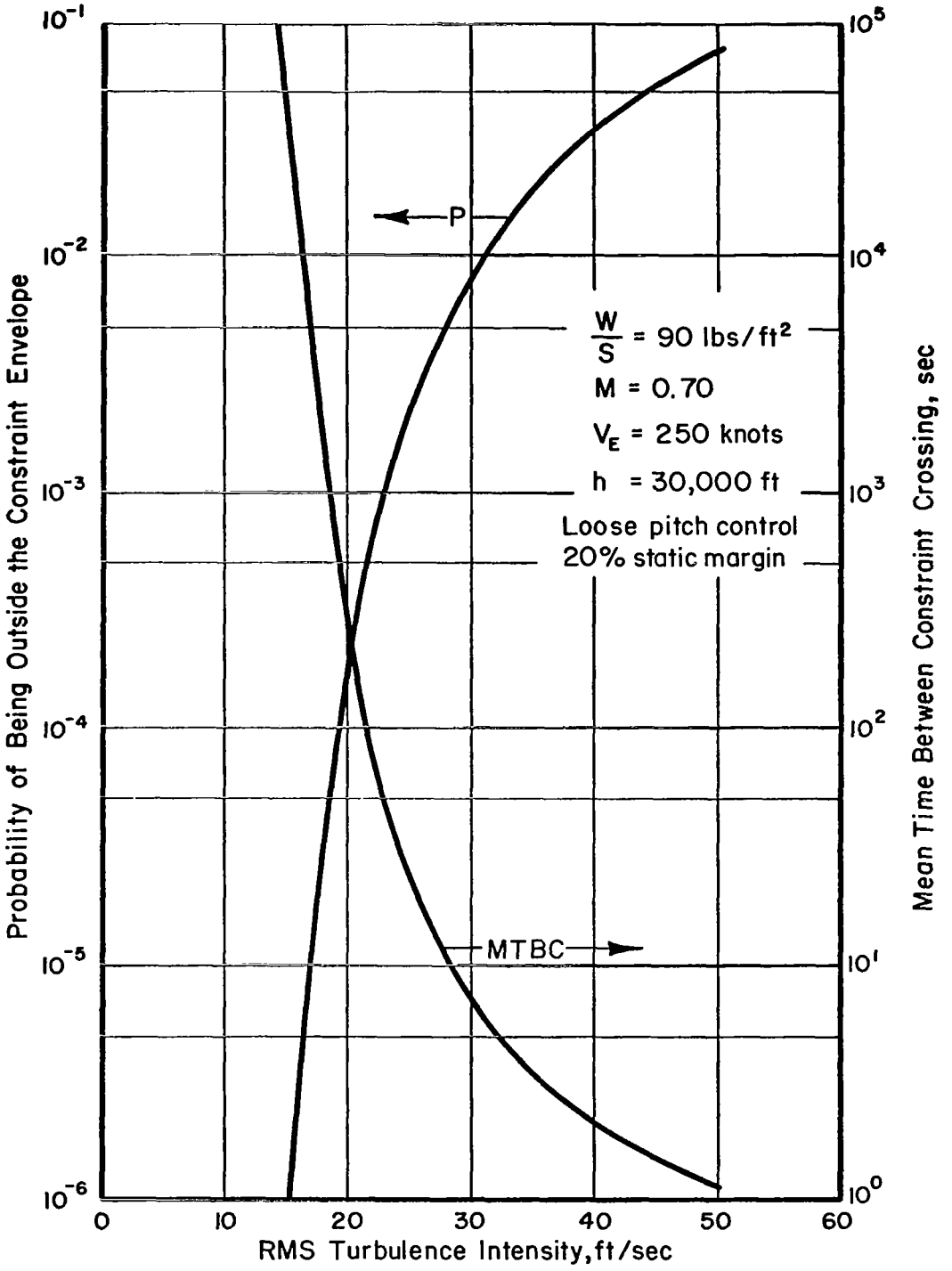

FIGURE 10. EFFECT OF TURBULENCE INTENSITY ON PROBABILITY OF BEING OUTSIDE THE CONSTRAINT ENVELOPE, AND UPON THE MEAN TIME BETWEEN CROSSING CONSTRAINT BOUNDARIES

Figure 11 shows the linearized constraint boundaries (and resulting envelopes) for three mass parameter values, all at a true velocity of 800 ft/sec. These boundaries are formally independent of size. The constraint envelope for $(W/S)/\sigma = 197$ lb/ft^2, at the top of the figure, represents that of an aircraft trimmed at a relatively high lift coefficient, caused either by a high wing loading or a high altitude operating point. It is evident that this aircraft will probably encounter the upper buffet limit before the positive load factor limit is reached, whereas for negative angle of attack disturbances the negative load factor limit is reached first. The minimum control speed, corresponding to the 1-g stall speed, is fairly close to the origin or trim point because of the high trim lift coefficient.

The constraint envelopes for lower values of $(W/S)/\sigma$ illustrate the tendency of the positive load factor constraint to predominate the lower wing loadings or lower altitudes. For the lowest value of $(W/S)/\sigma$, the upper buffet boundary has ceased to define any portion of the envelope.

The decreasing tolerance for angle of attack disturbances as $(W/S)/\sigma$ decreases is illustrated by the narrowing of the distance between the positive and negative load factor limits. However, Figure 9(b) shows that the rms angle of attack response to a unit turbulence input decreases as $(W/S)/\sigma$ decreases. Based only upon an inspection of Figures 9 and 11, an accurate evaluation of the relative turbulence-penetration performance for the three cases would appear to be quite difficult to obtain because of the interwoven effects of constraint boundary changes and aircraft response differences as basic parameters are varied. This evaluation, however, can be performed mathematically by determining the probability of being outside the constraint envelope and the mean time between crossing the closest constraint limit.

Figure 12 shows the results for three values of $(W/S)/\sigma$ as a function of aircraft size. Perhaps the most striking attribute of the turbulence-penetration probability criterion is its decisiveness, since the numberical values shown for the three $(W/S)/\sigma$ cases are markedly different. For a medium-sized aircraft, subjected to the horizontal and vertical 20 ft/sec rms turbulence the probability of being outside the constraint envelope is 30 times greater for the highest wing loading case compared to that for the intermediate wing loading, while the lowest wing loading results in a probability value about 300 times greater. Once again, the comparative insensitivity of results to aircraft size is observed.

Generalized Probability Contours

Neglecting aircraft size effects, the turbulence-penetration performance criterion becomes amenable to contour plotting as was done earlier for the aircraft responses. Figure 13 shows these generalized exceedance probability contours in the normalized-wing-loading/velocity plane. To generate these results, the same cases were used as for the generalized aircraft response data of Figure 9, and the rms turbulence intensities (horizontal and vertical) were assumed to be 30 ft/sec, representing severe thunderstorm turbulence.

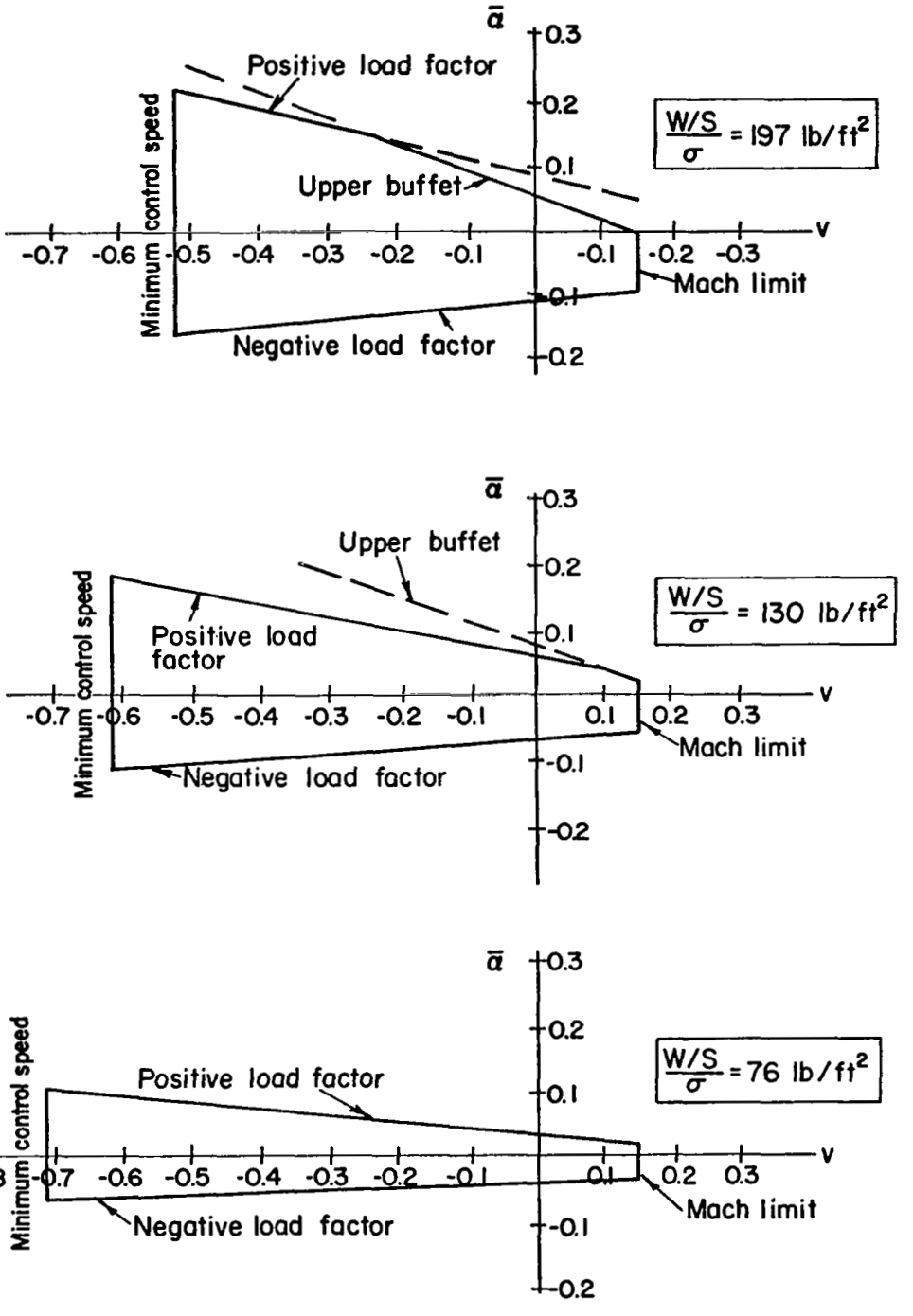

FIGURE 11. EFFECT OF MASS PARAMETER ON LINEARIZED CONSTRAINT ENVELOPES AT A TRUE AIRSPEED OF 800 FT/SEC

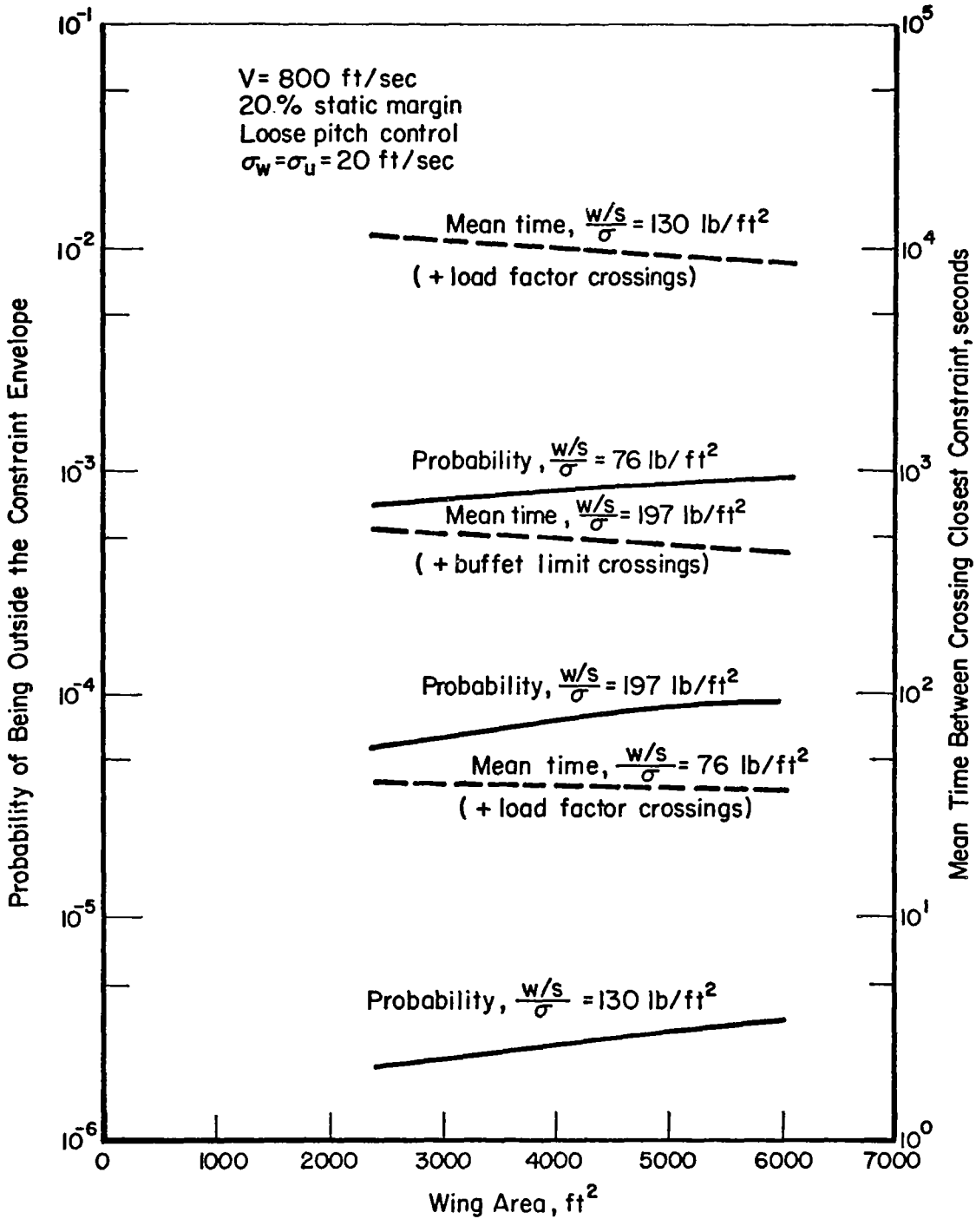

FIGURE 12. EFFECTS OF MASS PARAMETER AND SIZE ON TURBULENCE-PENETRATION PERFORMANCE

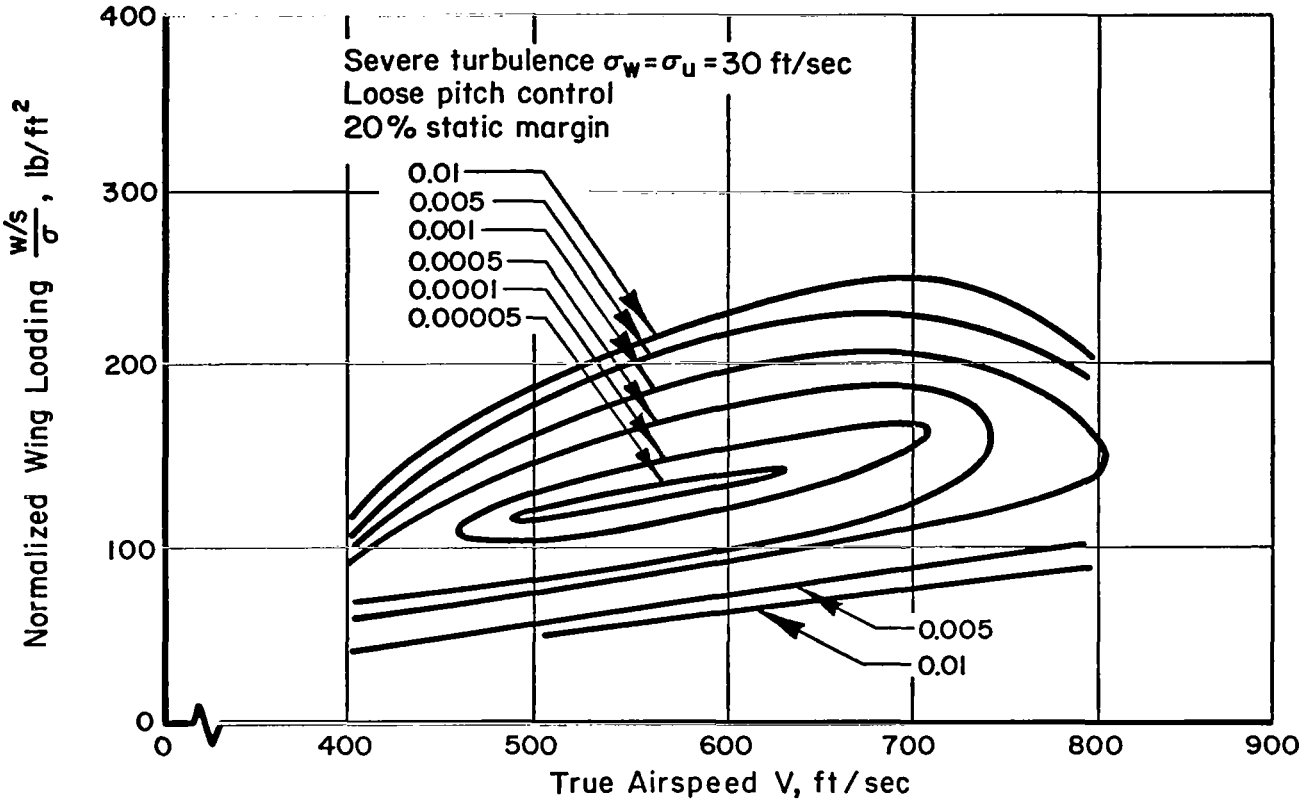

FIGURE 13. CONTOURS OF EQUAL PROBABILITY OF EXCEEDING CONSTRAINT ENVELOPE

As shown in Figure 13, a narrow, sharp depression in the probability surface exists in which the value is less than .00005. While operating in this small region, the probability of exceeding any of the constraints is less than one in twenty thousand, even in this severe turbulence environment. This may be compared with operation near the outer contour, where the probability has increased by a factor of 200.

The generalized data of Figures 9 and 13 can be made more meaningful from an operational point of view by selecting a wing loading and mapping the response and probability contours into a conventional flight envelope defined in the altitude equivalent-airspeed plane. The equivalent airspeed, V_E, is used instead of true airspeed because of its more common usage in aircraft operations. The 1962 ICAO standard atmosphere serves to relate altitude to density ratio. The flight envelopes, with contours of rms angle of attack and load factor for unit turbulence-intensity inputs, are given for three wing loadings in Figure 14. These data were obtained from Figure 9 by a simple transformation of variables along lines of constant response magnitude. Both the angle of attack and load factor contours plot virtually as straight lines within the flight envelope, although it must be borne in mind that the assumption neglecting aeroelastic effects on nondimensional derivatives may be somewhat strained when computations over the entire flight envelope are made. Keeping in mind the various assumptions discussed in earlier sections of this report and in the Appendices, the qualitative conclusion may be drawn that increasing altitude at fixed equivalent airspeeds tends to reduce both the load factor and angle of attack responses to turbulence. It will be recalled, on the other hand, that the results in Figure 9 showed that altitude increases at fixed true airspeeds caused increases in the angle of attack responses to turbulence.

By the same transformation of variables, the exceedance probability contours of Figure 13 have been mapped into the flight envelopes of Figure 15 for the same three wing loadings. These contours have not been drawn near the dynamic pressure or maximum equivalent airspeed since limits. This limit was not considered in generating the linearized constraint envelopes used for the numerical data plotted in Figure 13. For a particular aircraft, however, this constraint could be included and the exceedance probability contours could be calculated for the complete flight envelope. For each wing loading, the closed contours of the probability function in the h-V_E plane outline regions of minimum likelihood of constraint exceedance. Interestingly, the effect of increased wing loading is to move the optimum region to lower altitudes. Even for wing loadings that are quite low for current subsonic jet transports, the region of minimum exceedance probability is well below normal cruising altitudes.

The contours at the higher altitudes reflect the fact that the primary constraint at these flight conditions is the buffet limit. In this region, the contours assume the general shape of the 1-g low speed and high speed buffet limits defining the boundaries of the flight envelope at higher altitudes. In the lower-altitude, high-speed region of Figure 15(a), the 0.001 contour has the general shape of the constant rms load factor response contour of Figure 14(a), a consequence of the fact that the load factor limit is the primary constraint in this region.

For the 90 lbs/ft^2 wing loading case in Figure 15(b), the approximate locus of the optimum turbulence-penetration speeds, based on minimum exceedance probability, has been sketched. Beginning at the highest altitudes, the curve follows the peaks of the contours. Below about 18,000 ft, the relative

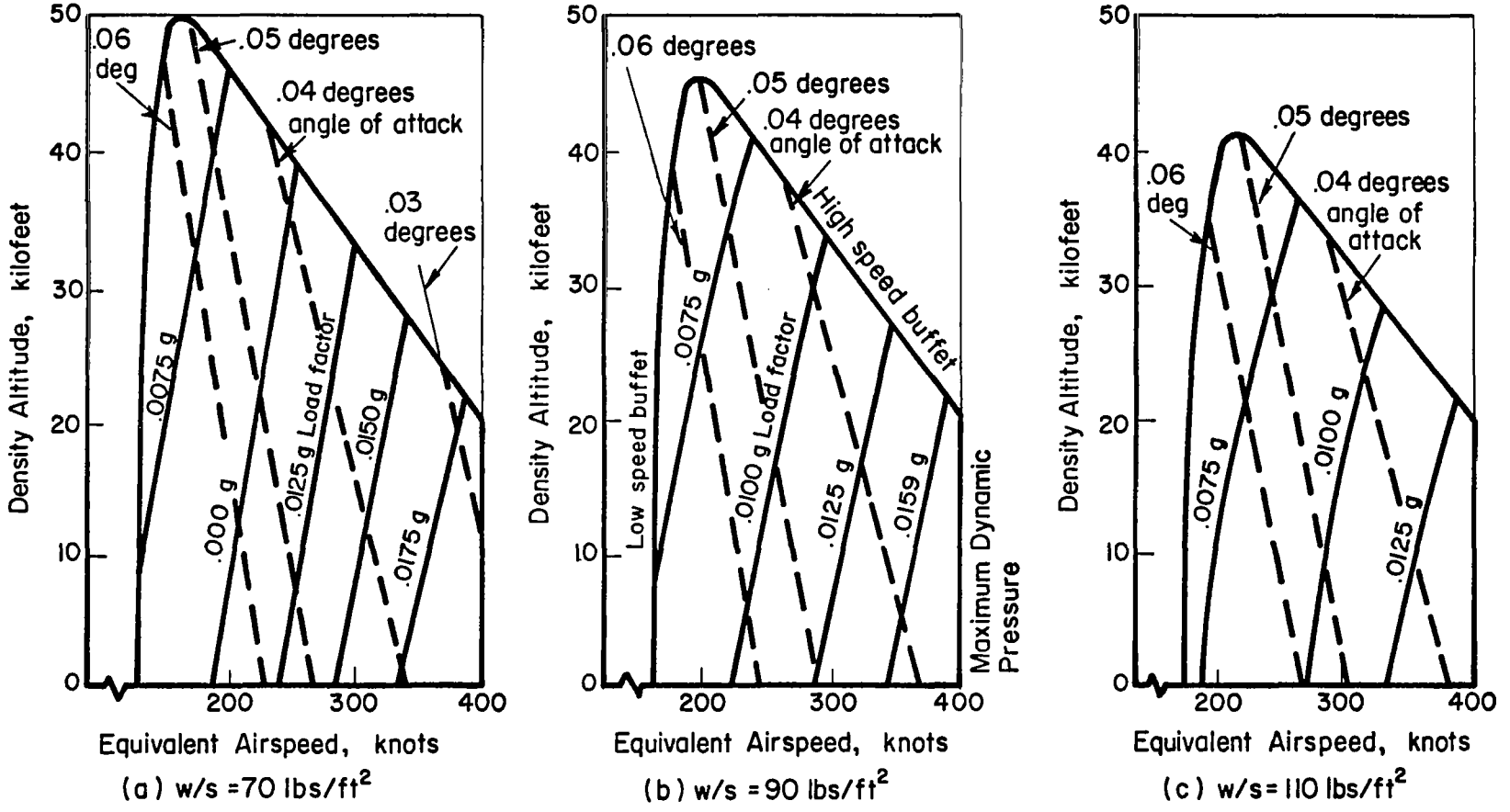

FIGURE 14. AIRCRAFT RESPONSE CONTOURS AS A FUNCTIONS OF WING LOADING FOR UNIT TURBULENCE INTENSITY, LOOSE PITCH CONTROL, AND 20% STATIC MARGIN

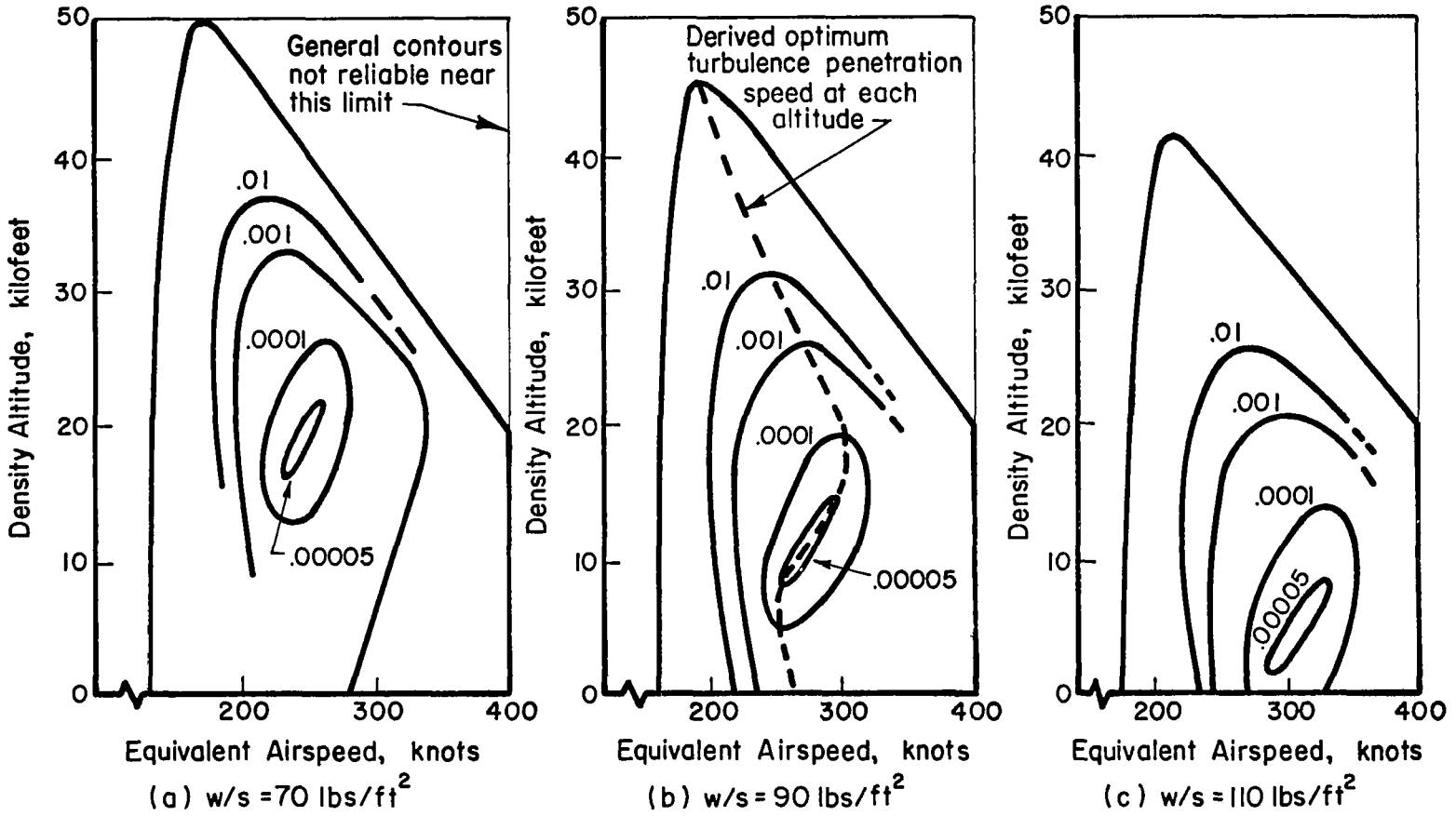

FIGURE 15. PROBABILITY CRITERION CONTOURS AS A FUNCTION OF WING LOADING FOR SEVERE TURBULENCE, ($\sigma_w = \sigma_u = 30$ FT/SEC), LOOSE PITCH CONTROL, AND 20% STATIC MARGIN

importance of the buffet limit diminishes and the load factor limit becomes the dominant constraint. Consequently, the optimum turbulence-penetration speed is reduced with decreasing altitudes. At altitudes below about 7,500 ft, the increased rms angle of attack response to turbulence with decreases in equivalent airspeed (see Figure 14) becomes significant and causes an approximately constant optimum turbulence-penetration speed at the lower altitudes.

Sensitivity of Results to Other Parameter Variations

As mentioned in the previous sections, the optimum turbulence penetration region based on minimum constraint exceedance capability is below the normal cruise altitudes of current subsonic jet transports. The effects of some parameter changes were examined at a fixed cruise altitude, chosen as 30,000 ft because of the relatively high constraint exceedance probability at this altitude. Figures 16 and 17 show the aircraft responses to unit turbulence inputs and the exceedance probabilities as functions of the equivalent airspeed for three wing loadings. Figure 17 shows that for the conditions of these results the lowest wing loading case has the lowest exceedance probability. This is because the lowest wing loading has the lowest angle of attack response to turbulence inputs, as shown in Figure 16, and as shown previously, the dominant constraint at this altitude is the buffet limit. The lowest wing loading has the largest load factor response to turbulence but the load factor limit is of less importance compared to the buffet limit.

To portray in more detail the manner in which the constraints and the aircraft responses interact, Figures 18 and 19 have been prepared. Figure 18 displays for a low equivalent airspeed of 200 knots, the aircraft response covariance ellipses and the constraint envelopes for the highest and lowest wing loadings. Similar data are shown in Figure 19 for the higher equivalent airspeed of 300 knots. The mean times between crossings of each constraint are given in several units of time or are denoted as approaching infinity if the mean time is greater than one day.

From Figure 18, it is readily apparent that the difference in the resultant exceedance probabilities for the two wing loadings is strongly affected by the location of the constraint envelope relative to the trim point rather than on differences in aircraft response. In particular, the upper buffet limit is very near the trim point for the higher wing loading case. The minimum control speed limit could also be expected to be crossed occasionally for the higher wing loading case but the other constraints are insignificant. For the lower wing loading case, the upper buffet limit is the only significant constraint.

Similar data are presented in Figure 19 for the high speed cruise situation. For the lower wing loading case, the upper buffet limit is most dominant with the Mach limit and positive load factor limit of somewhat less

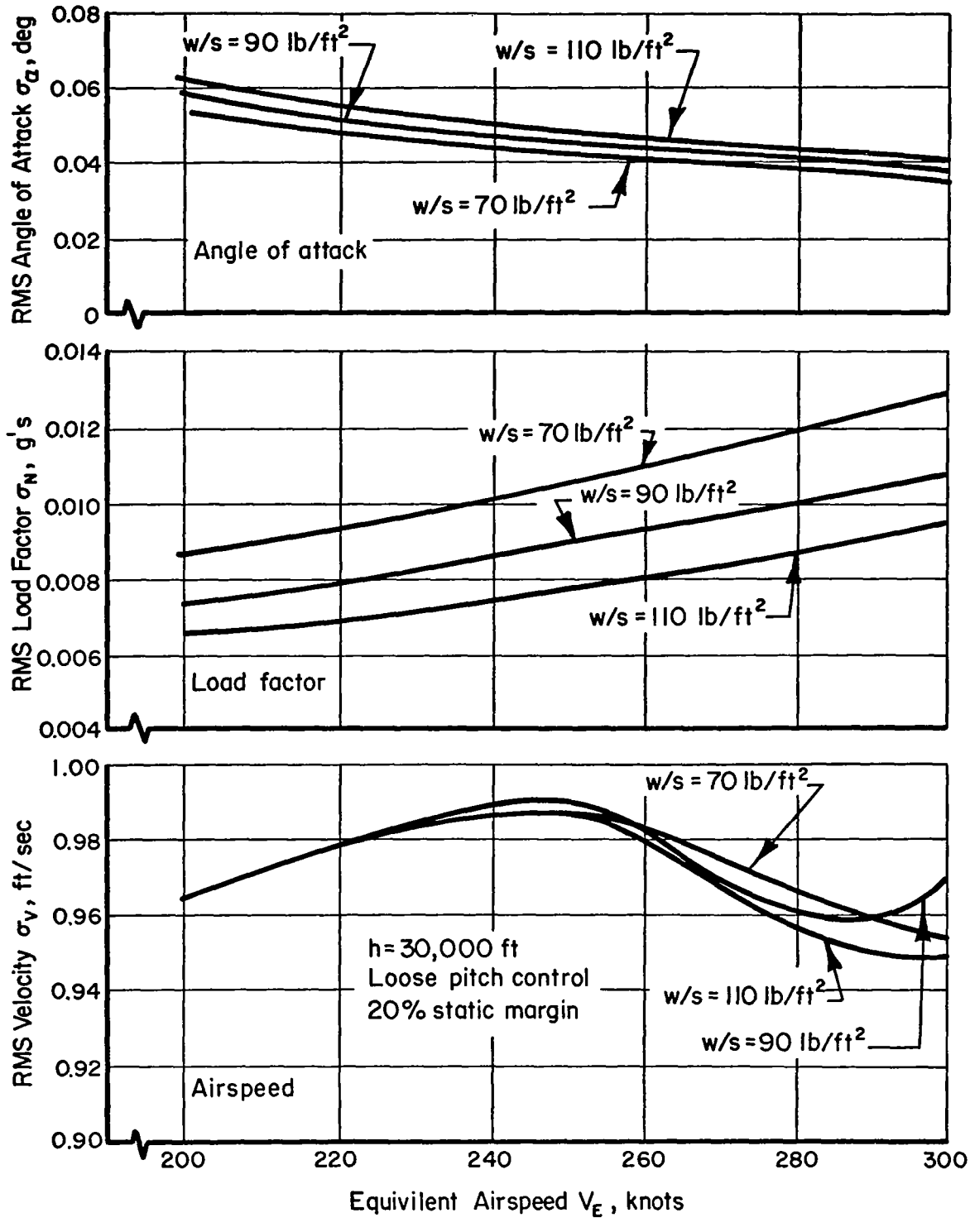

FIGURE 16. EFFECT OF WING LOADING ON RMS RESPONSES TO UNIT TURBULENCE INTENSITY

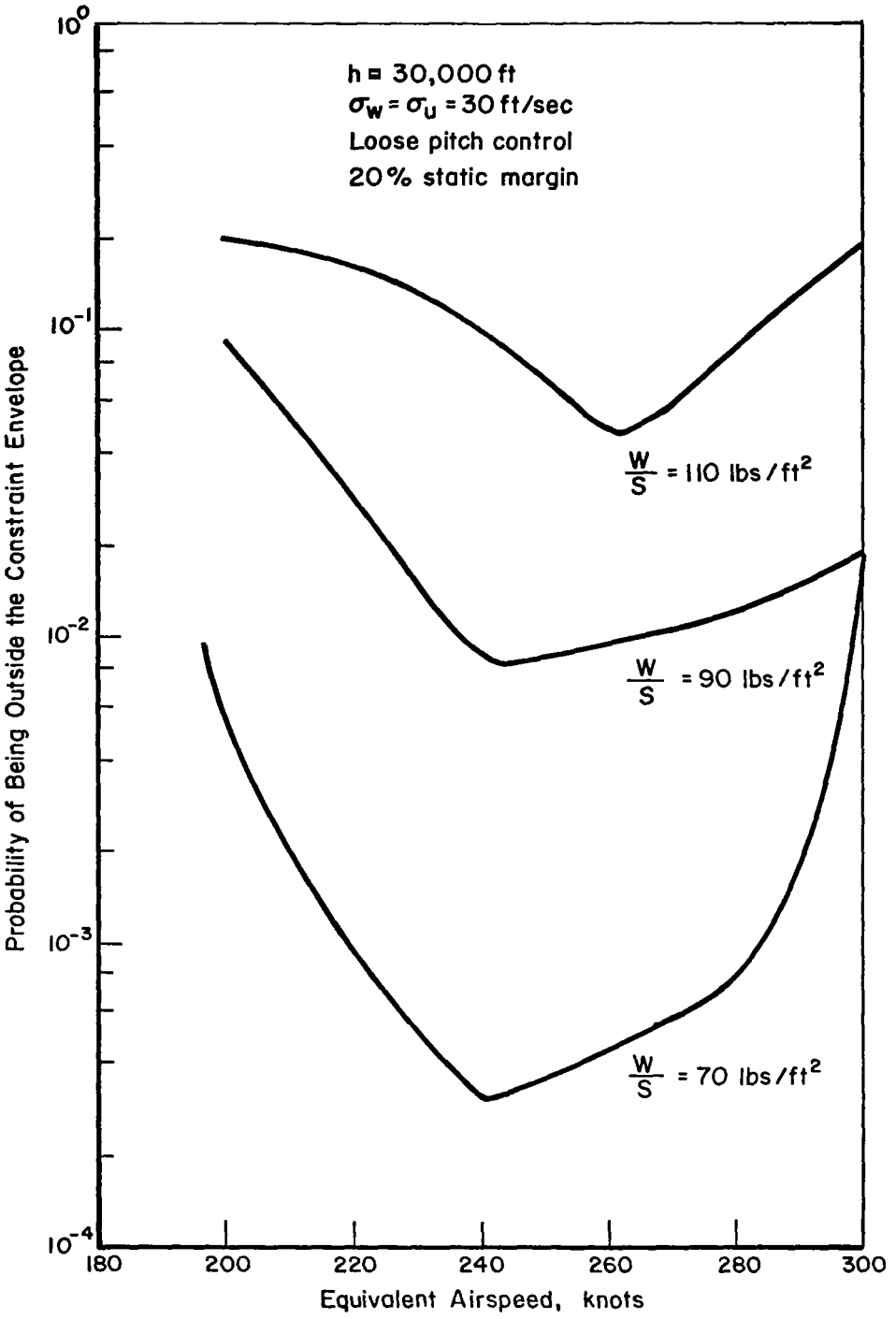

FIGURE 17. EFFECT OF WING LOADING ON PROBABILITY OF BEING OUTSIDE THE CONSTRAINT ENVELOPE

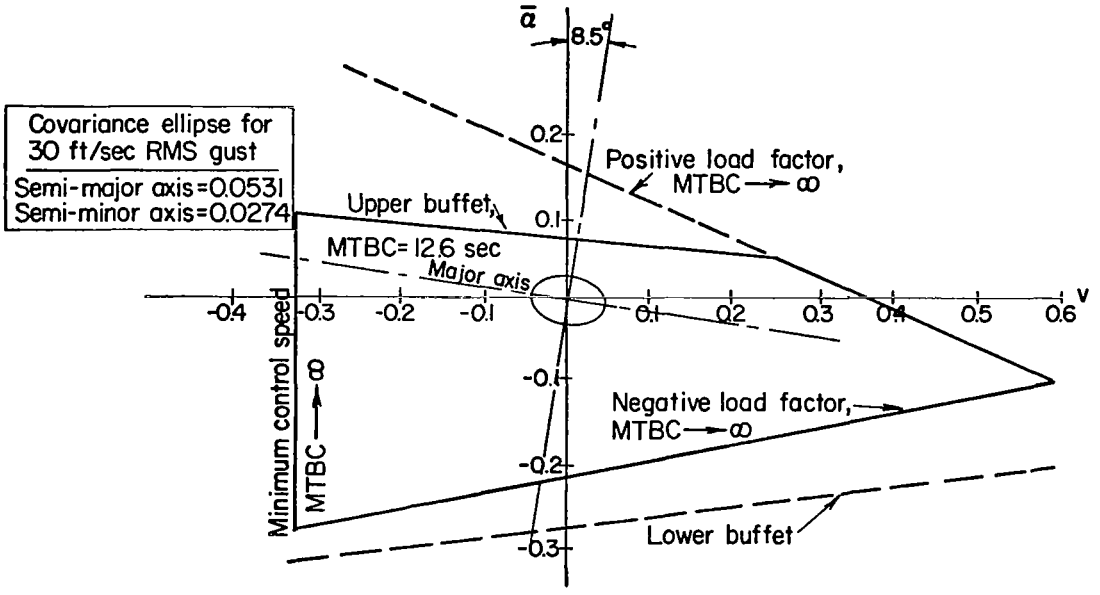

(a) W/S = 70 lb/ft^2; Exceedance Probability = 0.0056

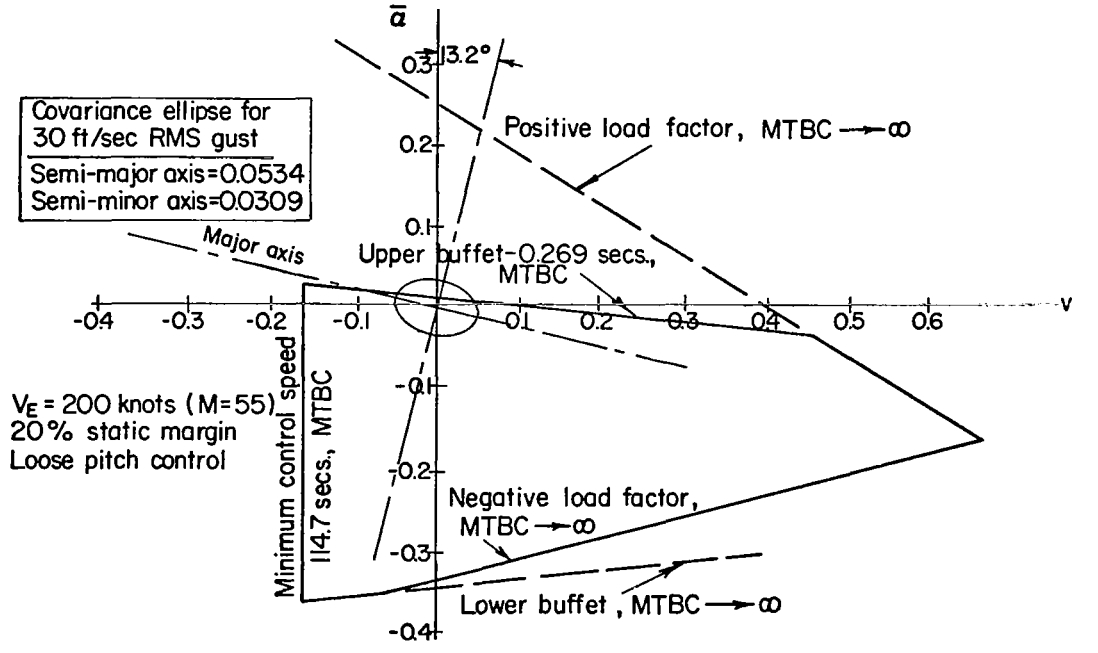

(b) W/S = 110 lb/ft^2; Exceedance Probability = 0.20

FIGURE 18. CONSTRAINT ENVELOPES AT LOW SPEED FOR 30,000 FT CRUISE ALTITUDE

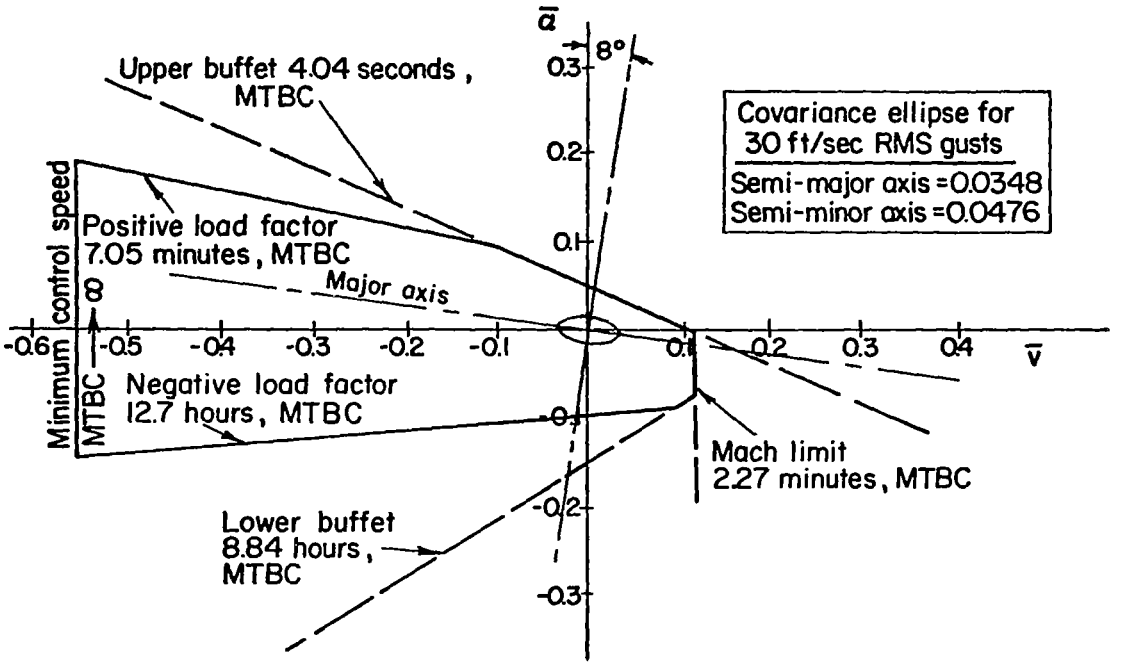

(a) W/S = 70 lb/ft^2; Exceedance Probability = 0.014

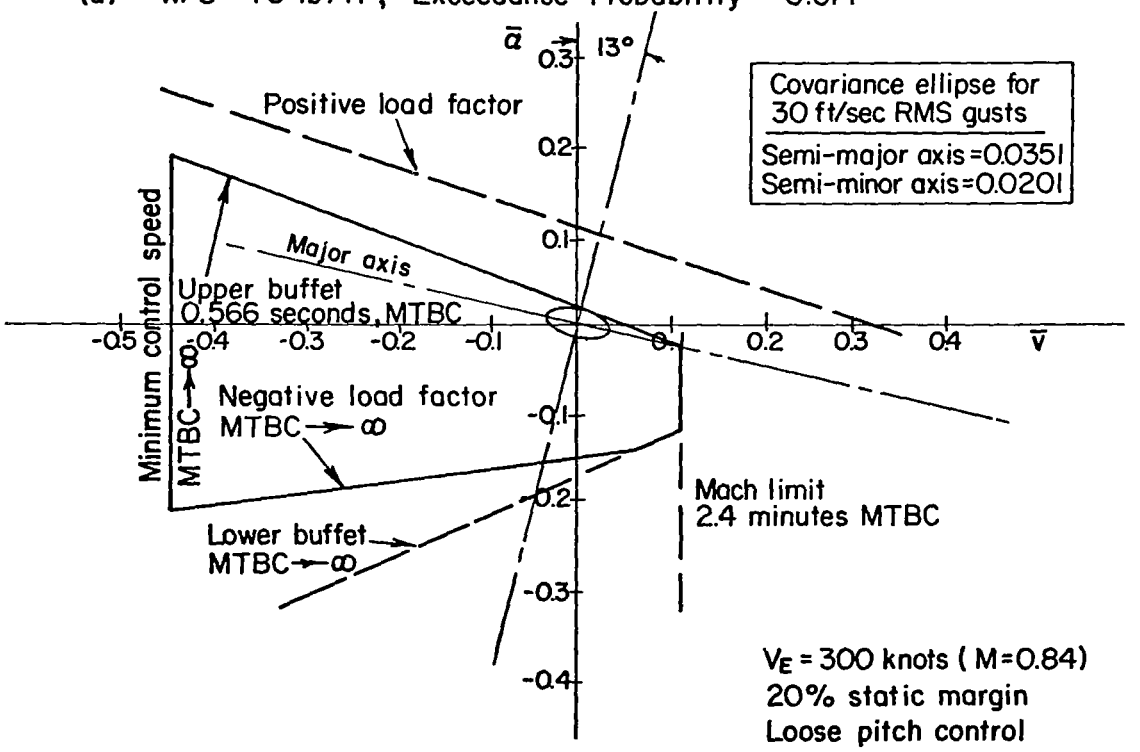

(b) W/S = 110 lb/ft^2; Exceedance Probability = 0.19

FIGURE 19. CONSTRAINT ENVELOPES AT HIGH SPEED FOR 30,000 FT CRUISE ALTITUDE

significance. For the higher wing loading case, the upper buffet limit again moves very near the trim point and dominates the exceedance probability, although the Mach limit cannot be completely disregarded.

Close scrutiny of the results in Figures 18 and 19 exposes several possible shortcomings of the turbulence-penetration performance evaluation as presently formulated. First, all the constraints are viewed with equal seriousness regardless of their physical origin; although it is quite possible that load factor limit exceedances should be weighted more heavily than occasional excursions beyond the buffet limit. Secondly, a rational basis for properly weighting each constraint is not obvious. For instance, it is difficult to assess the seriousness of exceeding either the Mach limit or the minimum control speed limit as compared to exceeding the buffet limit. Examination of these questions was beyond the scope of this study.

The effects of variations in static margin, atmospheric turbulence model, and control criteria on aircraft response and turbulence-penetration performance were also examined in this study.

The effect of a rearward movement of the center of gravity was found to be detrimental, from the load factor standpoint, by Pratt and Bennett.[13] The results of the study reported herein confirm this finding. As illustrated in Figure 20, decreased static margin has an adverse effect on the load factor and angle of attack responses to unit turbulence inputs while the airspeed response is not significantly changed. Figure 20 also shows the two response parameters, altitude and pitch rate, which were not, in general, computed for most of the cases of this study since they are not directly involved in the turbulence-penetration performance evaluation procedure. However, altitude and pitch rate responses to turbulence are of interest because altitude is important from the air traffic control standpoint and pitch rate can influence passenger comfort. Figure 20 shows that the altitude response to a unit turbulence input is influenced by the trim airspeed but is not greatly affected by static margin, whereas the pitch rate response shows a strong dependence on center of gravity location and no significant influence of trim airspeed.

The effects of changes in the atmosphere turbulence model are shown in Figure 21. The Case II (Dryden) model yields smaller responses in load factor and angle of attack than does the Case I (Von Karman) model which has been used throughout this study. The response reductions with the Dryden model are due to the slightly lower power spectral density amplitude of this model in the short period frequency range for both the horizontal and vertical turbulence components.

The consequences effects of reducing the scale length from 5,000 ft to 2,000 ft are shown in Figure 21 for the Von Karman model. This change increases the relative level of the turbulence power at the important short period frequencies and consequently causes large increases in the load factor and angle of attack responses to a unit rms turbulence input. It is observed from Figure 21 that the correlation coefficient relating angle of attack and

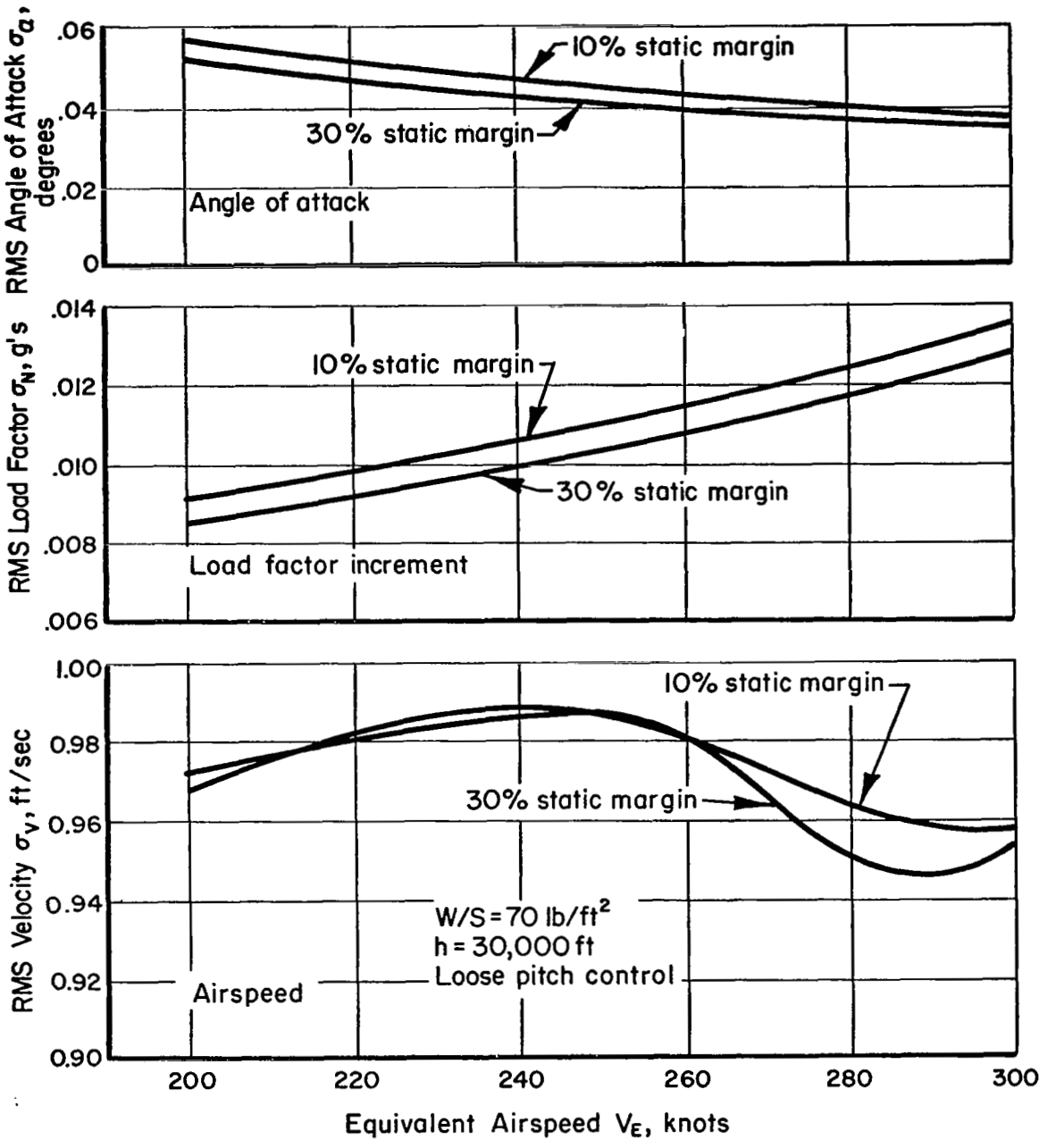

FIGURE 20. EFFECT OF TRIM SPEED AND STATIC MARGIN ON RMS RESPONSES TO UNIT TURBULENCE INTENSITY

(CONTINUED)

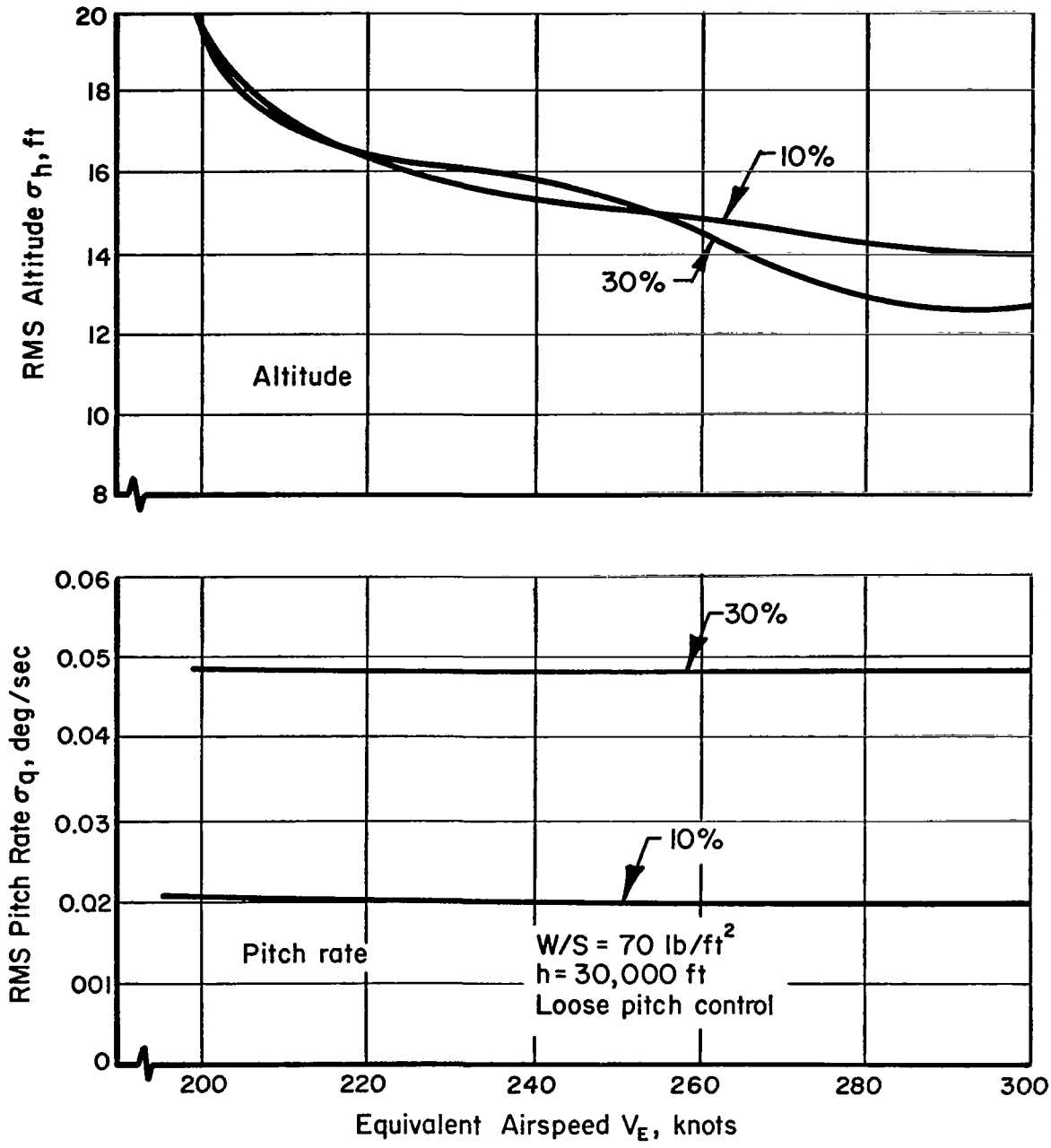

FIGURE 20. (CONCLUDED)

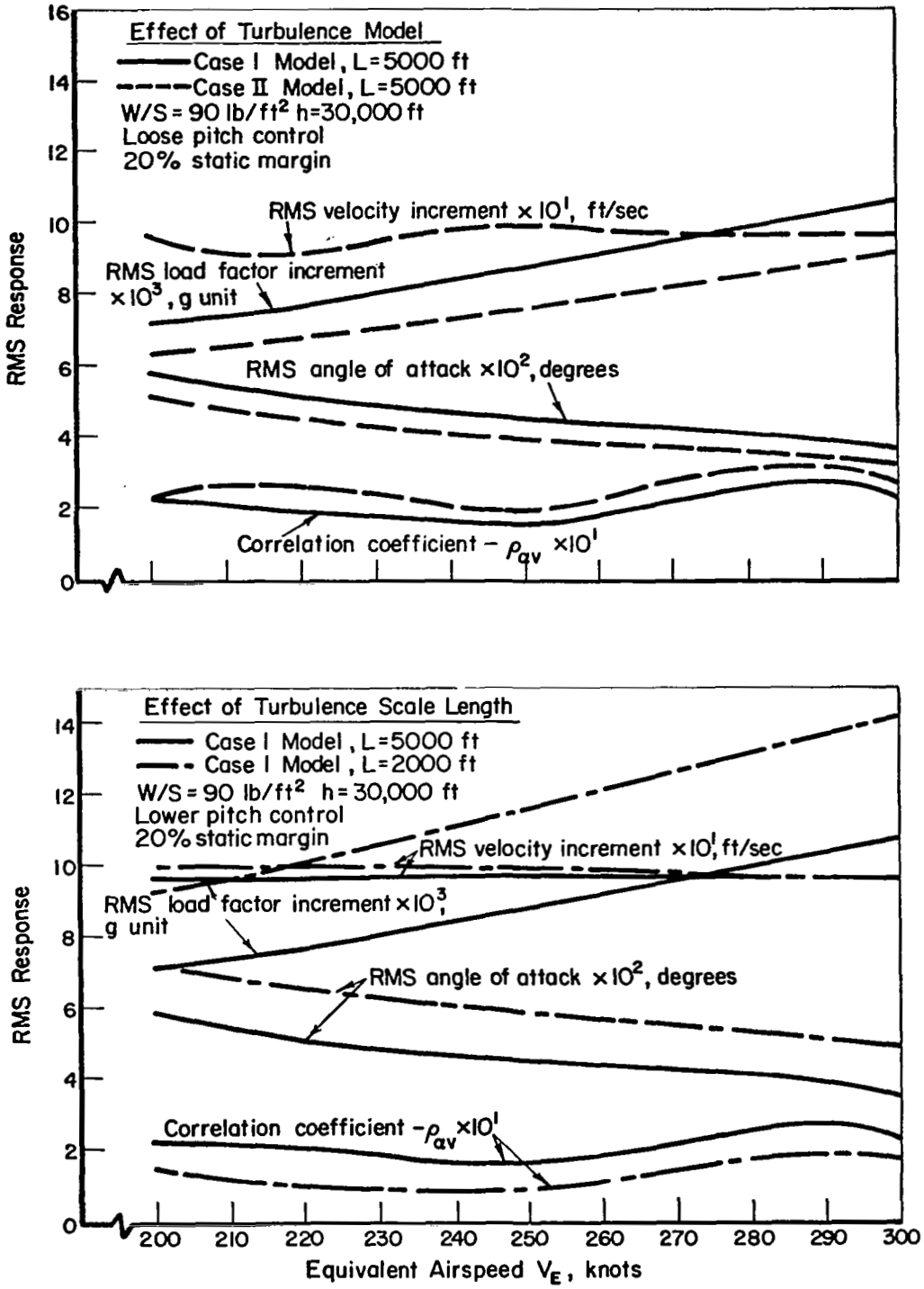

FIGURE 21. EFFECT OF TURBULENCE PARAMETERS ON RESPONSES TO UNIT TURBULENCE INTENSITY

velocity responses is dependent upon both the turbulence model and the scale length. Consequently, the shape of the covariance ellipses, such as shown in Figures 18 and 19 would be affected by these factors. Further exploration of the influence of the turbulence model and the scale length on turbulence-penetration performance was not performed in this study.

The effects of using different control systems on the response to unit turbulence inputs and on the turbulence-penetration performance were investigated for one equilibrium flight condition. This included a more detailed study of the aircraft's response behavior with a pitch autopilot having pitch angle and pitch rate error signals fed to the elevator control. Since two gain settings are involved with this control system, the procedure used was to first select the pitch angle feedback gain, since this determines the tightness of control, and then adjust the pitch rate feedback gain to provide 0.7 critical damping of the short period mode. The responses to a unit turbulence input and the turbulence-penetration performance are presented in Figure 22 as functions of the pitch feedback gain. Also shown in this figure are the results for the loose pitch control used in all earlier work and those for a pitch autopilot with short period damping. The trim flight condition corresponds to the optimum turbulence penetration speed of 250 knots at 30,000 ft for a wing loading of 90 lbs/ft^2 (see Figure 15(b)).

As expected, the results in Figure 22 indicate that increasing the closed-loop short period damping to 0.7 with the pitch rate feedback is beneficial in reducing the angle of attack and load factor responses compared to those for the loose pitch control. Increasing the pitch feedback gain while maintaining 0.7 critical damping of the short period decreases the pitch rate response to unit turbulence inputs. The turbulence-penetration performance in terms of probability of being outside the constraint envelope is not greatly affected by the tightness of pitch control, although all cases with higher short period damping are superior to the loose pitch control case. Although these few results are certainly not conclusive, they indicate that the turbulence-penetration performance may not be heavily dependent on the pitch control gains as long as the closed loop system is reasonably good based upon subjective judgment of tightness and damping.

More complex control systems were also investigated for the same trim flight condition. Figure 23 shows the aircraft's rms responses to unit turbulence inputs for a variety of systems utilizing elevator and thrust control. It should be emphasized here that all the feedback gains except those of the basic pitch autopilot with pitch angle and pitch rate feedback loops were selected in a very arbitrary fashion based purely on subjective judgment. These data are therefore for illustrative purposes only, and do not represent the final results of a systematic investigation. The pitch autopilot, which was used in all the control systems studied and shown in Figure 23, had a pitch feedback gain $K_\theta = -0.6$ and a pitch rate feedback gain $K_{\dot{\theta}} = -0.64$ 1/sec which provided 0.7 critical damping of the short period mode. It should be pointed out that the final damping ratio of the closed-loop short period mode was affected by the additional feedbacks used in the more complex control systems. The following control systems were investigated:

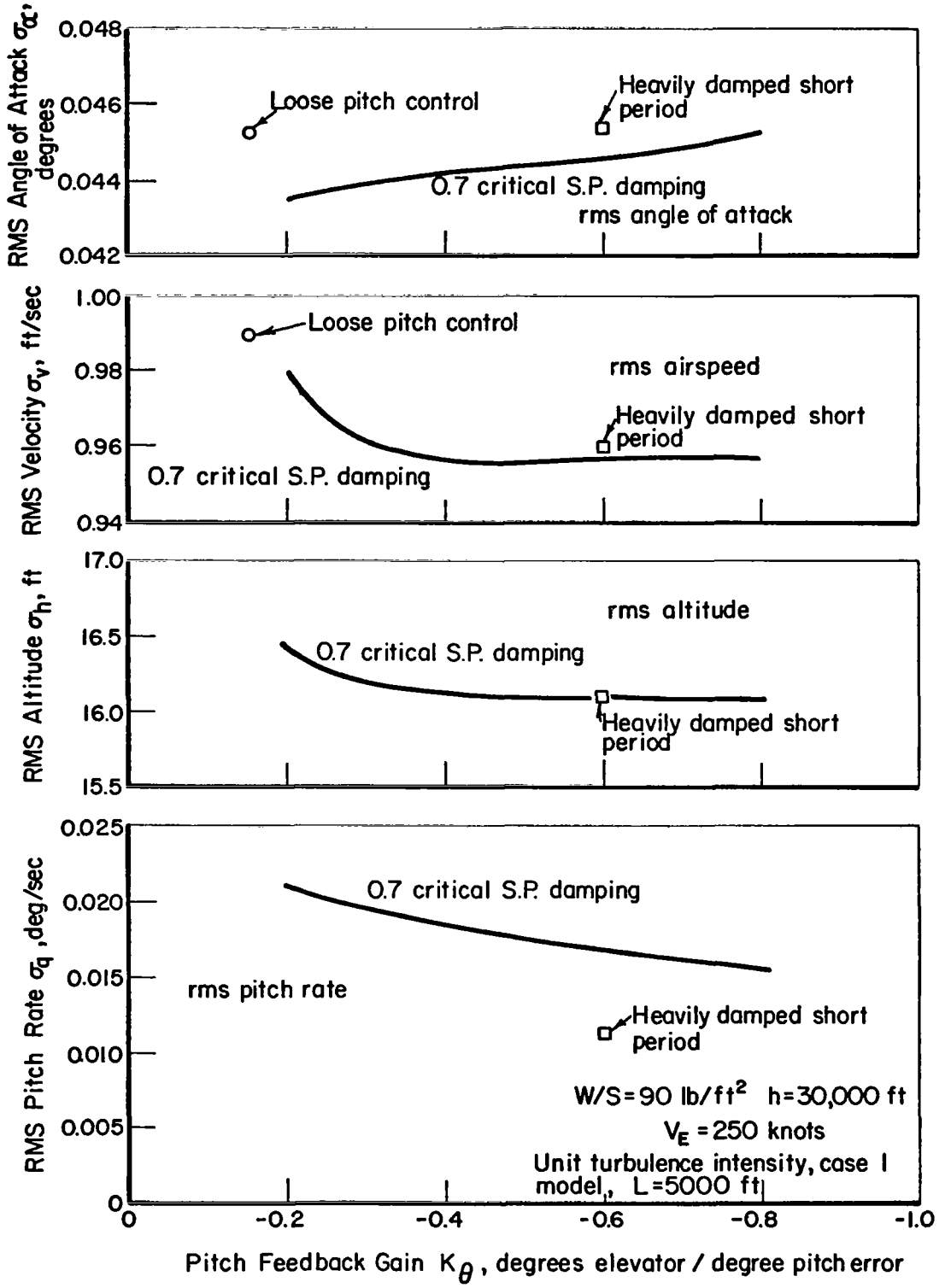

FIGURE 22. EFFECT OF TIGHTENED PITCH CONTROL: PITCH AUTOPILOT WITH 0.7 CRITICAL DAMPING OF SHORT PERIOD MODE (CONTINUED)

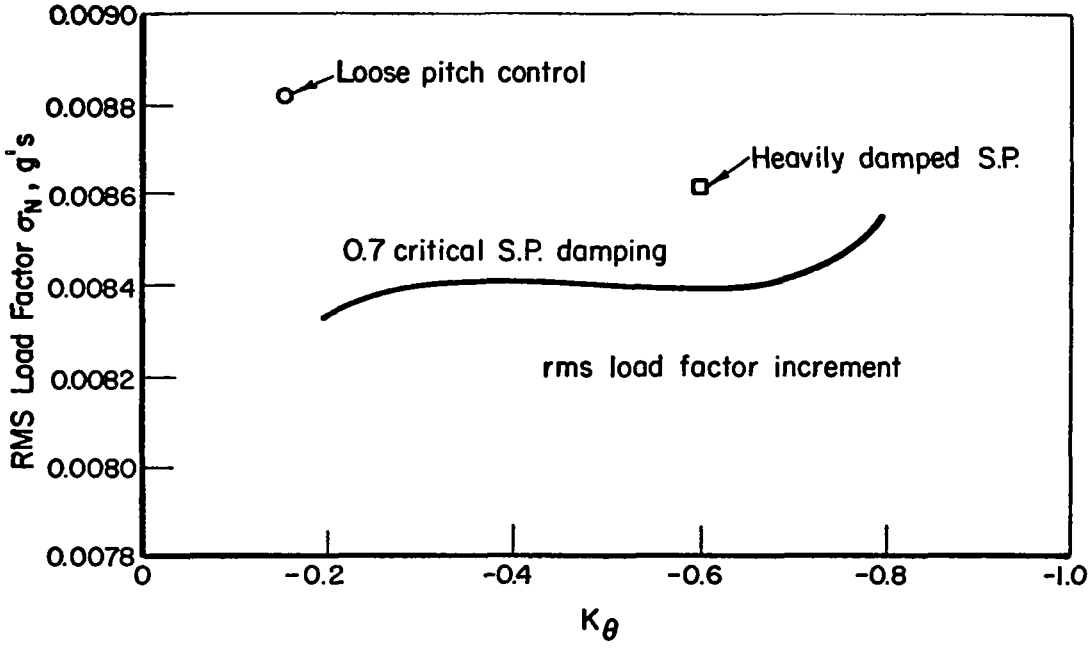

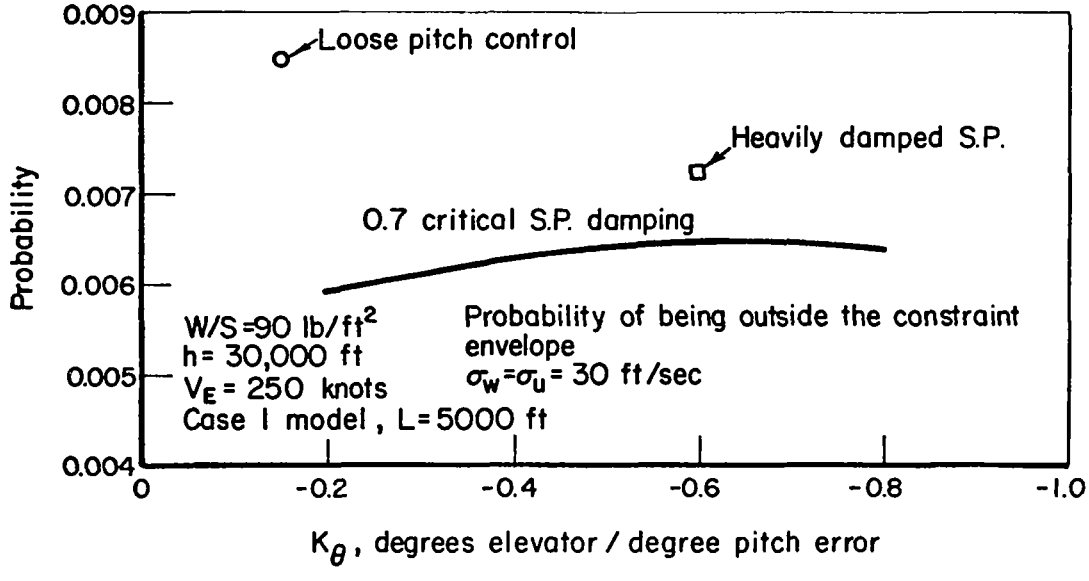

FIGURE 22. (CONCLUDED)

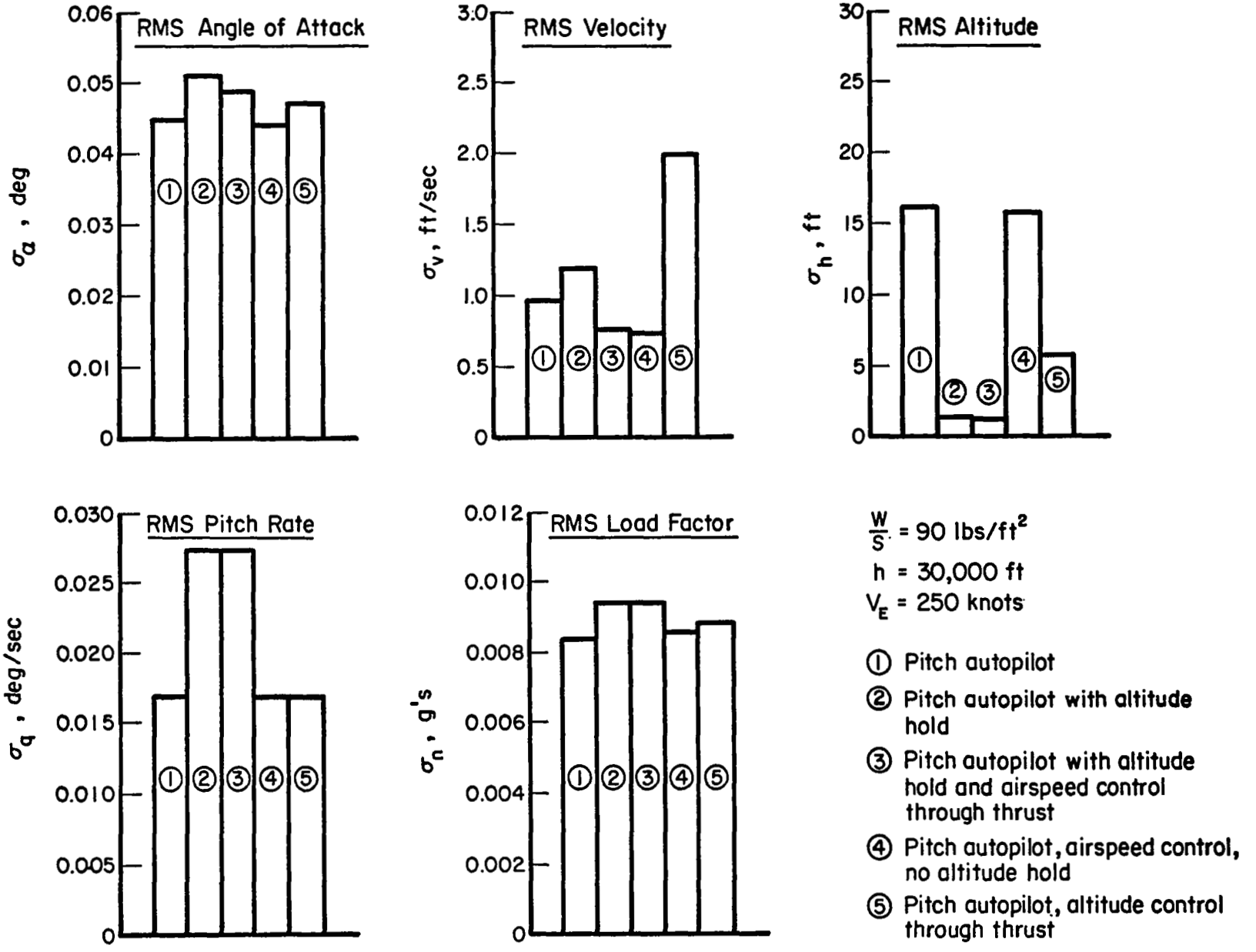

FIGURE 23. EFFECT OF CONTROL SYSTEM ON RMS RESPONSES TO UNIT TURBULENCE INPUTS

(1) Pitch autopilot.

(2) Pitch autopilot with altitude hold, mechanized by feeding altitude and altitude rate signals as commands into the autopilot. Gains were P_h = -0.001 rad/ft, $P_{\dot{h}}$ = -0.002 rad/ft·sec

(3) System (2) airspeed control, mechanized by feeding airspeed and airspeed rate error signals to the throttles. Gains were T_V = -1, $T_{\dot{V}}$ = -1 1/sec.

(4) System (3) with altitude hold removed.

(5) Pitch autopilot with altitude controlled by positioning the throttles as a function of altitude and altitude rate error signals. Gains were T_h = -0.0001 rad/ft, $T_{\dot{h}}$ = -0.004 rad/ft·sec.

Figure 23 shows that some of the responses were affected very little by the type of control system. In particular, the angle of attack and load factor responses are relatively constant for the five systems. This is probably due to the fact that these two responses are dominated by the pitch autopilot, which was an integral part of all the systems. Control systems (2) and (3), with altitude hold achieved by pitch autopilot commands, are quite effective in reducing the unit turbulence input, rms altitude response at the expense of the other variables, notably the pitch rate. The addition of airspeed control through thrust, as used in control systems (3) and (4), improved the airspeed response significantly and had little effect on the other variables. This can be seen by comparing the responses for systems (1) and (4) without altitude hokd, and systems (2) and (3) with altitude hold. System (5), using altitude control through thrust in conjunction with the pitch autopilot, is not as effective in reducing the altitude response compared to systems (2) and (3) using altitude hold through pitch command. Furthermore, the airspeed response for system (5) drastically increased, a consequence of using thrust changes for altitude corrections while attempting to maintain a fixed pitch attitude.

Figure 24 shows the turbulence-penetration performance for each of the control systems. Systems (1) and (4) have essentially the same probability of the aircraft being outside the constraint envelope for the trim flight condition used. Systems (2) and (3), and to some extent system (5), have poorer performance when evaluated with the specific constraint envelope used. These are the systems that were most effective in reducing the altitude response. It is interesting to note that system (4) would result in an rms altitude response of 468 ft in the severe 30 ft/sec rms turbulence environment, whereas system (3) would only result in an rms altitude response of slightly over 40 ft. Although turbulence of this magnitude is infrequent, the very large altitude response which results with system (4) might represent problems from the air traffic control standpoint. Consequently, consideration of including an altitude constraint as part of the constraint envelope may be warranted.

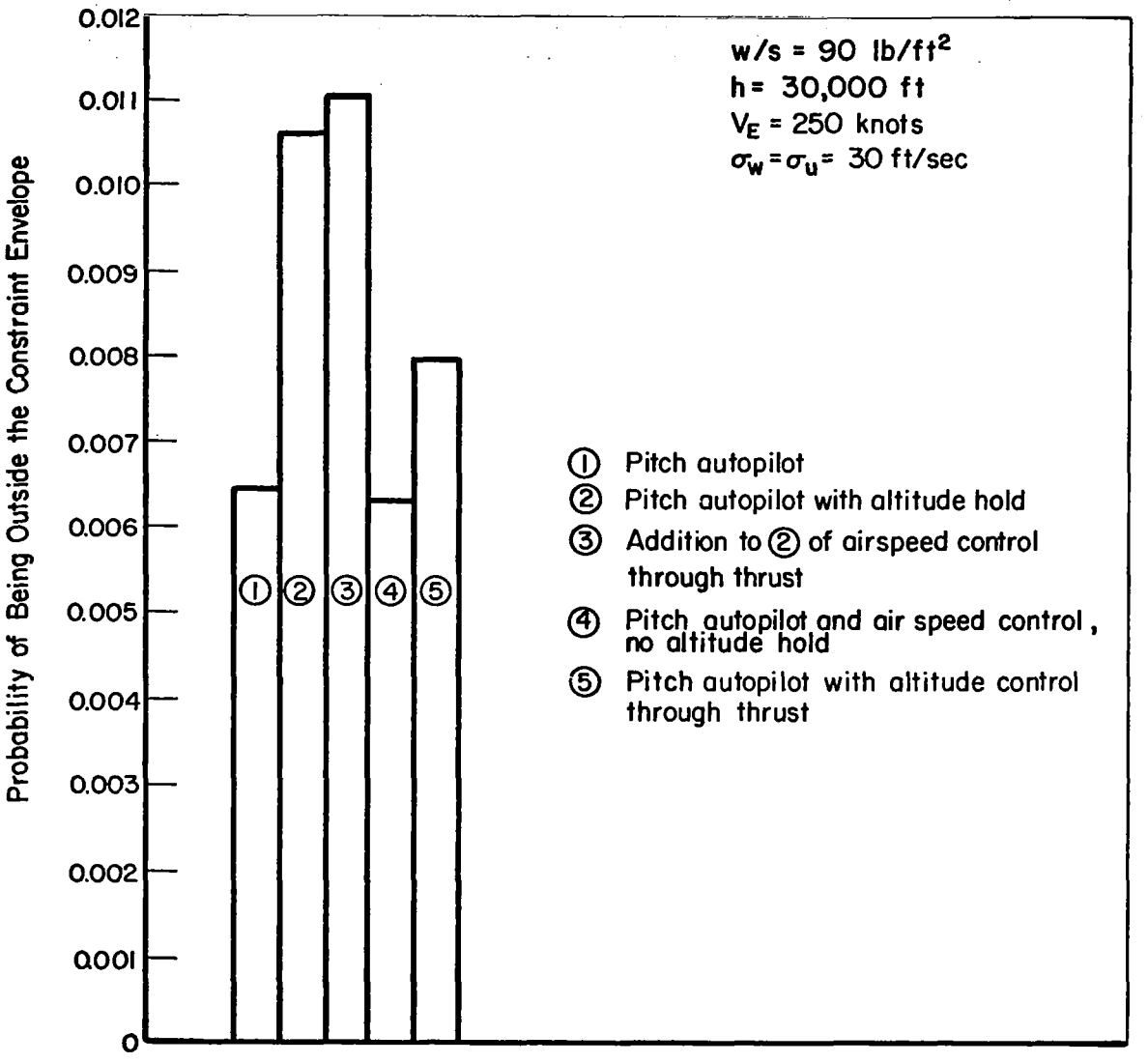

FIGURE 24. EFFECT OF CONTROL SYSTEM ON TURBULENCE-PENETRATION PERFORMANCE

The data in Figures 23 and 24 reveal an interesting subtlety of the turbulence-penetration performance evaluation procedure reported herein. According to Figure 24, system (3) is slightly worse than system (2). However, the opposite conclusion might be drawn from the angle of attack and airspeed responses shown in Figure 23. A close examination of this apparent anomaly revealed that differences in the covariance ellipse orientation were responsible for changing the relative performance for these two systems. This illustrates the difficulty of assessing the turbulence-penetration performance by simply examining the individual parameter responses to unit turbulence inputs.

It should be noted that the relative turbulence-penetration performance of these five control systems shown in Figure 24 might be different at other trim flight conditions in the flight envelope. At the trim flight condition used to investigate the effects of different control systems, the upper buffet limit was the predominant constraint, and airspeed changes had a very small effect on the probability of being outside the constraint envelope. Airspeed changes might be more important if the trim flight condition were at a higher altitude or offset from the derived optimum turbulence-penetration speed.

Procedural Extensions and Applications

As a result of performing the work described in this report, certain insights were gained on possible refinements which could reasonably be made in the procedure for assessing turbulence-penetration performance and on potential applications of the procedure. These are briefly discussed in this section.

Possible extensions to the evaluation procedure which appear to be of value and practical from both a formulation and computational standpoint are the following:

(1) Increased Dimensions of Constraint Space - The two-dimensional angle-of-attack/velocity constraint space used in this report could be extended to include altitude limits established from air traffic control considerations, a deep-stall constraint limit, ride-quality limits, and possibly lateral-directional response limits. For aircraft with potential deep-stall problems, a constraint boundary established as a function of both angle of attack and pitch rate might be appropriate.[15] With regard to ride qualities, a discomfort index such as in Reference 16 could be used. Although an extension of the constraint space to include

lateral-directional response limits may appear useful, the tendency for a low degree of correlation between longitudinal and the lateral-directional responses may permit separate examination of these motions and the development of a relatively simple procedure for combining their effects on turbulence-penetration performance. It should be noted that a potential limitation on increasing the constraint space dimensions is the increased complexity in integrating the multi-variate probability distribution function throughout the region. This difficulty would appear to grow geometrically as the number of dimensions of the space is increased. It is encouraging, however, that the two-dimensional integration used in this study required only 0.2 seconds per case on a CDC 6400 computer.

(2) Inclusion of Primary Structural Modes - The analytical model of the aircraft used in determining turbulence responses could be expanded to include primary structural dynamic modes. Such modes would be required if the constraint space included a ride qualities discomfort index relating acceleration spectra at selected points in the aircraft to human objective responses. Furthermore, if structural modes were included the load factor constraint boundary could be replaced or supplemented by structural stress limits at selected critical locations in the aircraft. The aircraft/control system dynamic model would be substantially more complex with the inclusion of elastic modes, and the number of parameters involved would probably inhibit generalization of results. This complication appears to be warranted only for the investigation of turbulence-penetration performance of specific aircraft.

(3) Inclusion of Nonlinear Aerodynamic and Control System Characteristics - The addition of nonlinear characteristics in the analytical model of the aircraft/control system appears to be desirable, particularly for assessing turbulence-penetration performance of aircraft operating in or near the transonic speed region. Unfortunately, including the nonlinear characteristics presents special analysis problems. For analyzing nonlinear systems, there are exact approaches such as using the Fokker-Planck Equation[17], but this method might prove excessively difficult for dynamic systems greater than second order. Two less exact analysis approaches are the use of a random-input describing function[18] which allows Gaussian-type computations but suffers from an uncertainty in the validity

of the results, and the use of the Monte-Carlo method[19] which is moderately simple to apply but has the disadvantage of low confidence levels for low-probability events such as are involved in determining turbulence-penetration performance. In extending the procedure as described above, one might also account for the variations with altitude of the probabilities of encoutering turbulence of a given magnitude for, say, nominal mission profiles.

(4) Improvement in Constraint Envelope Formulation - It might be very desirable to formulate the constraint envelope with differential weighting of the various turbulence-penetration performance limits, or to replace some of the discrete boundaries with gradients representing increasingly proper performance as the boundary is penetrated. A prerequisite to such improvements must be a better quantitative understanding of hazards in the general state-space, than now exists.

There are several potential applications of the turbulence-penetration performance assessment procedure, even in its simplified form as described in this report. Some of these are as follows:

(1) The comparative evaluation of various types of aircraft to delineate particular problems in terms of the relationship between the basic physical and aerodynamic characteristics and the intended operational environment,

(2) The selection of optimum turbulence penetration speeds for specific aircraft,

(3) The definition of the gross closed-loop control requirements for an autopilot turbulence mode of operation.

In addition, refinements of the procedure for assessing turbulence-penetration performance, as discussed above, could lead to tools adequately sophisticated for the investigation of optimal controller configurations and/or path geometry and speeds for automatic approaches in turbulence.

Conclusions

From an examination of the results of this work, the following conclusions are drawn:

(1) The procedure for assessing turbulence-penetration performance by evaluating the probability of being outside a constraint envelope produces quantitative comparative results which are in general agreement with subjective engineering judgments and operationally derived procedures.

(2) The computational effort required to apply turbulence-penetration assessment procedure is well within the capability of digital computers.

(3) The assessment procedure is decisive, in that large differences in the numerical value of the probability function can result from reasonable changes in the important inertial, aerodynamic, and control system characteristics of the aircraft and in the trim flight condition.

(4) The parameters which appear to have the most influence on the turbulence-penetration performance are the normalized wing loading, $(W/S)/\sigma$, and the trim airspeed.

(5) For the range of aircraft sizes considered in this study, increasing aircraft size has a relatively insignificant detrimental effect on over-all turbulence-penetration performance.

(6) The optimum turbulence-penetration altitudes derived from using the turbulence-penetration performance assessment procedure are below the normal cruise altitudes for current jet transport aircraft. The procedure was used to define optimum turbulence penetration speeds for the complete altitude range for aircraft with different wing loadings.

(7) The conventional means of longitudinal control (horizontal tail surfaces and engine thrust) used in this study were found to be limited to an improvement of turbulence-penetration performance in that part of the temporal frequency spectrum below the short-period frequency, where the excursions of most concern

generally occur. Consequently, little dramatic improvement may be expected over the performance obtained by a simple control philosophy based upon smooth pitch control to inhibit the lower frequency motion. On the other hand, an improper choice of control feedback can have large adverse effects on the criterion rating.

Nomenclature

a = speed of sound, ft/sec

A,B,C = arbitrary designations for coefficient matrices

$\bar{c}$ = length of mean aerodynamic chord, ft

C_L = lift coefficient

$C_{L_{max}}$ = maximum lift coefficient

C_{L_α} = lift curve slope $(\partial C_L/\partial\alpha)$

$(C_T)_1$ = perturbation in thrust coefficient caused by throttle displacement

$f(\bar{\alpha},v)$ = probability density function

g = gravitational constant, 32.2 ft/sec^2

h = density altitude, ft

I_{yy} = pitching moment of inertia, slug ft^2

$I_{\bar{\alpha}\bar{\alpha}}$, I_{vv} = second-moments of the $\bar{\alpha}$ and v output spectra, 1/ft^2

$I_{\bar{\alpha}v}$ = second-moment of the $\bar{\alpha}$, v cross spectrum, 1/ft^2

K_q = pitch rate feedback gain to elevator, rad/(rad/sec)

K_θ = pitch angle feedback gain to elevator, rad/rad

L = scale of turbulence, ft

m = aircraft mass, slugs

M = Mach number

P_h = ratio of pitch angle command to altitude error, rad/ft

$P_{\dot{h}}$ = ratio of pitch angle command to altitude rate, rad/(ft/sec)

S = wing area, ft^2

T_h = ratio of throttle displacement to altitude error, rad/ft

$T_{\dot{h}}$ = ratio of throttle displacement to altitude rate, rad/(ft/sec)

T_v = ratio of throttle displacement to nondimensional airspeed error, rad

$T_{\dot{v}}$ = ratio of throttle displacement to nondimensional airspeed rate, rad/sec

v = nondimensionalized airspeed perturbation

V = true airspeed, ft/sec

V_E = equivalent airspeed, $\sqrt{\sigma}\, V_{true}$, knots

V_{g_h} = horizontal component of gust velocity, ft/sec

V_{g_v} = vertical component of gust velocity, ft/sec

W = aircraft weight, lbs

X_i = designation for state variables, where i = 1, 2, . . . N

X_{sm} = static margin: ratio of the distance of the c.g. forward of neutral point, to the length of the mean aerodynamic chord

α = angle of attack, radians unless otherwise stated

$\bar{\alpha}$ = angle of attack perturbation from trim, radians

δ_e = elevator deflection from trim, radians

δ_t = throttle displacement from trim setting, radians

θ = pitch attitude displacement from trim, radians

θ_{comm} = commanded pitch angle, radians

ρ = atmospheric density, slugs/ft^3

ρ_{SL} = sea level atmospheric density, slugs/ft^3

$\rho_{\bar{\alpha}v}$ = correlation coefficient relating $\bar{\alpha}$ and v

σ = ratio of ambient atmospheric density to sea level value (ρ/ρ_{SL}); or, with subscript, root mean square response

σ_u, σ_w = root mean square of horizontal and vertical gust components, respectively

$\sigma_{\bar{\alpha}}^2, \sigma_v^2$ = variances of angle of attack and dimensionless airspeed, respectively

$\Phi(\Omega)$ = power spectral density of atmospheric turbulence, ft^3/sec^2

$\Phi_{\bar{\alpha}\bar{\alpha}}, \Phi_{vv}$ = output power spectra for $\bar{\alpha}$ and v, ft

Ω = turbulence spatial frequency, rads/ft

* = superscript denoting "equilibrium flight condition"

References

1. Hunsaker, J. C., Behavior of Aeroplanes in Gusts; Part I - Experimental Analysis of Inherent Longitudinal Stability for a Typical Biplane, NACA Report 1, 1915.

2. Wilson, E. B., Behavior of Aeroplanes in Gusts; Part II - Theory of an Aeroplane Encountering Gusts, NACA Report 1, 1915.

3. Rhode, R. V., and Lundquist, E. E., Preliminary Study of Applied Load Factors in Bumpy Air, NACA TN 374, 1931.

4. Pratt, Kermit G., and Walker, Walter G., A Revised Gust-Load Formula and a Reevaluation of V-G Data Taken on Civil Transport Airplanes From 1933 to 1950, NACA Report 1206, 1954.

5. Press, Harry, Meadows, May T., and Hadlock, Ivan, A Reevaluation of Data on Atmospheric Turbulence and Airplane Gust Loads for Application in Spectral Calculations, NACA Report 1272, 1956.

6. Soderlind, Capt. Paul A., Jet Transport Operation in Turbulence, 1st AIAA Annual Meeting, Washington, D. C., June 29-July 2, 1964, AIAA Paper No. 64-53.

7. Andrews, William H., Butchart, Stanley P., Sisk, Thomas R., and Hughes, Donald L., Flight Tests Related to Jet-Transport Upset and Turbulent-Air Penetration, NASA SP-83, Conference on Aircraft Operating Problems, Langley Research Center, May 10-12, 1965.

8. Bray, Richard S., and Larsen, William E., Simulator Investigations of the Problems of Flying a Swept-Wing Transport Aircraft in Heavy Turbulence, NASA SP-83, Conference on Aircraft Operating Problems, Langley Research Center, May 10-12, 1965.

9. Sadoff, M., Bray, R. S., and Andrews, W. H., Summary of NASA Research on Jet Transport Control Problems in Severe Turbulence, AIAA Journal of Aircraft, Vol. 3, No. 3, p 193-200, 1966.

10. FAA Turbulence Test Program Study, prepared for the Federal Aviation Agency by General Dynamics Convair on Contract No. FA66WA-1467, April 27, 1966.

11. Hitchcock, Lloyd Jr., and Morway, Donald A., A Dynamic Simulation Study of the Swept Wing Transport Aircraft in Severe Turbulence, U. S. Naval Air Development Center Report No. NADC-MR-6807, Federal Aviation Agency Report No. FAA-DS-68-12, October 30, 1968.

12. Houbolt, John C., Steiner, Roy, and Pratt, Kermit G., Dynamic Response of Airplanes to Atmospheric Turbulence Including Flight Data on Input and Response, NASA Technical Report R-199, Langley Research Center, June, 1964.

13. Pratt, Kermit G., and Bennett, Floyd V., Charts for Estimating the Effects of Short-Period Stability Characteristics on Airplane Vertical-Acceleration and Pitch-Angle Response in Continuous Atmospheric Turbulence, NACA TN 3992, June, 1957.

14. Huntley, E., Spectral Gust Alleviation Factor, ICAS Paper No. 68-47, Sixth Congress of the International Council of the Aeronautical Sciences, Munich, Germany, September, 1968.

15. Montgomery, R. C. and Moul, M. T., Analysis of Deep-Stall Characteristics of T-Tailed Aircraft Configurations and Some Recovery Procedures, Journal of Aircraft, Vol. 3, No. 6, November-December, 1966.

16. Grande, D. L., Some Effects of Random Turbulence on Weapon System Performance, Aerospace Engineering, pp 35-43, October, 1962.

17. Robinson, Alfred C., On the Second-Order Properties of the Output of Certain First- and Second-Order Nonlinear Systems With Random Inputs, Ph.d. Thesis, University of Michigan, 1962.

18. Thaler, G. J. and Pastel, M. R., Analysis and Design of Nonlinear Feedback Control Systems, New York, McGraw-Hill, 1962.

19. Hammersley, J. M., and Handscomb, D. C., Monte Carlo Method, New York, John Wiley and Sons, 1964.

Appendix A

Aircraft and Control System Model

Table of Contents

Appendix A

Aircraft and Control System Model

Introduction

The mathematical model of the aircraft and control system used in this study was based on the following assumptions:

(1) Three degrees-of-freedom longitudinal rigid-body modes of motion were considered.

(2) The equations were linearized about a level flight equilibrium condition.

(3) Atmospheric density was assumed to be an exponential function of altitude.(A-1)

(4) The control system involved pure gain feedbacks with no equalization, and sensor and actuator dynamics were ignored.

(5) Both longitudinal and vertical gust velocity components were included.

(6) The lag in vertical gust penetration between the wing and the horizontal tail was represented as an effective aerodynamic pitching rate.

(7) The aerodynamic lag in lift growth on the wing following gust penetration (Kussner function) was included in approximate form; the unsteady aerodynamic effects of aircraft motion (Wagner function) were ignored.

Nomenclature

$\bar{c}$ = mean aerodynamic chord length, ft

C_D = drag coefficient

C_L = lift coefficient

C_T = thrust coefficient

$(C_T)_1$ = perturbation in thrust coefficient caused by throttle displacement

$(C_T)_2$ = perturbation in thrust coefficient due to changes in flight variables.

C_{D_α} = $\partial C_D/\partial\alpha$. 1/rad.

$C_{D_{\delta_e}}$ = $\partial C_D/\partial\delta_e$, 1/rad.

C_{D_M} = $\partial C_D/\partial M$

C_{L_α} = $\partial C_L/\partial\alpha$, 1/rad.

$C_{L_{\delta_e}}$ = $\partial C_L/\partial\delta_e$, 1/rad.

C_{L_M} = $\partial C_L/\partial M$

C_{L_q} = $\partial C_L/\partial \left(\frac{q\bar{c}}{2V}\right)$, 1/rad.

C_m = pitching moment coefficient

C_{m_α} = $\partial C_m/\partial\alpha$, 1/rad.

$C_{m_{\dot{\alpha}}}$ = $\partial C_m/\partial \left(\frac{\dot{\alpha}\bar{c}}{2V}\right)$, 1/rad.

$C_{m_{\delta_e}}$ = $\partial C_m/\partial\delta_e$, 1/rad.

C_{m_q} = $\partial C_m/\partial \left(\frac{q\bar{c}}{2V}\right)$, 1/rad.

C_{m_M} = $\partial C_m/\partial M$

$C_{m_{C_T}}$ = $\partial C_m/\partial T$, 1/lb

g = acceleration of gravity, ft/sec^2

h = increment in altitude from reference condition, ft

$\bar{I}$ = unit vector along x body axis

I_{yy} = pitch moment of inertia, slug-ft^2

k_y = pitch radius of gyration, ft

$K_\alpha = \partial\delta_e/\partial\alpha$

$K_q = \partial\delta_e/\partial q$

K_T = static gain relating thrust coefficient to throttle position

$K_v = \partial\delta_e/\partial v$

$K_{\dot{v}} = \partial\delta_e/\partial\dot{v}$

$K_\theta = \partial\delta_e/\partial\theta$

ΔL = increment in total lift force, lbs

M = mach number

m = airplane mass, slugs

$$M_\alpha = \frac{\rho V^2 S\bar{c}}{2I_{yy}} C_{m_\alpha}, \text{ 1/sec}$$

$$M_{\dot{\alpha}} = \frac{\rho V S\bar{c}^2}{4I_{yy}} C_{m_{\dot{\alpha}}}, \text{ 1/sec}$$

$$M_{C_T} = \frac{\rho V^2 S\bar{c}}{2I_{yy}} C_{m_{C_T}}$$

$$M_{\delta_e} = \frac{\rho V^2 S\bar{c}}{2I_{yy}} C_{m_{\delta_e}}, \text{ 1/sec}$$

$$M_q = \frac{\rho V S\bar{c}^2}{4I_{yy}} C_{m_q}, \text{ 1/sec}$$

$$M_v = \left[\frac{\rho V^2 S\bar{c}}{2I_{yy}} C_{m_M} M + C_{m_{C_T}} \frac{V\bar{c}}{I_{yy}} \left(\frac{\partial T}{\partial V} - 2 \frac{T}{V} \right) \right], \text{ 1/sec}$$

Δn = incremental change in normal load factor

$P_h = \partial\theta_{com}/\partial h$, rad/ft

$P_{\dot{h}} = \partial\theta_{com}/\partial\dot{h}$, rad/(ft/sec)

q = pitch rate, rad/sec

q_g = equivalent aerodynamic pitch rate due to vertical gust penetration, rad/sec

S = wing area, ft^2

T = total engine thrust, lbs

t = time, sec

$T_v = \partial\delta_T/\partial v$, rad

$T_{\dot{v}} = \partial\delta_T/\partial\dot{v}$, rad-sec

$T_h = \partial\delta_T/\partial h$, rad/ft

$T_{\dot{h}} = \partial\delta_T/\partial\dot{h}$, rad/(ft/sec)

V = true airspeed, ft/sec

V_g = gust velocity relative to inertial reference, ft/sec

V_{g_h} = horizontal component of gust velocity, ft/sec

V_{g_v} = vertical component of gust velocity, ft/sec

V_i = inertial velocity, ft/sec

v = normalized airspeed = $\frac{\Delta V}{V}$

W = aircraft weight, lbs

$X_\alpha = \left[\frac{g}{V} - \frac{\rho VS}{2m} C_{D_\alpha}\right]$, 1/sec

$X_{\delta_e} = \left[-\frac{\rho VS}{2m} C_{D_{\delta_e}}\right]$, 1/sec

$$X_T = \frac{\rho VS}{2m}, \text{ 1/sec}$$

$$X_\theta = -\frac{g}{V}, \text{ 1/sec}$$

$$X_v = \left[\frac{1}{m}\left(\frac{\partial T}{\partial V} - 2\frac{T}{V}\right) - C_{D_M}\right], \text{ 1/sec}$$

$$Z_\alpha = -\frac{\rho VS}{2m} C_{L_\alpha}, \text{ 1/sec}$$

$$Z_{\delta_e} = -\frac{\rho VS}{2m} C_{L_{\delta_e}}, \text{ 1/sec}$$

$$Z_q = \left[1 - \frac{\rho VS}{2m} C_{L_q}\left(\frac{\bar{c}}{2V}\right)\right], \text{ 1/sec}$$

$$Z_v = \left[-\frac{2g}{V} - \frac{\rho VS}{2m} C_{L_M}\right], \text{ 1/sec}$$

α = angle of attack, rad.

β = exponential factor in atmospheric density equation, 1/ft

δ_e = elevator deflection from trim, rad.

δ_T = throttle deflection from trim setting, rad.

η = transfer function approximation to Kussner function

θ = pitch attitude, rad.

θ_{com} = commanded pitch attitude, rad.

λ = Laplace operator, 1/sec

ρ = atmospheric density, slugs/ft^3

τ_T = time constant of engine, sec

ω = temporal frequency, rad/sec

The subscripts x and z refer to standard NACA body-fixed reference axes.

Aircraft Equations of Motion

The development of the basic aircraft equations of motion follows standard techniques and is outlined below.

If an earth-fixed reference system is assumed to constitute an inertial reference, the inertial velocity of the aircraft's center of gravity is the vector sum of its aerodynamic velocity and the instantaneous velocity of the air mass.

$$\bar{V}_i = \bar{V} + \bar{V}_g$$

In the inertial reference frame, Newtonian mechanics states that,

$$\bar{F} = m \dot{\bar{V}}_i \tag{A-1}$$

where $\bar{F}$ is the total applied external force vector, composed of aerodynamic, thrust, and gravity force components.

In a conventional body axes system constrainted to rotate in pitch with the aircraft, the time derivative of inertial velocity becomes,

$$\dot{\bar{V}}_i = \left[\dot{V}_x + \dot{V}_{g_x} + q\left(V_z + V_{g_z}\right)\right]\bar{i} + \left[\dot{V}_z + \dot{V}_{g_z} - q\left(V_x + V_{g_x}\right)\right]\bar{k} \tag{A-2}$$

The force vector, $\bar{F}$, of Equation (A-1) is assumed to be composed of a lift force, acting normal to the aerodynamic velocity vector; drag and thrust forces acting parallel to the aerodynamic velocity vector; and a weight force acting downward. The components of this force are:

$$\begin{aligned} F_x &= \frac{\rho V S}{2}\left(C_L V_z - C_D V_x + C_T V_x\right) - mg \sin\theta \\ F_z &= \frac{\rho V S}{2}\left(-C_L V_x - C_D V_z + C_T V_z\right) + mg \cos\theta \end{aligned} \tag{A-3}$$

The horizontal and vertical gust velocity components are transformed into body axis components through the transformation,

$$V_{g_x} = V_{g_h} \cos\theta + V_{g_v} \sin\theta$$

$$V_{g_z} = V_{g_h} \sin\theta - V_{g_v} \cos\theta \qquad \text{(A-4)}$$

Equation (A-1) then can be written as,

$$\frac{\dot{V}}{V} \cos\alpha - \dot{\alpha} \sin\alpha = \frac{\rho VS}{2m}\left[C_L \sin\alpha - C_D \cos\alpha + C_T \cos\alpha\right] - \frac{g}{V} \sin\theta - \frac{\dot{V}_{g_h}}{V} \cos\theta - \frac{\dot{V}_{g_v}}{V} \sin\theta - q \sin\alpha \qquad \text{(A-5)}$$

$$\frac{\dot{V}}{V} \sin\alpha + \dot{\alpha} \cos\alpha = \frac{\rho VS}{2m}\left[- C_L \cos\alpha - C_D \sin\alpha + C_T \sin\alpha\right] + \frac{g}{V} \cos\theta - \frac{\dot{V}_{g_h}}{V} \sin\theta + \frac{\dot{V}_{g_v}}{V} \cos\theta + q \cos\alpha$$

In Equation (A-5), the angle of attack, α, is defined by,

$$\frac{V_x}{V} = \cos\alpha$$

$$\frac{V_z}{V} = \sin\alpha \qquad \text{(A-6)}$$

Equation (A-5) is then linearized about straight and level flight.

$$\dot{v} = \left(\frac{\rho VS}{2m}\right)_o \left[C_T - C_D\right] + \frac{g}{V_o}\alpha - \frac{g}{V_o}\theta - \frac{\dot{V}_{g_h}}{V_o}$$

$$\dot{\alpha} = \left(-\frac{\rho VS}{2m}\right)_o C_L - \frac{g}{V_o}\frac{\rho}{\rho_o} + \frac{\dot{V}_{g_v}}{V_o} - \frac{2g}{V_o} v + q \qquad \text{(A-7)}$$

Here, the subscript "o" denotes equilibrium values, while the nonsubscripted variables are perturbations from the equilibrium state.

It is assumed that the lift, drag, and thrust coefficients can be expressed as functions of the following variables:

$$C_L = C_L\left(\alpha, \frac{q\bar{c}}{2V_o}, M, \delta_e\right)$$

$$C_D = C_D\left(\alpha, M, \delta_e\right) \qquad \text{(A-8)}$$

$$C_T = C_T\left(\delta_T, V, \rho\right)$$

The first two equations are expanded in a first order Taylor's series as,

$$C_L = C_{L_\alpha}\alpha + C_{L_q}\left(\frac{q\bar{c}}{2V_o}\right) + C_{L_M} M v + C_{L_{\delta_e}}\delta_e$$

$$\qquad \text{(A-9)}$$

$$C_D = C_{D_\alpha}\alpha + C_{D_M} M v + C_{D_{\delta_e}}\delta_e$$

The total increment in thrust coefficient is considered to be made up of two parts:

$$(C_T)_1 = (C_T)_1 \delta_T$$

$$(C_T)_2 = \frac{\partial C_T}{\partial v} v + \frac{\partial C_T}{\partial \rho}\rho \qquad \text{(A-10)}$$

$(C_T)_1$ is the contribution of the throttle deflection, acting through the engine dynamics equation, A-18, which follows. $(C_T)_2$ on the other hand, is the increment in thrust coefficient which arises because of the functional dependence of the throttle-fixed engine thrust upon the airspeed and atmospheric density.

Since

$$C_T = \frac{2\Delta T}{\rho V^2 S},$$

$$(C_T)_2 = \left[\frac{2}{\rho_o V_o S}\left(\frac{\partial T}{\partial V} - 2\frac{T_o}{V_o}\right)\right] v + \left[\frac{C_{T_o}}{\rho_o}\right] \rho \qquad \text{(A-11)}$$

From the last equation, a simplification can be made if the assumption is made that thrust is directly proportional to atmospheric density, at constant thrust level setting. Since an idealized turbojet engine has these characteristics at altitudes above the tropopause, and it is nearly correct at other altitudes, we will invoke this assumption. So,

$$\frac{\partial C_T}{\partial \rho} = 0. \qquad \text{(A-12)}$$

Equation (A-10) then becomes,

$$C_T = (C_T)_1 + \frac{2}{\rho_o V_o S}\left[\frac{\partial T}{\partial V} - 2\frac{T_o}{V_o}\right] \qquad \text{(A-13)}$$

The atmospheric density can be related to altitude through the following relations:

Assume, $\rho' = \rho'_o e^{-\beta h'}$,

where ρ'_o is the density at the reference altitude from which h' is measured.

Then, $\frac{d\rho'}{dh'} = -\beta\rho'$.

So, the perturbation value of ρ caused by deviations from the reference altitude, h, is:

$$\frac{\rho}{\rho_o} = - \beta h \tag{A-14}$$

A constant value of $\beta = .0000362\ ft^{-1}$ is used throughout this study.

Substituting Equations (A-9), (A-13), and (A-14) into Equation (A-17) yields the final form of the linearized translational equations. The subscripts are dropped for clarity, but it is understood that quantities within the brackets are evaluated at the reference flight condition.

$$\begin{aligned} \dot{v} = &\left[\frac{g}{V} - \frac{\rho VS}{2m} C_{D_\alpha}\right] \alpha + \left[\frac{1}{m}\left(\frac{\partial T}{\partial V} - 2\frac{T}{V}\right) - C_{D_M} M\right] v + \left[-\frac{g}{V}\right] \theta \\ &+ \left[\frac{\rho VS}{2m}\right] \left(C_T\right)_1 + \left[-\frac{\rho VS}{2m} C_{D_{\delta_e}}\right] \delta_e + \left[-\frac{1}{V}\right] \dot{V}_{g_h} \\ \dot{\alpha} = &\left[-\frac{\rho VS}{2m} C_{L_\alpha}\right] \alpha + \left[-\frac{2g}{V} - \frac{\rho VS}{2m} C_{L_M} M\right] v + \left[1 - \frac{\rho VS}{2m} C_{L_q}\left(\frac{\bar{c}}{2V}\right)\right] q \\ &+ \left[-\frac{\rho VS}{2m} C_{L_{\delta_e}}\right] \delta_e + \left[\frac{g\theta}{V}\right] h + \left[\frac{1}{V}\right] \dot{V}_{g_v} \end{aligned} \tag{A-15}$$

Since the pitching axis is a principal axis, the pitching moment equation is simply,

$$I_{yy}\dot{q} = C_m \frac{\rho V^2 S\bar{c}}{2}$$

And, since $C_m = 0$ at equilibrium,

$$\dot{q} = \left[\frac{\rho V^2 S\bar{c}}{2I_{yy}}\right]_o C_m \tag{A-16}$$

Following Etkin[A-2], the vertical gust imposes an effective pitching rate equal to,

$$q_g = - \frac{\dot{V}_{g_v}}{V}$$

The total pitching moment coefficient is taken to be a function of the following variables,

$$C_m = C_m (\alpha, \dot{\alpha}, q, q_g, M, \delta_e, C_T).$$

The Taylor's series expansion is, then,

$$C_m = C_{m_\alpha} \alpha + C_{m_{\dot{\alpha}}} \left(\frac{\dot{\alpha}\bar{c}}{2V}\right) + C_{m_q} \left(\frac{q\bar{c}}{2V}\right) - C_{m_q} \frac{\bar{c}}{2V} \frac{\dot{V}_{g_v}}{V} + C_{m_M} Mv + C_{m_{\delta_e}} \delta_e + C_{m_{C_T}} C_T$$

From which, using Equation (A-13) and (A-16), the linearized pitching moment equation is,

$$\dot{q} = \left[\frac{\rho V^2 S\bar{c}}{2I_{yy}} C_{m_\alpha}\right] \alpha + \left[\frac{\rho V S\bar{c}^2}{4I_{yy}} C_{m_{\dot{\alpha}}}\right] \dot{\alpha} + \left[\frac{\rho V S\bar{c}^2}{4I_{yy}} C_{m_q}\right] q$$

$$+ \left[\frac{\rho V^2 S\bar{c}}{2I_{yy}} C_{m_{C_T}}\right] (C_T)_1 + \left[\frac{\rho V^2 S\bar{c}}{2I_{yy}} C_{m_{\delta_e}}\right] \delta_e + \left[- \frac{\rho V S\bar{c}^2}{4I_{yy}} \frac{C_{m_q}}{V}\right] \dot{V}_{g_v} \qquad \text{(A-17)}$$

$$+ \left[\frac{\rho V^2 S\bar{c}}{2I_{yy}} C_{m_M} M + C_{m_{C_T}} \frac{V\bar{c}}{I_{yy}} \left(\frac{\partial T}{\partial V} - 2 \frac{T}{V}\right)\right] v$$

Engine Dynamics

A second-order lag is assumed to represent the engine dynamic response to throttle deflections. The form of the transfer function relating thrust coefficient to throttle deflection is,

$$\frac{C_T}{\delta_T}(\lambda) = \frac{K_T}{(1 + \tau_T\lambda)\ (1 + 1.1\ \tau_T\lambda)}$$

The 1.1 factor is introduced to avoid possible mathematical difficulties with repeated roots during portions of the computation.

The engine transfer function can be expressed as the following second order differential equation,

$$\left(\ddot{C}_T\right)_1 = \left(\frac{K_T}{1.1\ \tau_T^2}\right)\delta_T - \left(\frac{1}{1.1\ \tau_T^2}\right)\left(C_T\right)_1 - \frac{2.1}{1.1\ \tau_T}\left(\dot{C}_T\right)_1 \qquad \text{(A-18)}$$

A value of $\tau_T = 4$ seconds was used throughout this study.

Unsteady Aerodynamics Effects

The unsteady effects of the build-up of aerodynamic lift following penetration of a vertical gust were approximated by multiplying the vertical gust velocity forcing function terms by a transfer function which approximates the Kussner lift growth function.

The aircraft under consideration in this study all have swept wing planform, and no readily usable analytical approximations were found for the Kussner functions for such wings. As an expediency, the approximation given by Jones[A-3] for elliptical wings of aspect ration = 3 was used to represent the indicial response function for the higher aspect ratio, but swept, wings of concern in this study.

Jones' approximation to the lift build-up function, expressed in terms of time is,

$$\eta\ (t) = 1. - .679\ e^{-.558\left(\frac{2V}{\bar{c}}\right)t} - .227\ e^{-3.20\left(\frac{2V}{\bar{c}}\right)t}$$

The desired transfer function is then obtained by taking the Laplace transform of the time derivative of the indicial response.(A-2)

$$\eta(\lambda) = \left[1 - \frac{.679\ \lambda}{\lambda + .558\left(\frac{2V}{\bar{c}}\right)} - \frac{.227\ \lambda}{\lambda + 3.20\left(\frac{2V}{\bar{c}}\right)}\right] \tag{A-19}$$

Feedback Control Equations

The control system equations involved only pure gain feedbacks with no equalization. In addition, sensor and actuator dynamics were ignored. The elevator control equation used was

$$\delta_e = K_v\, v + K_\alpha\, \alpha + K_{\dot{v}}\left(\dot{v} + \dot{v}_{g_h}\right) + K_q\, q + K_\theta\left(\theta - \theta_{com}\right) \tag{A-20}$$

This equation could be used to approximate different stabilization, flight director, and autopilot modes. For example, the first two terms could be used to represent a simple flight director scheme employing only velocity and angle of attack information. A system, such as SCAT, based upon angle of attack and inertial acceleration feedback could be approximated by using the second and third terms. A conventional pitch autopilot would be approximated by using the last two terms.

An altitude control system operating through the elevator channel of a pitch autopilot was simulated by generating a pitch angle command as a function of altitude and altitude rate information. The following equation was used.

$$\theta_{com} = P_{\dot{h}}\, \dot{h} + P_h\, h \tag{A-21}$$

The throttle control system used pure gain feedbacks of airspeed and altitude signals and their rates as described by the following equation

$$\delta_T = T_{\dot{v}}\, \dot{v} + T_v\, v + T_{\dot{h}}\, \dot{h} + T_h\, h \tag{A-22}$$

Complete Dynamic Model

Equations (A-15), (A-17), (A-18), (A-20), (A-21), (A-22), and an additional equation relating altitude deviations to other perturbation variables, define the complete system which can be written in matrix form as:

$$[A] \begin{Bmatrix} v \\ \alpha \\ \theta \\ (C_T)_1 \\ h \\ \delta_e \\ \delta_t \\ \theta_{com} \end{Bmatrix} = \begin{bmatrix} \frac{\lambda}{V} \\ 0 \\ 0 \\ 0 \\ 0 \\ -K_v \frac{\lambda}{V} \\ 0 \\ 0 \end{bmatrix} V_{g_h} + \begin{bmatrix} 0 \\ -\frac{\lambda}{V}\eta(\lambda) \\ M_q \frac{\lambda}{V}\eta(\lambda) \\ 0 \\ -1 \\ 0 \\ 0 \\ 0 \end{bmatrix} V_{g_v} \qquad \text{(A-23)}$$

where the coefficient matrix [A] is shown on the following page.

Since the horizontal and vertical gust components are assumed to be uncorrelated, the responses to each component must be determined separately and combined only in the final statistical sense.

$$
\begin{bmatrix}
(\lambda + X_v) & X_\alpha & X_\theta & X_T & 0 & X_{\delta_e} & 0 & 0 \\
Z_v & (-\lambda + Z_\alpha) & Z_q\lambda & 0 & \frac{g}{V}\beta & Z_{\delta_e} & 0 & 0 \\
M_v & (M_{\dot{\alpha}}\lambda + M_\alpha) & (-\lambda^2 + M_q\lambda) & M_{C_T} & 0 & M_{\delta_e} & 0 & 0 \\
0 & 0 & 0 & \left(\lambda^2 + \frac{2.1}{1.1\tau_t}\lambda + \frac{1}{1.1\tau_T{}^2}\right) & 0 & 0 & \frac{K_T}{1.1\tau_T{}^2} & 0 \\
0 & -V & V & 0 & -\lambda & 0 & 0 & 0 \\
K_{\dot{v}}\lambda + K_v & K_\alpha & (K_q\lambda + K_\theta) & 0 & 0 & -1 & 0 & -K_\theta \\
T_{\dot{v}}\lambda + T_v & 0 & 0 & 0 & (T_{\dot{h}}\lambda + T_h) & 0 & -1 & 0 \\
0 & 0 & 0 & 0 & (P_{\dot{h}}\lambda + P_h) & 0 & 0 & -1
\end{bmatrix} \qquad \text{(A-24)}
$$

Expressions for each of the transfer functions of interest can be developed using standard techniques. For example, the transfer function relating pitch angle to horizontal gusts is,

$$
\frac{\theta}{V_{g_h}}(\lambda) = \frac{|[A']|\ (\lambda)}{|[A]|\ (\lambda)} \qquad \text{(A-25)}
$$

Where $|[A']|$ is the determinant of the matrix obtained by substituting the first column matrix on the right side of Equation (A-23) for the third column of the matrix [A].

Expressions for any of the other transfer functions of interest are obtained in a similar fashion, and by noting that;

$$
\frac{q}{V_g}(\lambda) = \lambda \frac{\theta}{V_g}(\lambda) \ .
$$

Because of the algebraic complexity of the transfer functions, no analytical derivations of these expressions were performed. Instead, the determinants of the respective matrices for the numerators and the denominator were expressed in polynomials in the operator, λ, by purely numerical means.

The polynomial expansions were obtained as follows, using the determinant of the coefficient matrix as an example. For each arbitrary value of λ substituted into Equation (A-24), a unique value of the determinant of the matrix was found using a standard computer library subroutine for determinant expansion. Furthermore, an examination of the [A] matrix shows that it is of 7th order, so there will be eight coefficients in the characteristic polynomial. If eight arbitrary, but different, values of λ are used to obtain eight values of the determinant, a set of eight linear simultaneous algebraic equations can be formed to solve for the coefficients of the characteristic polynomial.

The technique described above was employed for the numerators and the denominator of each of the transfer functions. Then, setting $\lambda = j\omega$, the polynomial numerator and denominator were converted to the complex frequency response functions of interest.

The load factor frequency response functions can be derived from the angle of attack and velocity functions as follows.

Defining the increment in load factor at the c.g. as,

$$\Delta n = \frac{\Delta L}{W}$$

Then,

$$\frac{\Delta L}{W} = \left(\frac{C_{L_\alpha}}{C_L}\right) \alpha + 2 \frac{dV}{V} \qquad \text{(A-26)}$$

$$\Delta n = \frac{Z_\alpha}{X_\theta} \alpha + 2v \quad .$$

This is a simplified representation of the load factor response, in that lift contributions caused directly by pitching rate and elevator deflection have been ignored. On the other hand, these omitted components act primarily on the horizontal tail surface, so the simplified mechanization of the load factor equation used here is a reasonably valid indication of wing structural load.

So, for either gust component,

$$\frac{\Delta n}{V_g}(j\omega) = \left[\frac{Z_\alpha}{X_\theta}\right]\frac{\alpha}{V_g}(j\omega) + 2\frac{v}{V_g}(j\omega) \qquad \text{(A-27)}$$

Idealized Aircraft Equations

Equations (A-15) and (A-17) can be rewritten,

$$\dot{v} = \left[\frac{g}{V} - \frac{\rho VS}{2m} C_{D_\alpha}\right]\alpha + \left[\frac{1}{m}\frac{\partial T}{\partial V} - \frac{2}{(L/D)}\frac{g}{V} - C_{D_M} M\right] v + \left[-\frac{g}{V}\right]\theta + \left[\frac{\rho VS}{2m}\right]\left(C_T\right)_1$$

$$+ \left[-\frac{\rho VS}{2m} C_{D_{\delta_e}}\right]\delta_e + \left[-\frac{1}{V}\right]\dot{V}_{g_h}$$

$$\dot{\alpha} = \left[-\frac{\rho VS}{2m} C_{L_\alpha}\right]\alpha + \left[-\frac{2g}{V} - \frac{\rho VS}{2m} C_{L_M} M\right] v + \left[1 - \frac{\rho VS}{2m} C_{L_q}\left(\frac{\bar{c}}{2V}\right)\right] q \qquad \text{(A-28)}$$

$$+ \left[-\frac{\rho VS}{2m} C_{L_{\delta_e}}\right]\delta_e + \left[\frac{g\beta}{V}\right] h + \left[\frac{1}{V}\right]\dot{V}_{g_v}$$

$$\dot{q} = \frac{1}{2}\left(\frac{\rho VS}{2m}\right)\left(\frac{2V}{\bar{c}}\right)\left(\frac{\bar{c}}{k_y}\right)^2\left[C_{m_\alpha}\,\alpha + C_{m_{\delta_e}}\,\delta_e + C_{m_{C_T}}\left(C_T\right)_1\right] +$$

$$\left(\frac{2V}{\bar{c}}\right)\left(\frac{\bar{c}}{k_y}\right)^2\left[\frac{1}{2}\left(\frac{\rho VS}{2m}\right)C_{m_M}\,M + \left(\frac{1}{2}\frac{\partial T}{\partial V}\frac{1}{m} - \left(\frac{g}{V}\right)\frac{1}{(L/D)}\right)C_{m_{C_T}}\right]v +$$

$$\frac{1}{2}\left(\frac{\rho VS}{2m}\right)\left(\frac{\bar{c}}{k_y}\right)^2\left[C_{m_{\dot{\alpha}}}\,\dot{\alpha} + C_{m_q}\,q - \frac{C_{m_q}}{V}\dot{V}_{g_v}\right]$$

Six parameters, aside from the derivatives, appear explicitly in Equation (A-28). These are:

$$V,\ \left(\frac{2V}{\bar{c}}\right),\ \frac{\rho VS}{2m},\ \left(\frac{\bar{c}}{k_y}\right)^2,\ \frac{L}{D},\ \text{and } M.$$

At this point, an assumption can be made concerning the nondimensional derivatives. These derivatives are, in general, functions of Mach number, altitude, trim lift coefficent, and static margin. If static elastic deformation with altitude is eliminated by considering only the Mach number effects, and if the further assumption is made that the speed of sound is constant, then all nondimensional derivatives become functions of V, C_{L_o}, and static margin.

The lift-drag ration can be assumed, to a first approximation, to be a function of only the velocity and the trim lift coefficient:

$$\frac{L}{D} = f\left(C_{L_o}, V\right)$$

Furthermore, it is easily demonstrated that

$$\frac{\rho VS}{2m} = \frac{g}{VC_{L_o}}$$

so that C_{L_o} is uniquely established by the parameters V and $\frac{\rho VS}{2m}$ and, therefore, C_{L_o} is not needed as an additional parameter.

The variation of thrust with velocity, $\frac{\partial T}{\partial V}$, can also be eliminated as a separate parameter by noting that the equilibrium thrust is directly proportional to mass. The development is as follows:

For unaccelerated flight,

$$T = D = \frac{L}{(L/D)} = \frac{mg}{L/D}$$

so,

$$\frac{T}{M} = \frac{g}{L/D}$$

But, since L/D is uniquely defined by C_{L_o} and V,

$$\frac{T}{m} = f\left(C_{L_o}, V\right) \quad .$$

Since the characteristics of the idealized turbojet engine are such that $\frac{\partial T}{\partial V}$ is proportional to thrust at a given velocity, it follows that

$$\frac{\partial T}{\partial V}\frac{1}{m} = f\left(C_{L_o}, V\right)$$

At this point in the consideration of an idealized aircraft, five parameters are required to describe the aircraft. They are:

$$V, \frac{2V}{\bar{c}}, \frac{\rho VS}{2m}, \left(\frac{\bar{c}}{k_y}\right)^2 ,$$

and the static margin.

In Appendix B, the assumption is made that the pitch radius of gyration is directly proportional to chord length. As a consequence, $\frac{\bar{c}}{k_y}$ has a fixed value for the rubberized aircraft, irrespective of its size.

The number of parameters required to completely define the idealized aircraft then reduces to four. These are V, $\frac{2V}{\bar{c}}$, $\frac{\rho VS}{2m}$, and static margin.

References

A-1. Porter, R. F., "The Linearized Long-Period Longitudinal Modes of Aerospace Vehicles in Equilibrium Flight", Air Force Flight Test Center, TN 61-2, Edward Air Force Base, California, January, 1961.

A-2. Etkin, Bernard, "Dynamics of Flight", John Wiley and Sons, Inc., New York, 1959.

A-3. Jones, R. T., "The Unsteady Lift of a Wing of Finite Aspect Ratio", NACA Technical Report 681, 1940.

Appendix B

Aircraft Characteristics

Table of Contents

List of Figures

List of Figures (Continued)

Appendix B

Aircraft Characteristics

Introduction

The aircraft's aerodynamic and inertial characteristics, together with the trim flight condition and the flight control system modes are important primary variables in the study of turbulence-penetration performance. In modeling the aircraft, it is desirable that the model be as flexible as possible in terms of the number of parameters treated as variables. However, the necessity to limit the number of variables to a managable quantity is also recognized. In this Appendix, selected characteristics are presented together with the criteria used in selection. The material is divided into the areas of physical, aerodynamic, propulsion, and operational characteristics.

Nomenclature

a = speed of sound, ft/sec

$\bar{c}$ = mean aerodynamic chord length, ft

C_D = drag coefficient

$(C_D)_L$ = drag coefficient component varying with lift

$(C_o)_M$ = drag coefficient component varying with Mach Number

C_L = lift coefficient

C_{L_o} = lift coefficient ($\alpha = 0$)

C_{L_α} = $\partial C_L / \partial \alpha$

$C_{L_{\delta_e}}$ = $\partial C_L / \partial \delta_e$

C_m = pitching moment coefficient

C_{M_o} = pitching moment coefficient ($\alpha = 0$)

$C_{M_{X_{cg}}} = \partial C_M / \partial X_{cg}$

$C_{M_\alpha} = \partial C_M / \partial \alpha$

$C_{M_{\delta_e}} = \partial C_M / \partial \delta_e$

D = drag, lb

g = gravitational constant, ft/sec^2

I_{yy} = pitching moment of inertia, $slugs\text{-}ft^2$

K_1 = defined in Equation (B-1)

K_2 = defined in Equation (B-2)

L = lift, lbs

M = Mach Number

N_o = neutral point, see Equation (B-28)

Q = dynamic pressure, lb/ft^2

r = aircraft's pitch radius of gyration, ft

S = wing area, ft^2

T = total engine thrust, lbs

$\bar{T}$ = total engine thrust at sea level, standard atmospheric conditions, lbs

T_{s_t} = static thrust, lbs

V = velocity, ft/sec

W = aircraft weight, lbs

X_{cg} = center of gravity, see Equation (B-10)

α = angle of attack, rad

δ_e = tailplane incidence, rad

δ_{t_2} = pressure correction factor

θ = pitch attitude, rad

ρ = atmospheric density, slugs/ft^3

Physical Characteristics

The primary physical characteristic parameters of interest are wing mean aerodynamic chord length ($\bar{c}$), wing area (S), pitching moment of inertia (I_{yy}), and aircraft gross weight (W).

In an attempt to simplify the problem somewhat, it is assumed that while the aircraft's size would be allowed to vary, its basic geometry would remain fixed. Here geometry is construed to include such factors as fuselage slenderness ratio, wing aspect ratio, wing sweep, and the general attachment position of the wing to the fuselage. Having assumed this, other assumptions can be made with fair accuracy. First, given various aircraft physical sizes, wing area will vary proportionally with the square of the mean aerodynamic chord length. That is,

$$S = K_1 \bar{c}^2 \tag{B-1}$$

Second, the aircraft's radius of gyration (r) about the center of gravity will vary approximately linearly with mean aerodynamic chord length. Thus,

$$r = K_2 \bar{c} \tag{B-2}$$

This latter assumption is made recognizing that the distribution of airframe mass is far more influential in determining r than are the masses of fuel and payload which vary as gross weight varies.

Pitching moment of inertia is a function of radius of gyration, gross weight, and the gravitational constant (g), as follows:

$$I_{yy} = r^2 \frac{W}{g} \tag{B-3}$$

Combining (B-2) and (B-3) to eliminate r gives

$$I_{yy} = K_2^2 \, \bar{c}^2 \, \frac{W}{g} \tag{B-4}$$

A reference aircraft is chosen to evaluate the proportionality constants, K_1 and K_2. It is one of the first-generation type, four engine, turbojet-powered transports with a mean aerodynamic chord length of 20 feet and a wing area of 2400 square feet. A reasonable mid-range value for this aircraft's radius of gyration is 27 feet. Using these values in equations (B-1) and (B-2), the values of K_1 and K_2 are found to be 6.0 and 1.35, respectively. Thus, equations (B-1) and (B-4) can be rewritten as

$$S = 6\bar{c}^2 \tag{B-5}$$

$$I_{yy} = 22.6 \, W \tag{B-6}$$

It is convenient to specify the aircraft's wing loading (W/S) as a parameter, instead of the W and S individually. Equations (B-5) and (B-6) can be combined to yield

$$I_{yy} = 135.6\bar{c}^2 \left(\frac{W}{S}\right) \tag{B-6a}$$

Based on the foregoing material, the process of fully describing the aircraft's physical characteristics can be viewed as a three-step process;

(1) Size the aircraft by selecting $\bar{c}$,

(2) Specify the wing loading $\left(\frac{W}{S}\right)$, and

(3) Calculate the pitching moment of inertia (I_{yy}).

Aerodynamic Characteristics

The longitudinal aerodynamic characteristics are of interest in this study and include the lift, drag, and pitching moment coefficients and derivatives. The nondimensionalized characteristics of the reference aircraft mentioned earlier will be used. These are, to a good order of approximation, applicable to an aircraft with the same geometrical configuration, even though it may differ in physical size. The aerodynamic characteristics presented in the following paragraphs are limited to the configuration with flaps and

landing gear retracted. Also, unlike the derivations in Appendix A, they involve values as measured from a zero angle-of-attack condition, and not the trim flight angle-of-attack.

Lift Characteristics

The equation below illustrates the dependence of lift coefficient (C_L) on aircraft angle of attack (α), and tailplane incidence (δ_e).

$$C_L = C_{L_o} + C_{L_\alpha} \cdot \alpha + C_{L_{\delta_e}} (\delta_e - \delta_{e_{ref}}) \qquad \text{(B-7)}$$

Here, $\delta_{e_{ref}}$ is a reference tailplane incidence of -4 degrees. Static airframe elasticity, and compressibility effects on C_L are accounted for by the fact that C_{L_o}, C_{L_α}, and $C_{L_{\delta_e}}$ are, in turn functions of flight Mach number (M), and flight altitude (h).

Figures B-1 through B-3 present the values of C_{L_o}, C_{L_α}, and $C_{L_{\delta_e}}$, respectively, as a function of Mach number and several flight altitudes.

Figure B-4 shows the aircraft's buffet boundary limit representing the limit C_L value as a function of Mach number. The dashed curve is a section of an ellipse approximating the boundary and will be used in generating the vehicle's flight envelopes, presented later in this Appendix, and the turbulence-penetration-constraint boundaries, discussed in Appendix C.

Drag Characteristics

The drag coefficient can be expressed in terms of incompressible drag, $(C_D)_L$ which varies with lift, and the drag rise due to Mach number, $(C_D)_M$.

$$C_D = (C_D)_L + (C_D)_M \qquad \text{(B-8)}$$

Figures B-5 and B-6 shows the variations of $(C_D)_L$ and $(C_D)_M$ with respect to C_L and M, respectively.

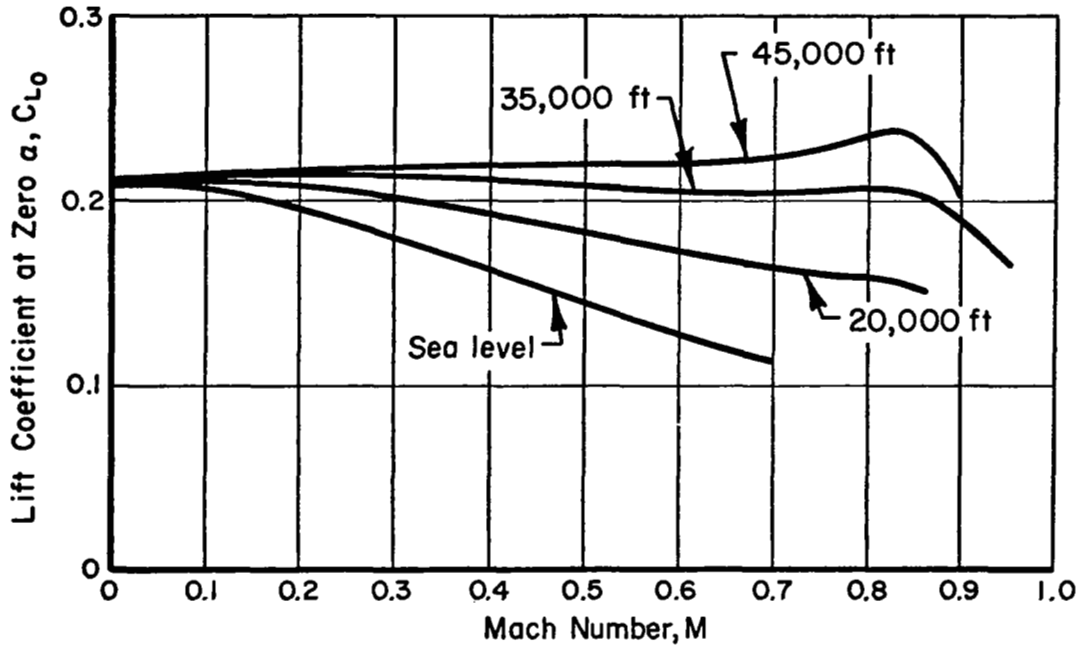

FIGURE B-1. VARIATION OF C_{L_O} WITH MACH NUMBER AND ALTITUDE

In addition to the basic drag coefficient, its rate of change relative to changes in both angle of attack and Mach number are of interest in studying the aircraft's dynamic response. The first of these derivatives, $\frac{\partial}{\partial\alpha}(C_D)_L$, is given by the following expression.

$$\frac{\partial}{\partial\alpha}(C_D)_L = \frac{\partial}{\partial C_L}(C_D)_L \cdot C_{L_\alpha} \qquad \text{(B-9)}$$

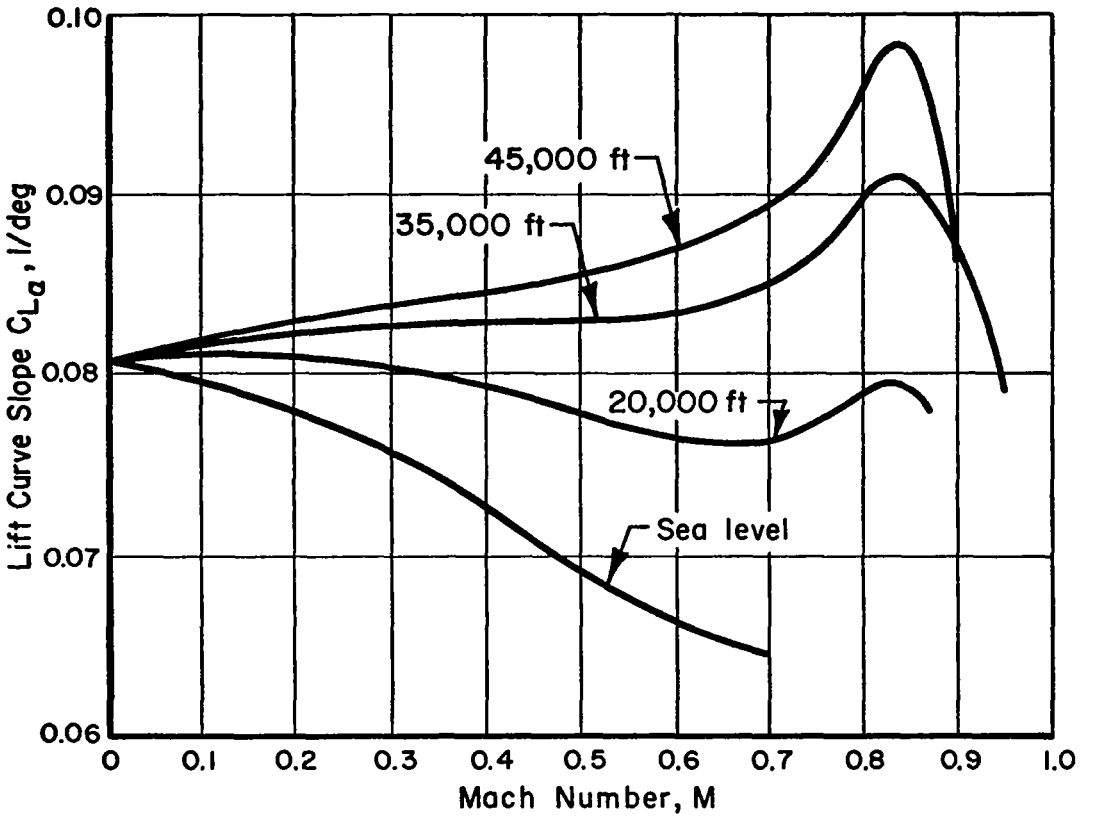

FIGURE B-2. VARIATION OF C_{L_α} WITH MACH NUMBER AND ALTITUDE

The data in Figure B-5 are used to obtain the characteristics of $\frac{\partial}{\partial \alpha} (C_D)_L$ for various values of C_L and C_{L_α}. The derivative $\frac{\partial}{\partial M} (C_D)_M$ is evaluated from the data presented in Figure B-6.

Figures B-7 and B-8 provide data on the derivatives $\frac{\partial}{\partial \alpha} (C_D)_L$ and $\frac{\partial}{\partial M} (C_D)_M$, respectively.

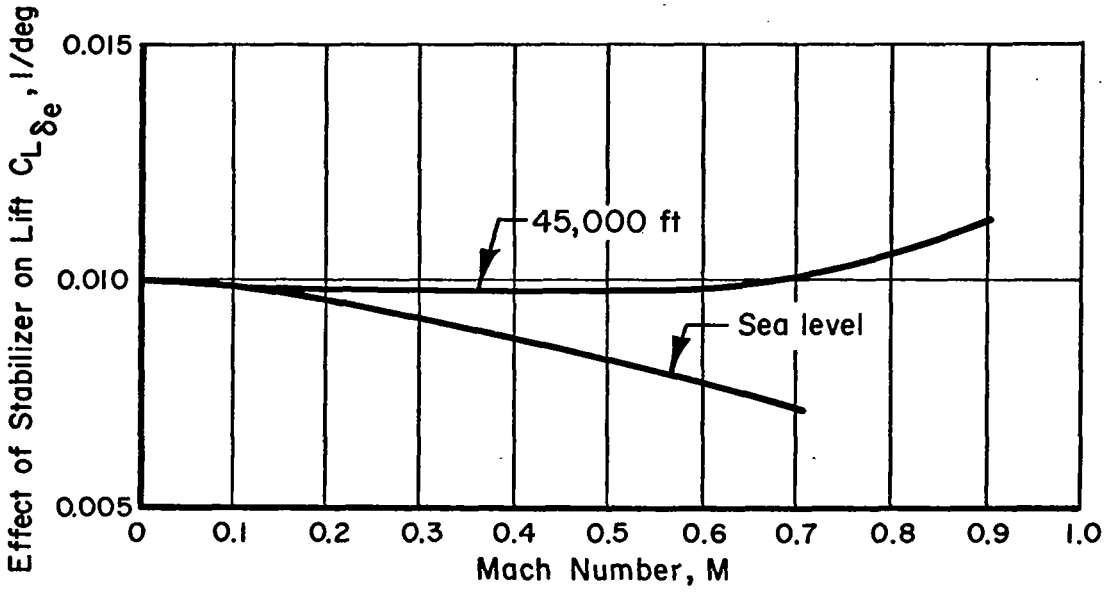

FIGURE B-3. VARIATION OF $C_{L_{\delta e}}$ WITH MACH NUMBER AND ALTITUDE

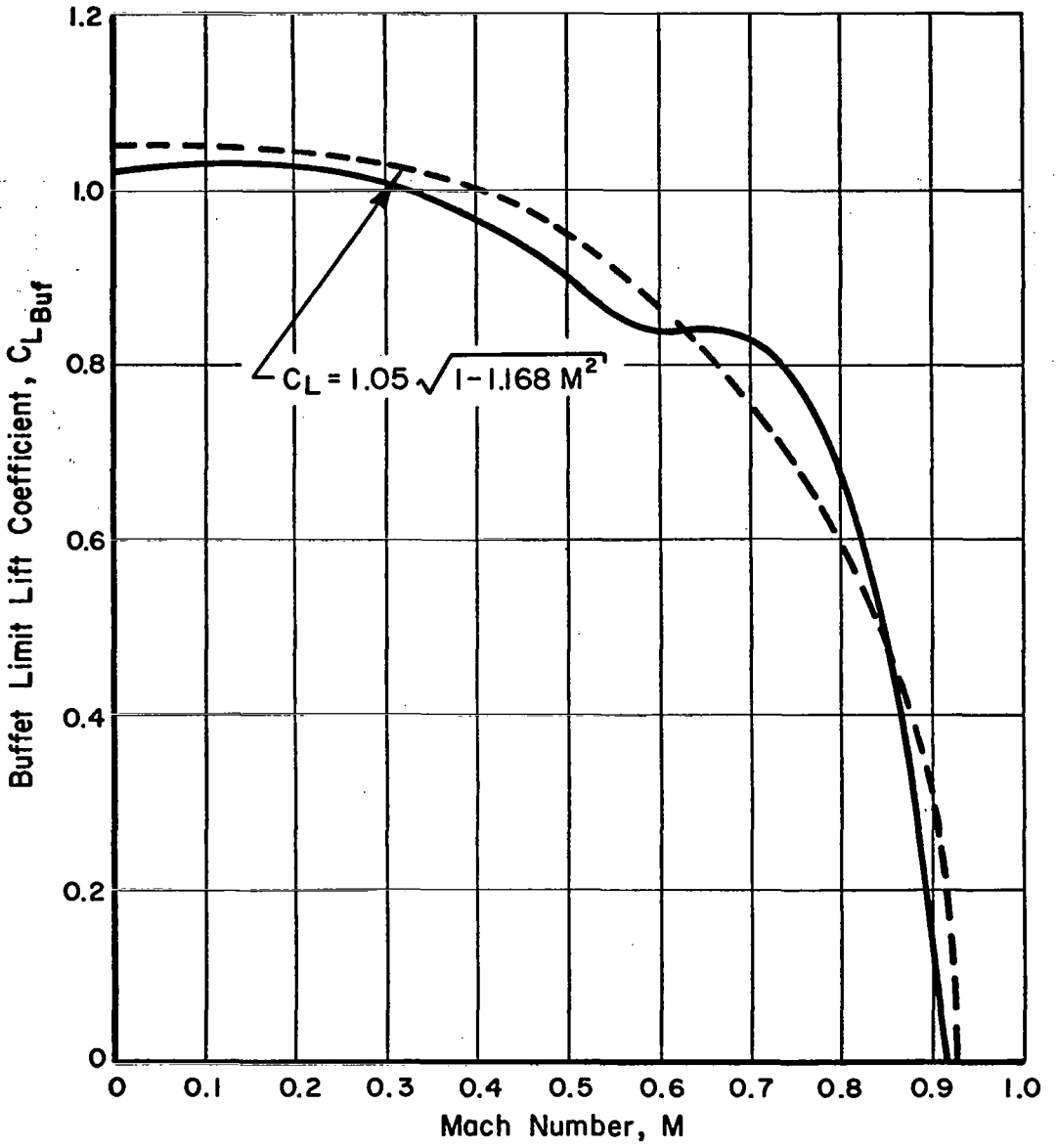

FIGURE B-4. BUFFET LIMIT LIFT COEFFICIENT VERSUS MACH NUMBER

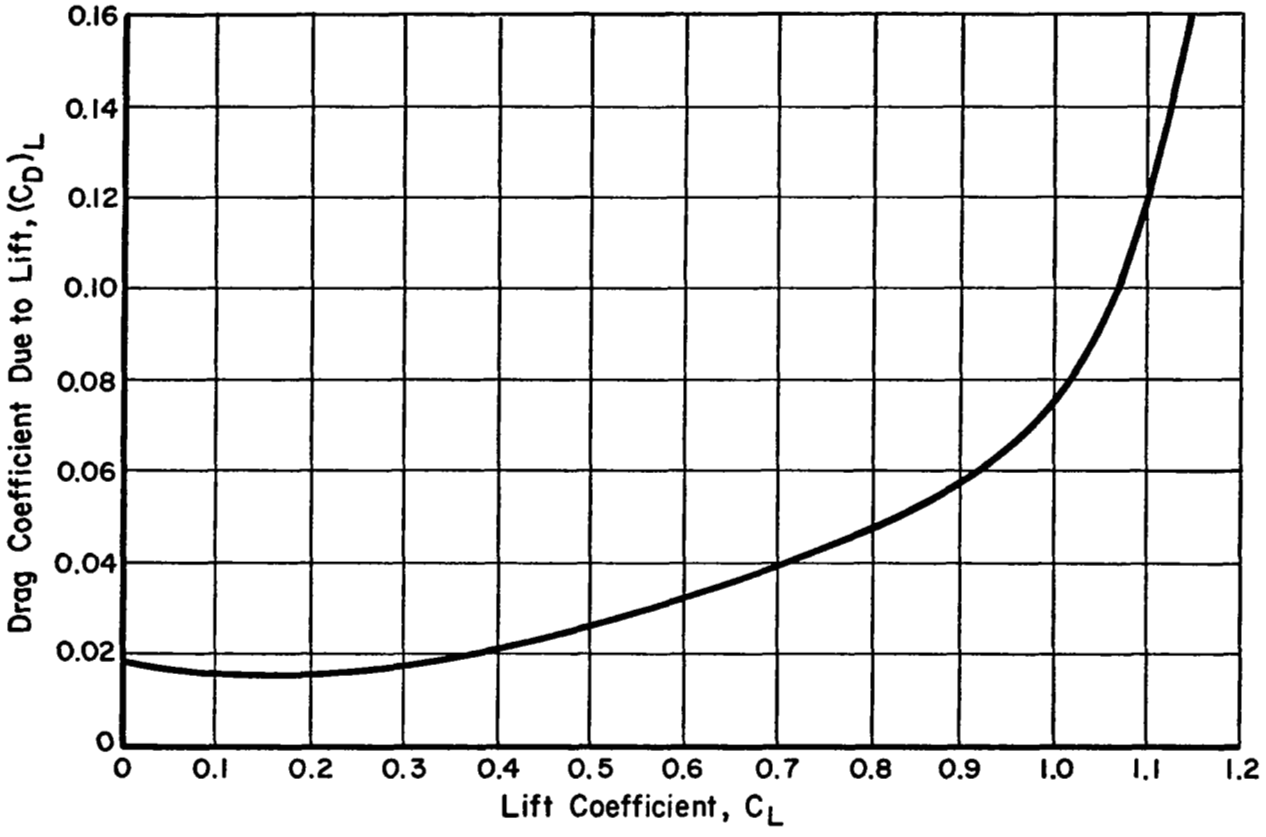

FIGURE B-5. DRAG COEFFICIENT DUE TO LIFT

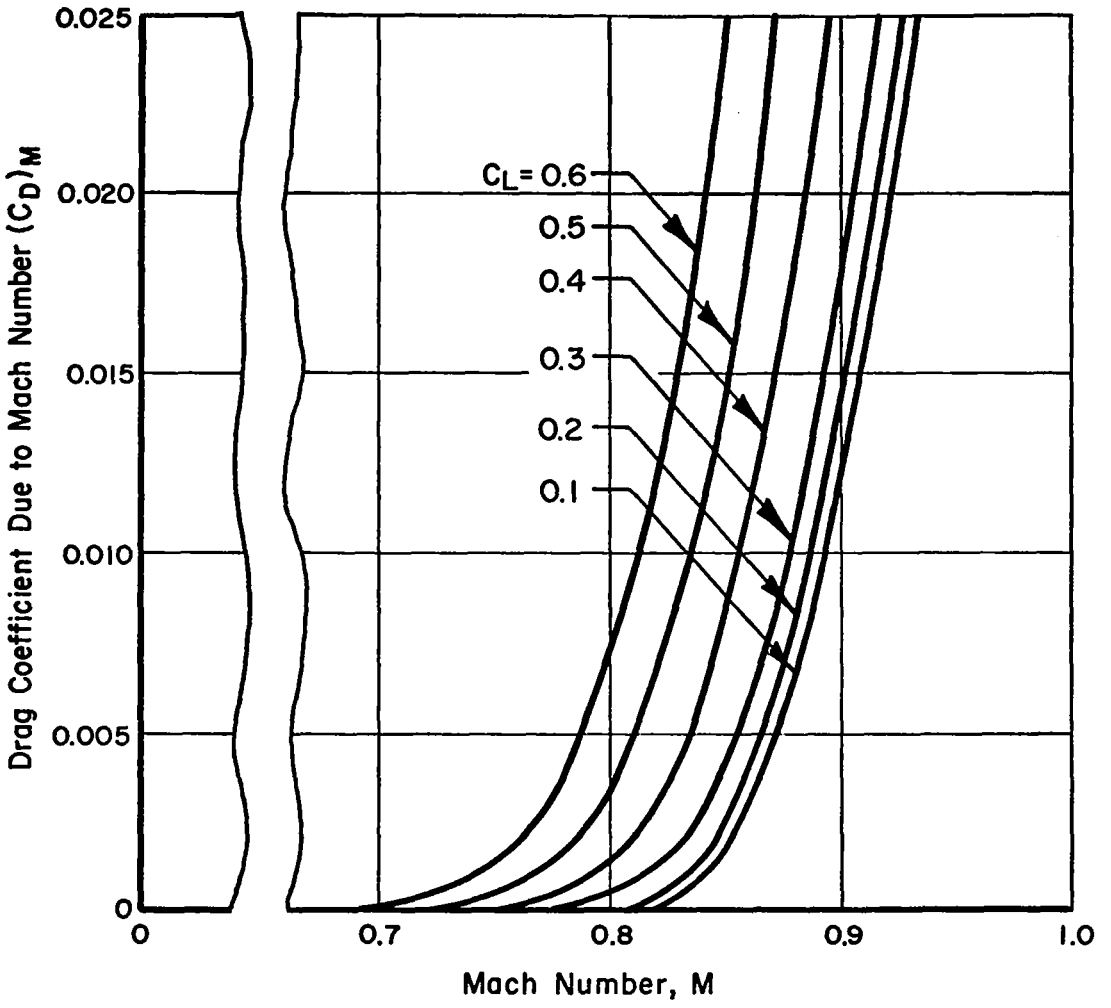

FIGURE B-6. DRAG COEFFICIENT DUE TO MACH NUMBER

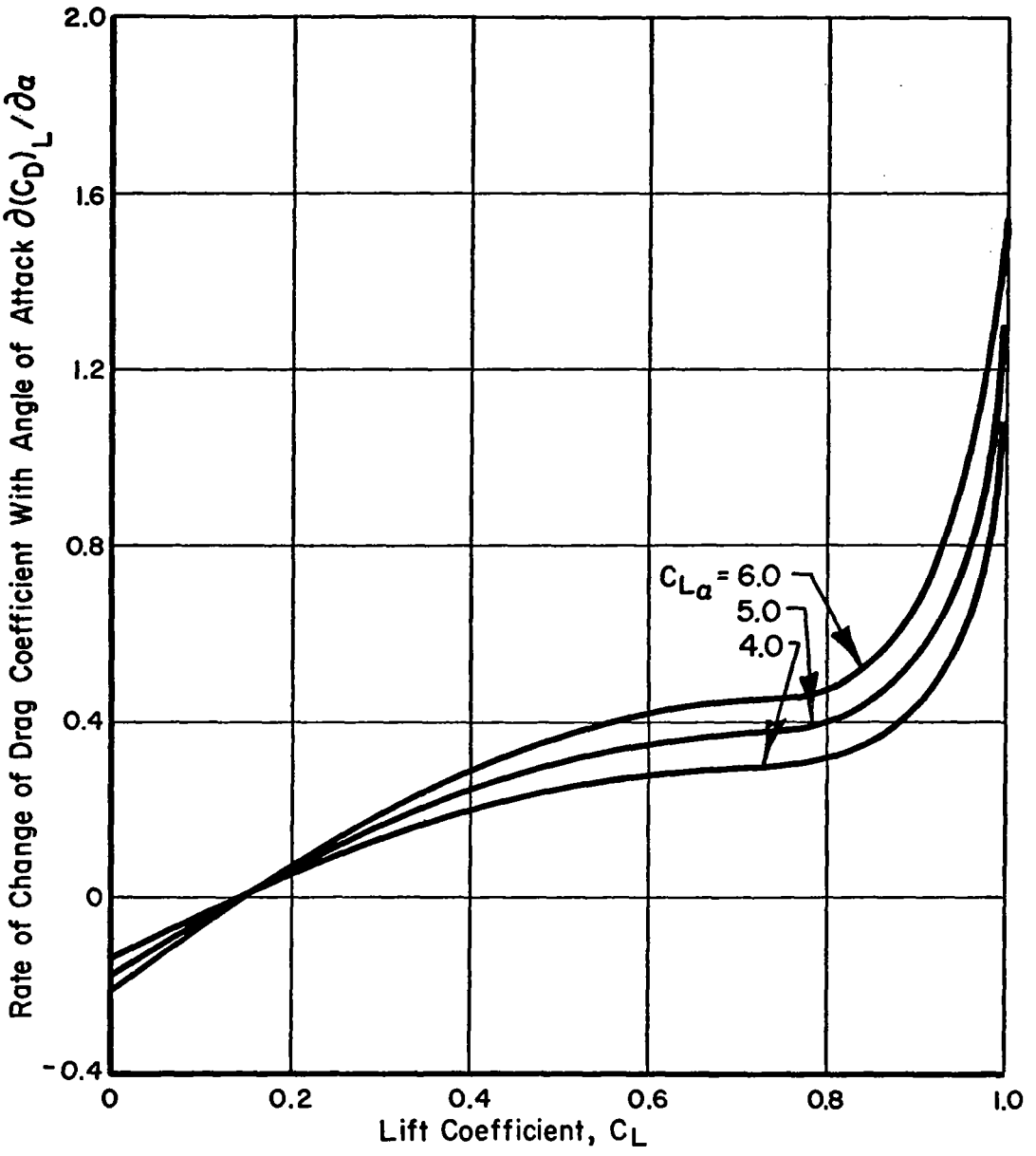

FIGURE B-7 VARIATION OF $\partial(C_D)_L/\partial\alpha$ WITH LIFT COEFFICIENT AND LIFT CURVE SLOPE

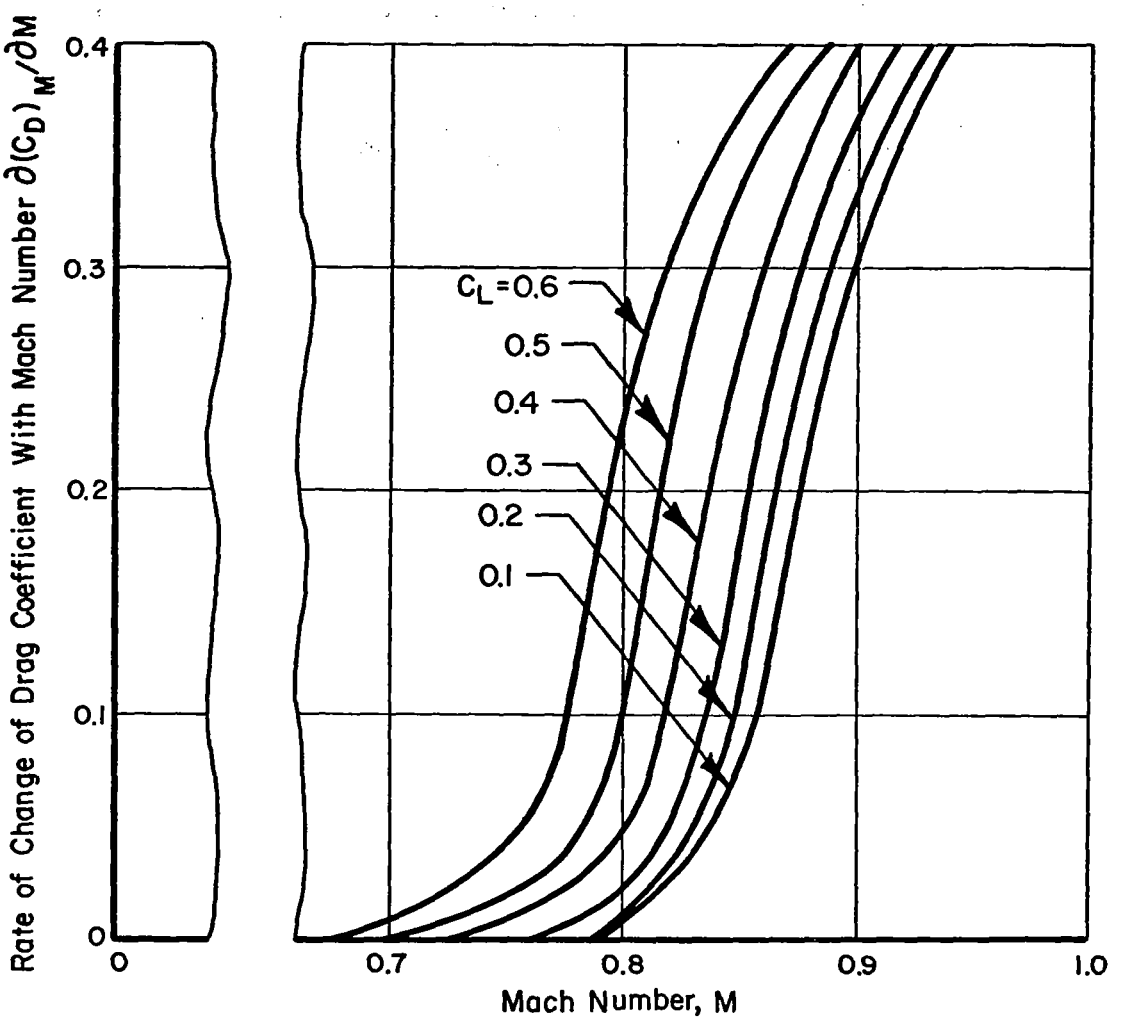

FIGURE B-8. VARIATION OF $\partial (C_D)_M / \partial M$ WITH LIFT COEFFICIENT AND MACH NUMBER

Pitching Moment Characteristics

An expression for the pitching moment coefficient is given as

$$C_m = C_{m_o} + \left(C_{m_\alpha}\right)_{ref} \cdot \alpha + C_{m_{\delta_e}} (\delta_e - \delta_{e_{ref}}) + C_{m_{X_{cg}}} (X_{cg} - X_{cg_{ref}})$$

$$+ \frac{\partial\left(C_{m_\alpha}\right)_{ref}}{\partial X_{cg}} (X_{cg} - X_{cg_{ref}})\, \alpha + \frac{\partial Cm}{\partial(\bar{c}\dot{\alpha}/2V)}\, \dot{\alpha} + \frac{\partial Cm}{\partial(\bar{c}\dot{\theta}/2V)}\, \dot{\theta} \qquad \text{(B-10)}$$

In this equation, X_{cg} is the ratio of the center of gravity distance forward of the 0.25 MAC position, to the length of the mean aerodynamic chord. Thus, $X_{cg_{ref}} = 0.25$. The value of $(C_{m_\alpha})_{ref}$ is referenced to the condition where X_{cg} equals $X_{cg_{ref}}$. The effects of airframe static elasticity and compressibility on C_m are reflected in the derivatives of Equation (B-10), all of which vary with flight Mach number and altitude.

Figures B-9 through B-13 give the characteristics of C_{m_o}, $(C_{m_\alpha})_{ref}$, $C_{m_{\delta_e}}$, $C_{m_{X_{cg}}}$, and $\dfrac{\partial(C_{m_\alpha})_{ref}}{\partial X_{cg}}$ as a function of M and h.

Figures B-14 and B-15 present data on the variation of C_m with angle of attack rate ($\dot{\alpha}$) and pitching rate ($\dot{\theta}$).

Propulsion Characteristics

In this study involving aircraft dynamic response in turbulence, no specific attempt is made to characterize the thrust capacity of the vehicle's engines. That is, having selected a vehicle configuration and flight condition, it is assumed that the necessary thrust for level flight is available. For equilibrium flight, the following two expressions are applicable:

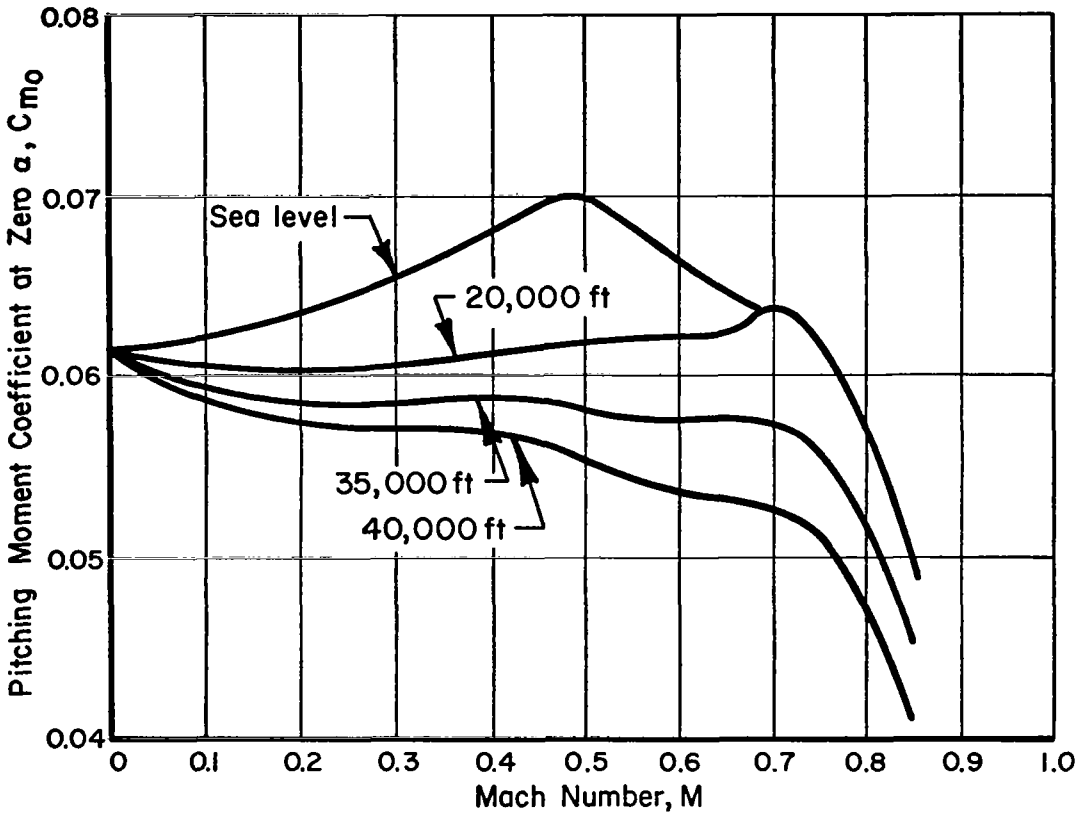

FIGURE B-9. VARIATION OF C_{m_0} WITH MACH NUMBER AND ALTITUDE

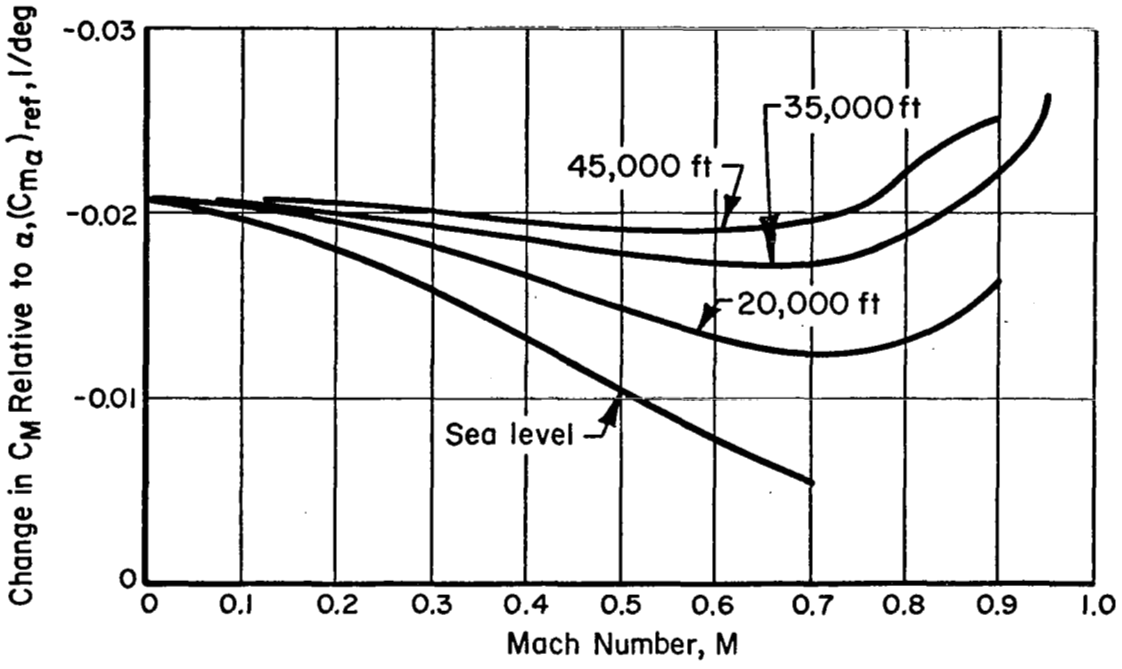

FIGURE B-10. VARIATION OF $(C_{m_\alpha})_{ref}$ WITH MACH NUMBER AND ALTITUDE

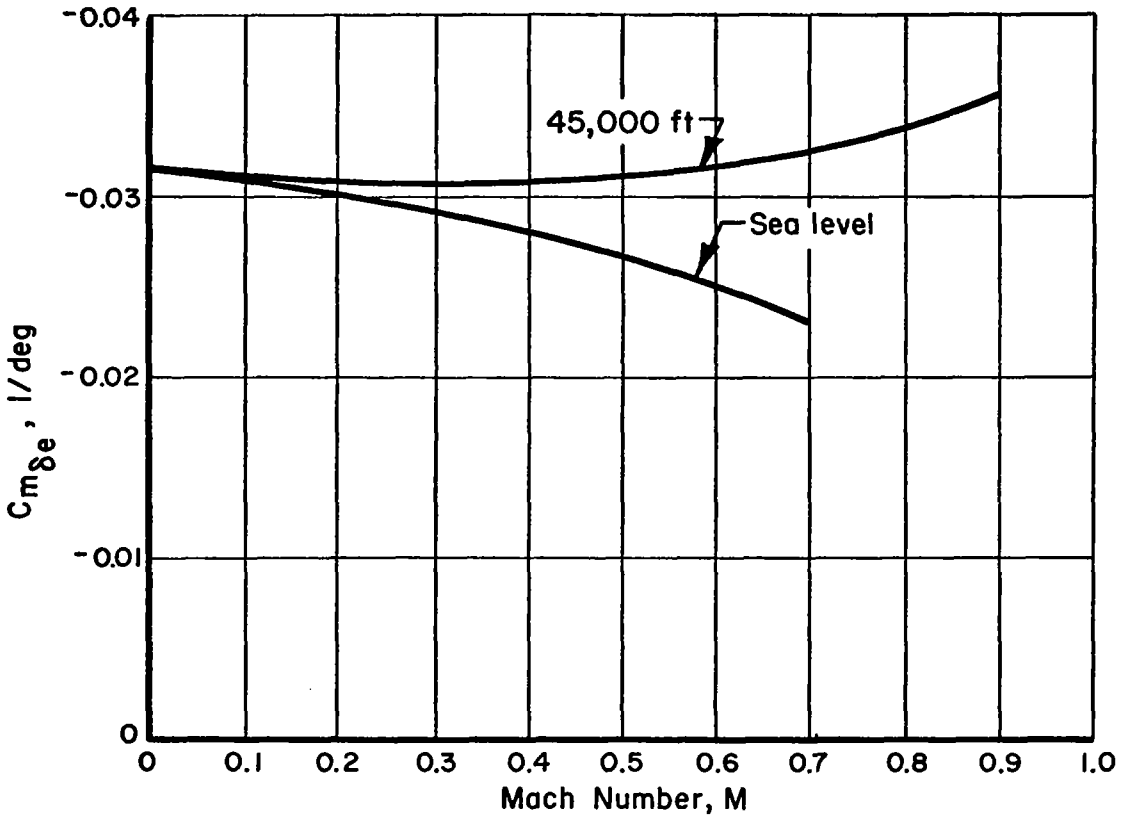

FIGURE B-11. VARIATION OF $C_{m_{\delta e}}$ WITH MACH NUMBER AND ALTITUDE

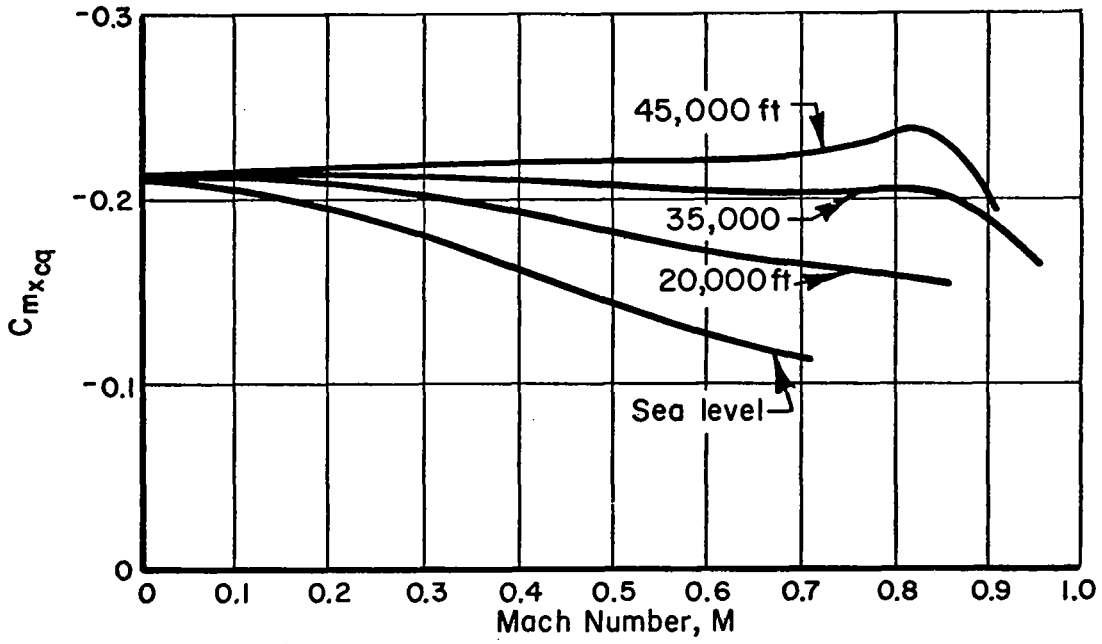

FIGURE B-12. VARIATION OF $C_{m_{xcq}}$ WITH MACH NUMBER AND ALTITUDE

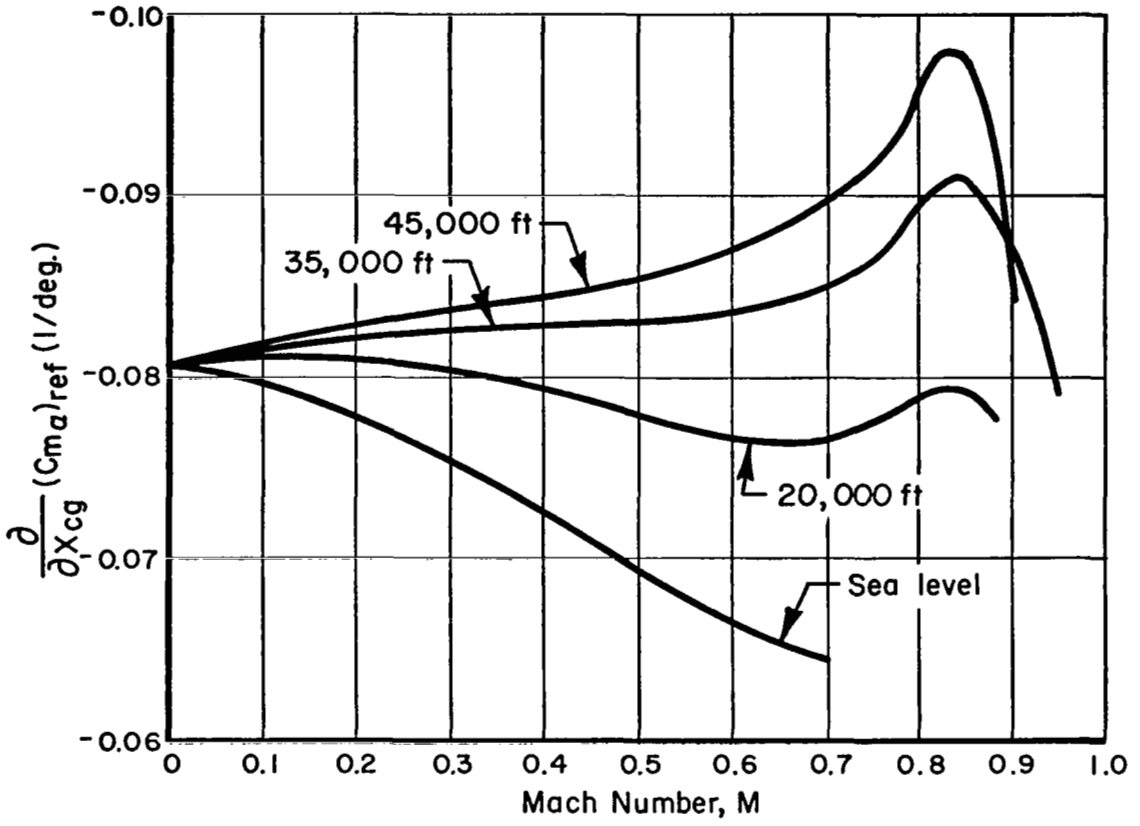

FIGURE B-13. VARIATION OF $\partial(C_{m_\alpha})_{ref}/\partial X_{cg}$ WITH MACH NUMBER AND ALTITUDE

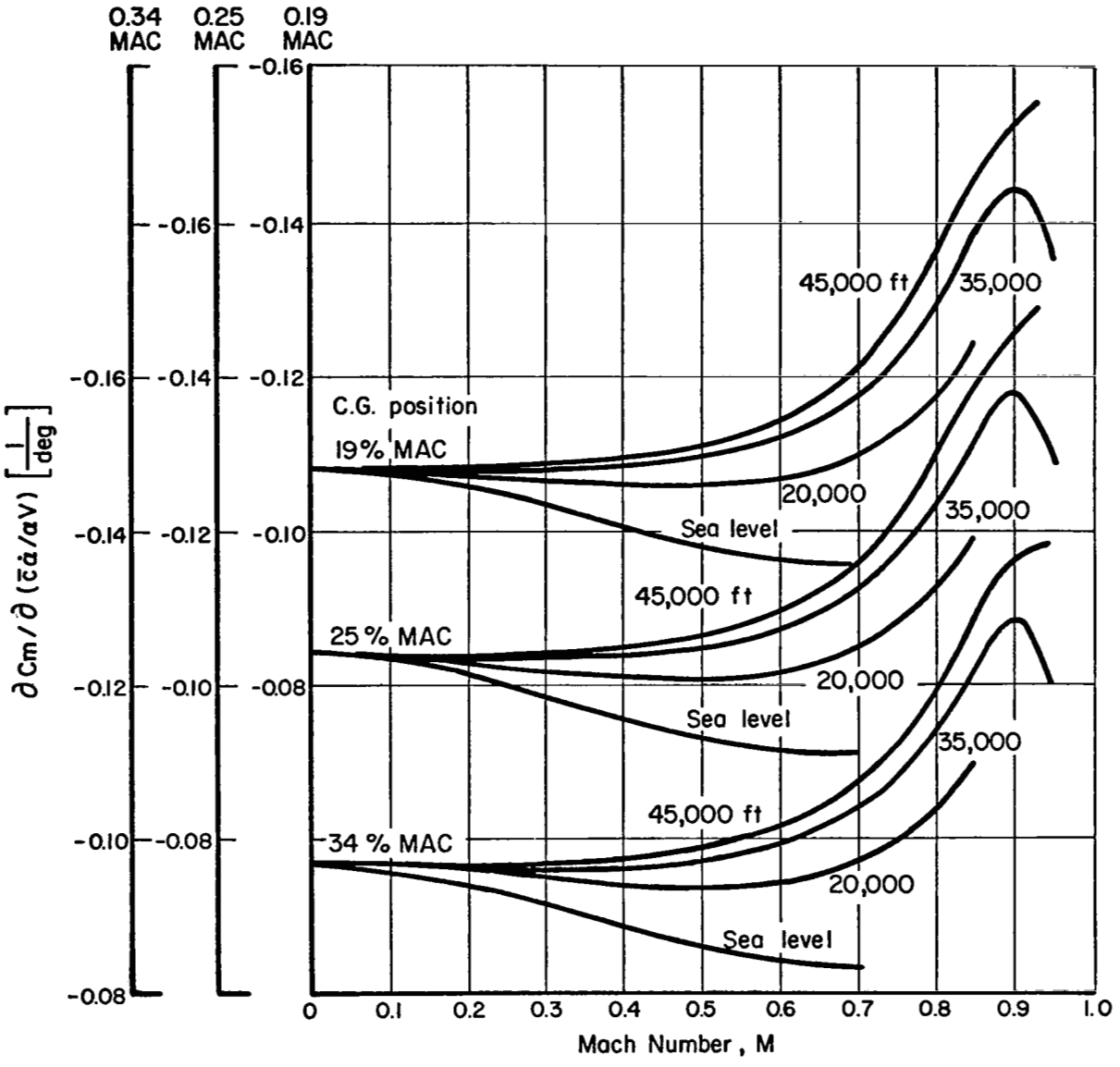

FIGURE B-14. VARIATION OF $\partial Cm/\partial(\bar{c}\dot{\alpha}/2V)$ WITH MACH NUMBER, ALTITUDE, AND C.G. POSITION

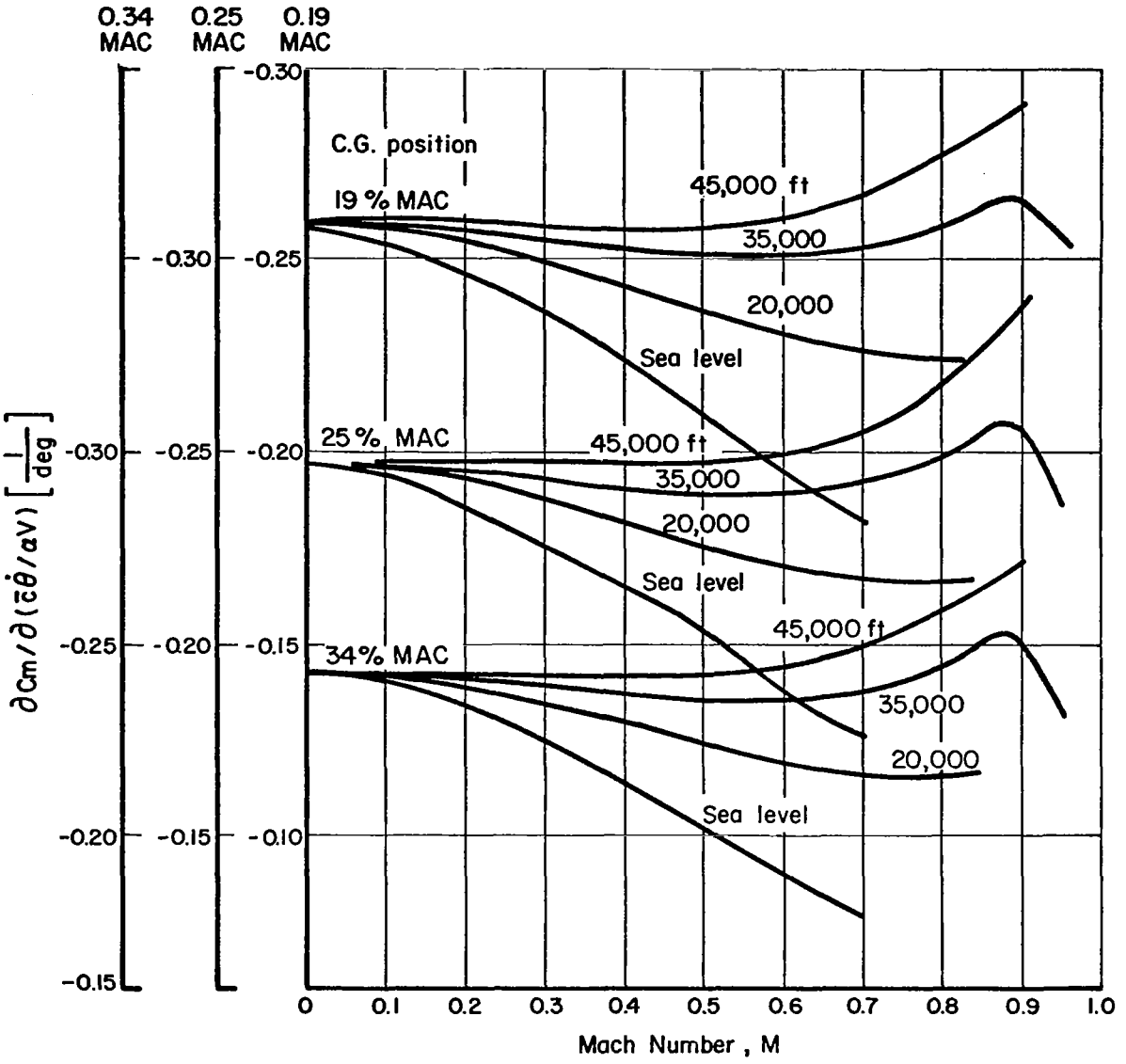

FIGURE B-15. VARIATION OF $\partial Cm/\partial (\bar{c}\dot{\theta}/2V)$ WITH MACH NUMBER, ALTITUDE, AND C.G. POSITION

$$T = C_D QS \tag{B-11}$$

$$W = C_L QS \quad . \tag{B-12}$$

These expressions can be combined to yield

$$\frac{T}{W} = \frac{C_D}{C_L} \tag{B-13}$$

Using Equation (B-8), (B-13) can be rewritten as

$$\frac{T}{W} = \frac{(C_D)_L + (C_D)_M}{C_L} \tag{B-14}$$

where $(C_D)_L$ is a function of C_L, and $(C_D)_M$ is a function of M.

Figure B-16 gives the equilibrium flight thrust-to-weight ratio $(\frac{T}{W})$ as a function of C_L and M. Its characteristics were determined from the data in Figures B-5 and B-6.

Now with regard to the aircraft's dynamic behavior, it is considered desirable to allow for the effects of velocity changes on thrust, as given by $\frac{\partial T}{\partial V}$. The thrust-velocity characteristics of a specific engine could not be used, as this would not be in harmony with the concept of a "rubberized" engine and the assumptions made above. Instead, the approach used involved the nondimensionalized characteristics of an idealized, constant-volume flow turbojet engine.

Figure B-17 shows the idealized thrust characteristics* as a function of Mach number of an axial-flow, turbojet engine operating on a constant-volume flow basis. These thrust characteristics are for maximum-rated fuel flow

---

* "Aerodynamics of Propulsion", by Dietrick Küchemann and Johanna Weber, McGraw-Hill Book Company, Incorporated, 1953, Sections 8-5.

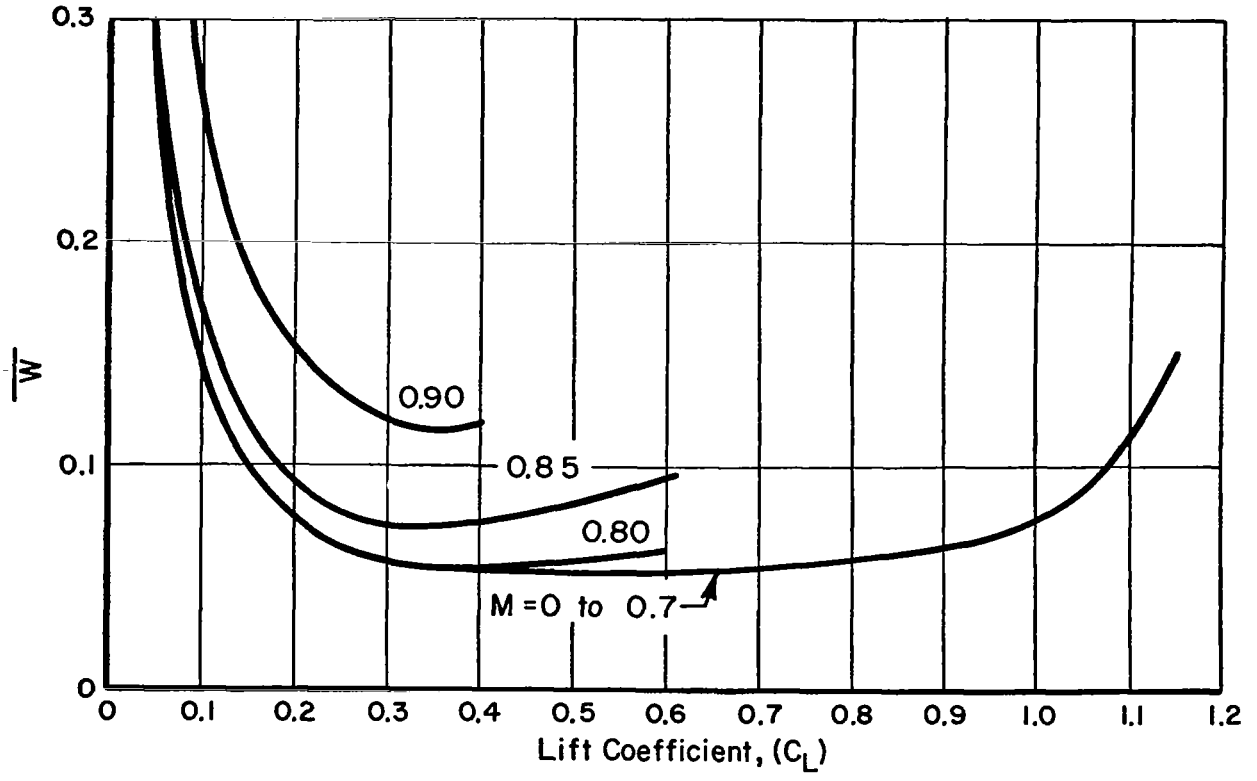

FIGURE B-16. VARIATION OF T/W WITH MACH NUMBER AND LIFT COEFFICIENT

(full throttle) at sea level standard conditions. The thrust is given as a ratio of actual thrust to the static thrust at zero flight speed. As shown in the figure, the characteristic curve is approximated analytically.

$\bar{T}_{max}$ represents the maximum thrust available at sea-level standard conditions and is given by

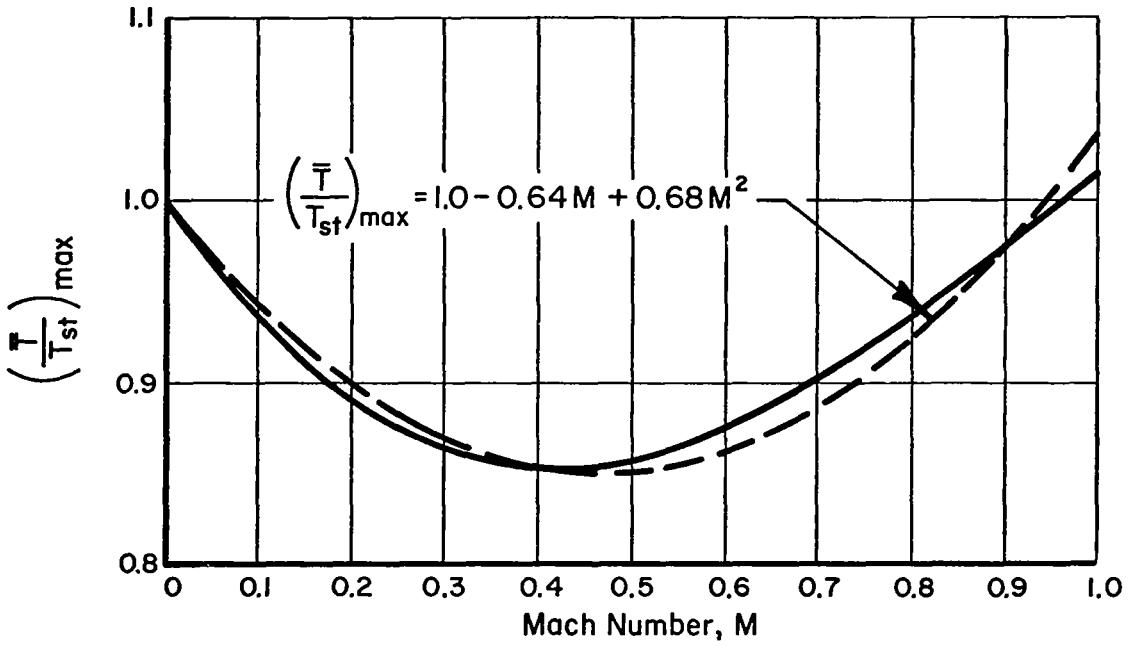

FIGURE B-17. VARIATION OF MAXIMUM SEA-LEVEL STANDARD THRUST WITH FLIGHT MACH NUMBER, FOR AN IDEALIZED TURBOJET ENGINE.

$$\bar{T}_{max} = \left(\frac{\bar{T}}{T_{st\ max}}\right) \cdot \left(T_{st}\right) \qquad \text{(B-15)}$$

If T_{max} is the maximum thrust available at a flight condition other than sea-level standard, it would be determined from

$$T_{max} = \left(\frac{\bar{T}}{T_{st}}\right)_{max} \cdot \left(T_{st}\right) \cdot \delta_{t_2} \tag{B-16}$$

where δ_{t_2} is the pressure correction factor. The thrust, T, required at some particular flight condition would in general be some fraction K of T_{max}; that is,

$$T = \left(\frac{\bar{T}}{T_{st}}\right)_{max} \cdot \left(T_{st}\right) \cdot \delta_{t_2} \cdot K \tag{B-17}$$

At this condition the rate of change of thrust with Mach number is

$$\frac{\partial T}{\partial M} = \frac{\partial(\bar{T}/T_{st})_{max}}{\partial M} \cdot (T_{st}) \cdot \delta_{t_2} \cdot K \tag{B-18}$$

Now, Equations (B-17) and (B-18) can be combined to eliminate the product $T_{st} \cdot \delta_{t_2} \cdot K$. Thus,

$$\frac{\partial T}{\partial M} = T \frac{\partial(\bar{T}/T_{st})_{max}/\partial M}{(\bar{T}/T_{st})_{max}} \tag{B-19}$$

The analytical expression used to fit the curve in Figure B-17 is

$$\left(\frac{\bar{T}}{T_{st}}\right)_{max} = 1.00 - 0.64M + 0.68M^2 \tag{B-20}$$

Differentiating it with respect to M gives

$$\frac{\partial\left(\frac{\bar{T}}{T_{st}}\right)_{max}}{\partial M} = -0.64 + 1.36M \tag{B-21}$$

Using (B-20) and (B-21), Equation (B-19) can be rewritten as

$$\frac{\partial T}{\partial M} = T \frac{(-0.64 + 1.36M)}{(1.00 - 0.64M + 0.68M^2)} \tag{B-22}$$

A change of variable was made from M to V, taking account of the fact that

$$\frac{\partial T}{\partial M} = \frac{\partial T}{\partial V} \cdot \frac{\partial V}{\partial M} \tag{B-23}$$

and since

$$V = Ma \quad , \tag{B-24}$$

where a is the speed of sound at a particular altitude, then

$$\frac{\partial V}{\partial M} = a \tag{B-25}$$

Using these identities, Equation (B-22) can be rewritten as

$$\frac{\partial T}{\partial V} = T \frac{-0.64a + 1.36V}{a^2 - 0.64Va + 0.68V^2} \tag{B-26}$$

With this expression, it is possible to obtain the thrust variation with velocity, given the equilibrium thrust level, the flight speed, and the speed of sound at the flight altitude involved.

Figure B-18 is a composite graph, based on Equation (B-26), which gives values for $\frac{\partial T}{\partial V}$ in terms of the other variables involved. By observing both this figure and the numberator of Equation (B-22), it is seen that for all cases $\frac{\partial T}{\partial V}$ is zero when M equals 0.47.

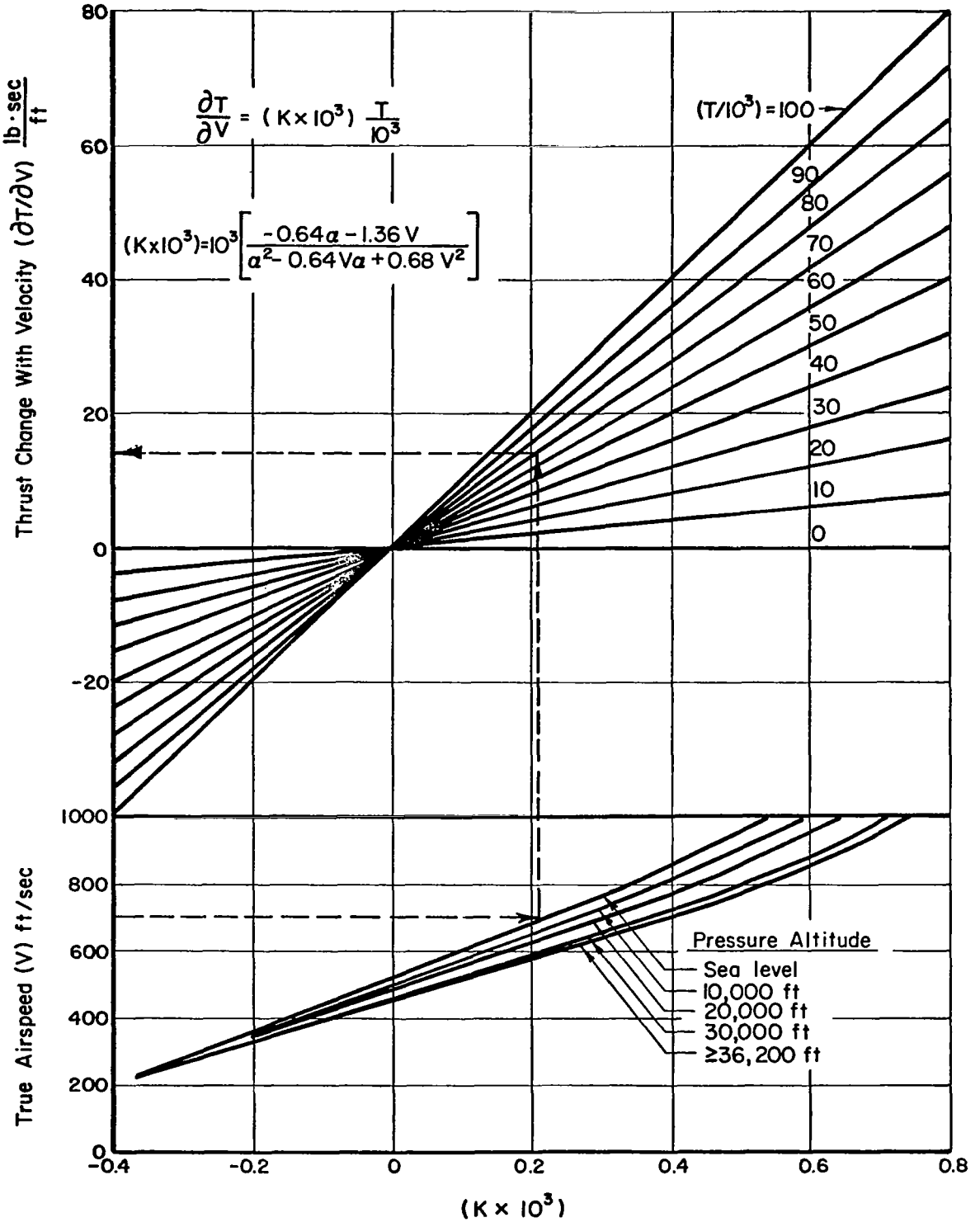

FIGURE B-18. THRUST CHANGE WITH VELOCITY FOR VARIOUS THRUST LEVELS AND FLIGHT CONDITIONS

Operational Characteristics

Figure B-19 is the altitude-airspeed operating envelope for the aircraft to be examined. The operational envelopes are seen to vary as a function of the wing loading $(\frac{W}{S})$. The buffet boundary limits were obtained by using the analytical representation of the buffet boundary shown in Figure B-4. Additionally, a dynamic pressure constraint is imposed by selecting an upper indicated airspeed limit of 400 knots.

It was decided that in specifying aircraft stability margins "static margin" would be selected in lieu of specific c.g. positions. Examination of Equation (B-10) shows that the effective C_{m_α} is given by

$$C_{m_\alpha} = \left(C_{m_\alpha}\right)_{ref} + \frac{\partial\left(C_{m_\alpha}\right)_{ref}}{\partial X_{cg}} \left(X_{cg} - X_{cg_{ref}}\right) \tag{B-27}$$

The neutral point (N_o) is the c.g. position (X_{cg}) at which C_{m_α} is zero. Thus,

$$N_o = X_{cg_{ref}} - \frac{\left(C_{m_\alpha}\right)_{ref}}{\partial\left(C_{m_\alpha}\right)_{ref}/\partial X_{cg}} \tag{B-28}$$

where

$$X_{cg_{ref}} = 0.25 \text{ MAC}$$

Static margin (X_{sm}) is defined by

$$X_{sm} = X_{cg} - N_o \tag{B-29}$$

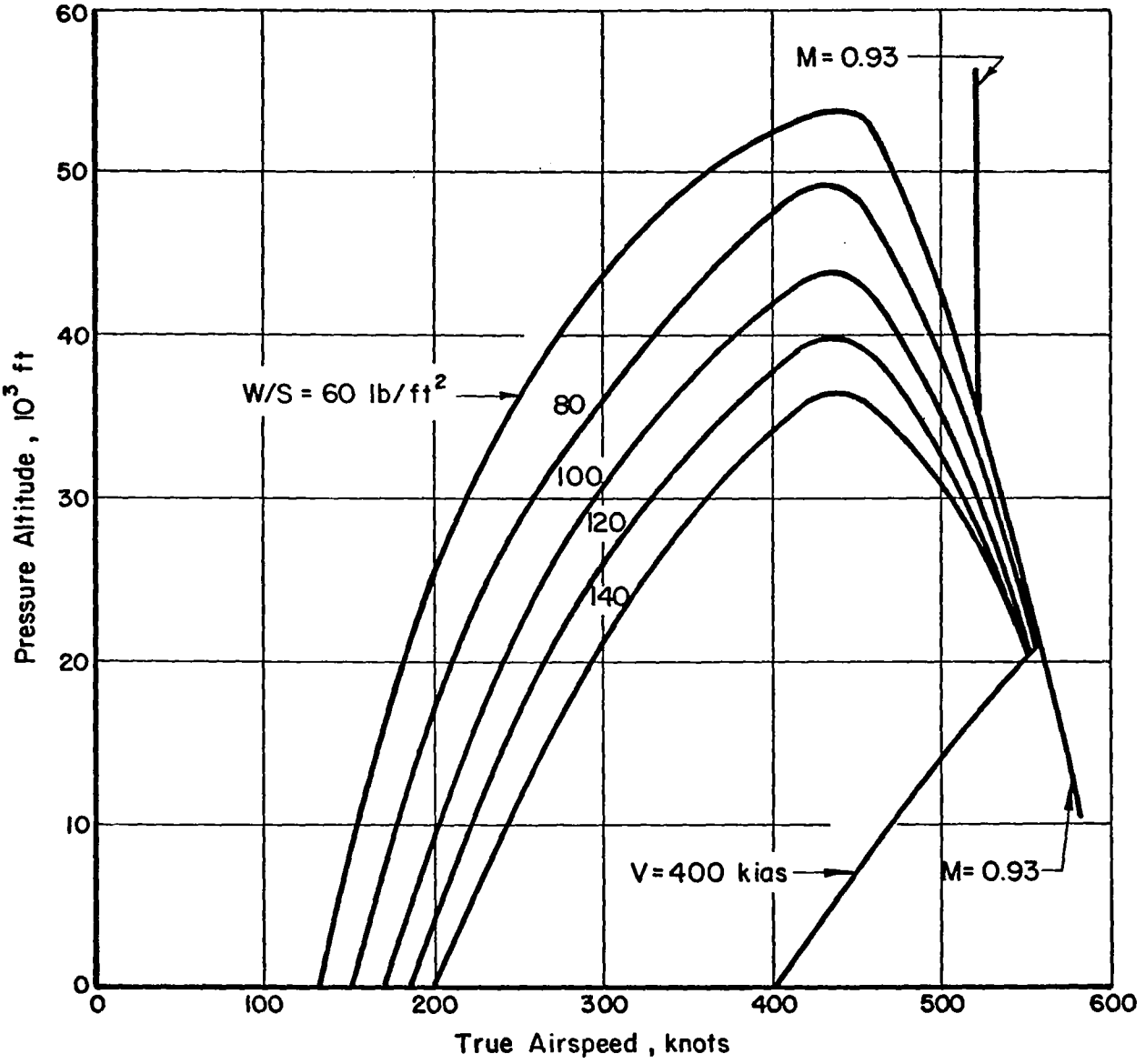

FIGURE B-19. ALTITUDE - AIRSPEED OPERATIONAL ENVELOPE

Substitution of (B-28) and (B-29) into (B-27) yields

$$\frac{\partial C_m}{\partial \alpha} = \frac{\partial \left(C_{m_\alpha}\right)_{ref}}{\partial X_{cg}} \cdot X_{sm} \qquad \text{(B-30)}$$

Stepwise Procedure for Acquiring Aircraft Data

One stepwise procedure for obtaining aircraft data for analysis purposes is illustrated below:

Specify $\bar{c}$

Find S (Equation B-5)

Specify $\frac{W}{S}$

Find W $\left(W = \frac{W}{S} \cdot S\right)$

I_{yy} (Equation B-6)

Specify M, h (Subject to Figure B-19)

Find C_{L_o} (Figure B-1)

C_{L_α} (Figure B-2)

$C_{L_{\delta_e}}$ (Figure B-3)

C_{m_o} (Figure B-9)

$\left(C_{m_\alpha}\right)_{ref}$ (Figure B-10)

$C_{m_{\delta_e}}$ (Figure B-11)

$C_{m_{X_{cg}}}$ (Figure B-12)

$\frac{\partial}{\partial X_{cg}}\left(C_{m_\alpha}\right)$ (Figure B-13)

ρ, a (standard atmosphere tables)

V ($V = Ma$)

C_L ($C_L = \frac{2W}{\rho S V^2}$)

C_D (Figures B-5 and B-6)

$\frac{\partial(C_D)_L}{\partial \alpha}$ (Figure B-7)

$\frac{\partial(C_D)_M}{\partial M}$ (Figure B-8)

$\frac{T}{W}$ (Figure B-16)

T ($T = \frac{T}{W} \cdot W$)

$\frac{\partial T}{\partial V}$ (Figure B-18)

Specify X_{sm}

Find C_{m_α} (Equation B-30)

N_o (Equation B-28)

X_{cg} (Equation B-29)

$\frac{\partial C_m}{2(\bar{c}\dot{\alpha}/2V)}$ (Figure B-14)

$$\frac{\partial C_m}{\partial(\dot{\bar{c}}\theta/2V)}$$ (Figure B-15)

Appendix C

Turbulence-Penetration Constraints

Table of Contents

List of Figures

Appendix C

Turbulence-Penetration Constraints

Introduction

For the purposes of this study, it is desirable to have a constraint envelope in the proper dimensional space, whose boundaries are defined by straight line segments. The following material describes the thinking and methods by which a constraint envelope is generated.

Nomenclature

a = speed of sound, ft/sec

A_i, B_i, . . . F_i = arbitrary coefficient designations

C_L = lift coefficient

C_{L_α} = $\partial C_L / \partial \alpha$

M = Mach number

S = wing area, ft^2

v = nondimensionalized airspeed perturbation

V = true airspeed, ft/sec

W = aircraft gross weight, lbs

α = angle of attack, radians

$\bar{\alpha}$ = perturbation from trim angle of attack, radians

ρ = atmospheric density, $slugs/ft^3$

$*$ = superscript denoting equilibrium flight condition

General Constraints

Figure C-1 illustrates the constraint boundaries considered, and their general appearance in the two-dimensional space of lift coefficient (C_L) and true airspeed (V). These constraint boundaries are discussed separately, below.

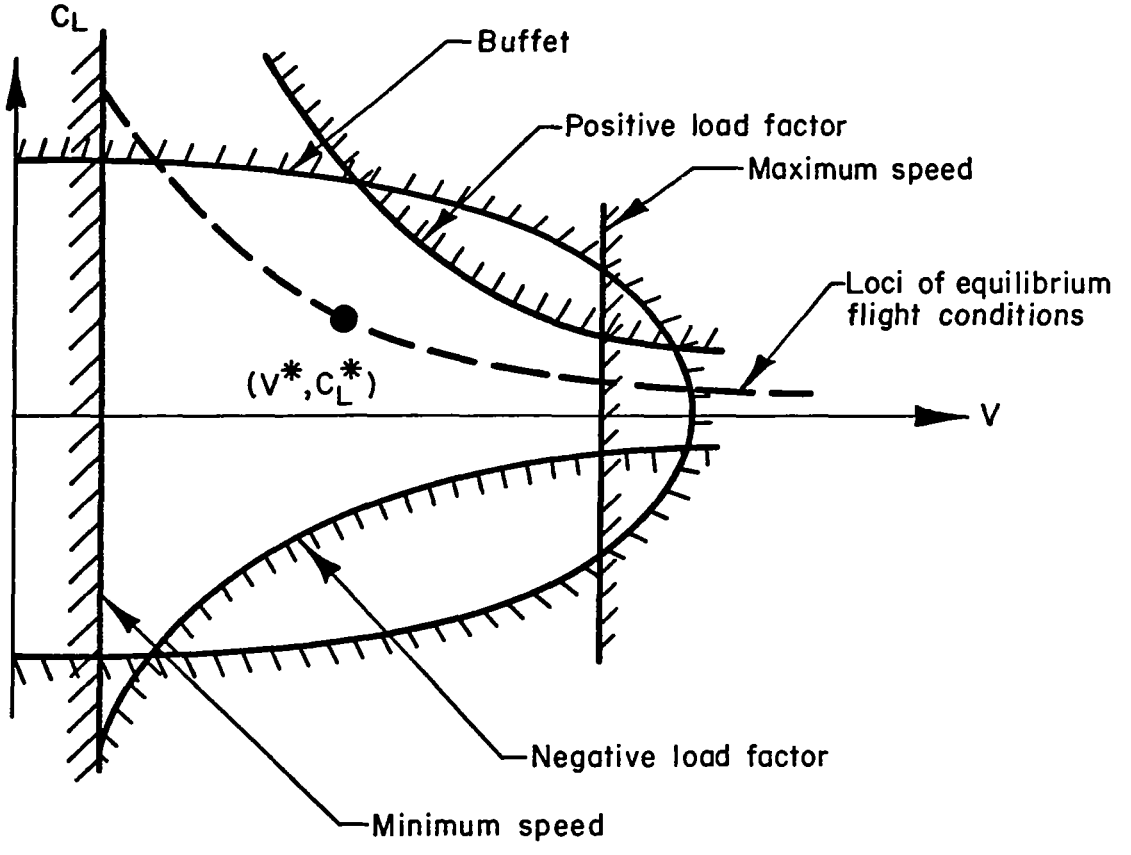

FIGURE C-1. NONLINEAR CONSTRAINT BOUNDARIES EXPRESSED IN THE C_L-V DIMENSIONS.

Buffet

In Appendix B, a buffet boundary for the study aircraft was approximated analytically by

$$C_L = 1.05 \left[1 - 1.168M^2\right]^{1/2} \tag{C-1}$$

where M is Mach number. However, since

$$M = V/a \tag{C-2}$$

where a is the speed of sound, Equation (C-1) can be rewritten in terms of V, instead of M, as

$$C_L = 1.05 \left[1 - (1.168/a^2)V^2\right]^{1/2} \tag{C-3}$$

Because of insufficient data on the nature of the buffet boundary in the negative C_L region, it was decided that the buffet boundary be taken as symmetrical about the V axis. Thus,

$$C_L = \pm 1.05 \left[1 - (1.68/a^2)V^2\right]^{1/2} \tag{C-4}$$

Positive Load Factor

The normal load factor (N) is given as the ratio of aerodynamic lift to aircraft weight. That is,

$$N = (\rho SV^2/2W)C_L \tag{C-5}$$

As discussed in Appendix A, the dynamic aeroelastic characteristics of the aircraft are not included in the study. For this reason, a constant load-factor boundary is assumed. For a positive load factor limit of 2.5, Equation (C-5) can be solved for C_L and expressed as

$$C_L = 5(W/S)/\rho V^2 \tag{C-6}$$

Negative Load Factor

A negative load factor limit of -1 is assumed. Using Equation (C-5), the C_L limits of this boundary, expressed in terms of the other variables, is

$$C_L = - 2(W/S)/\rho V^2 \qquad \text{(C-7)}$$

Minimum Speed

At sufficiently low airspeeds, for a particular altitude and load factor, the aerodynamic control surfaces are not effective enough to allow attitude control. A minimum speed limitation was postulated to take this fact into consideration. Since the threshold speed where control ineffectiveness occurs is a function of many factors, in this study, it is conservatively estimated to be the 1-g stall speed of the aircraft.

The 1-g stall speed, and hence the minimum speed boundary, corresponds to flight at the maximum lift coefficient and is given as

$$V_s = \left[2(W/S)\rho C_{L_{max}}\right]^{1/2} \qquad \text{(C-8)}$$

Maximum Speed

As presented in Appendix B, an indicated airspeed of 400 knots (675 ft/sec) is taken as the maximum permissible speed for the aircraft. The relationship between true and indicated airspeed is given by

$$V_{true} = \left[\rho_o/\rho\right]^{1/2} V_{indicated} \qquad \text{(C-9)}$$

where ρ_o is the sea level standard density, taken here as 0.002378 slug/ft^3. Therefore, the aircraft's maximum allowable true airspeed in feet per second is given by

$$V_m = 32.95/[\rho]^{1/2} \qquad \text{(C-10)}$$

From Figure C-1 it can be seen that under some flight conditions the maximum speed limit might be established by the buffet boundary. The maximum speed permitted by the buffet boundary can be obtained from Equation (C-4) for the case where C_L is zero. Thus,

$$V_m = \left[a^2/1.168\right]^{1/2} \tag{C-11}$$

Constraint Transformation

In order to be compatible with the dimensions employed in analyzing aircraft response (as given in Appendix A), the boundaries just discussed are transformed from the C_L - V axis system to a $\bar{\alpha}$ - v system, where

$$\bar{\alpha} = \alpha - \alpha^* \tag{C-12}$$

$$v = V/V^* - 1 \tag{C-13}$$

It can be shown that

$$C_L = C_L^* + C_{L_\alpha} \cdot \bar{\alpha} \tag{C-14}$$

and (C-13) can be rearranged to give

$$V = (v + 1)V^* \quad . \tag{C-15}$$

Using Equations (C-14) and (C-15) with the previously defined constraint boundaries, the transformed boundaries can be rewritten as

$$\bar{\alpha} = \pm K_1 \left[1 - K_2 \, (v + 1^2\right]^{1/2} - K_3 \qquad \text{(buffet)} \tag{C-16}$$

$$\bar{\alpha} = \left[K_4/(v + 1)^2\right] - K_3 \quad \text{(positive load factor)} \tag{C-17}$$

$$\bar{\alpha} = -\left[K_5/(v+1)^2\right] - K_3 \qquad \text{(negative load factor)} \tag{C-18}$$

$$v_{min} = K_6 \qquad \text{(minimum speed)} \tag{C-19}$$

$$v_{max} = K_7 \qquad \text{(maximum speed)} \tag{C-20}$$

$$v'_{max} = K_8 \qquad \text{(alternate maximum speed)} \tag{C-21}$$

where

$$K_1 = 1.05/C_{L_\alpha} \tag{C-22}$$

$$K_2 = 1.168V^{*2}/a^2 \tag{C-23}$$

$$K_3 = C_L^*/C_{L_\alpha} \tag{C-24}$$

$$K_4 = 5(W/S)/C_{L_\alpha}\ \rho V^{*2} \tag{C-25}$$

$$K_5 = 2(W/S)/C_{L_\alpha}\ \rho V^{*2} \tag{C-26}$$

$$K_6 = \left[2(W/S)\rho\ C_{L_{max}}\ V^{*2}\right]^{1/2} - 1 \tag{C-27}$$

$$K_7 = (32.95/V^*\sqrt{\rho}) - 1 \tag{C-28}$$

$$K_8 = \left[1/K_2\right]^{1/2} - 1 \tag{C-29}$$

Linearizing the Constraints

In the preceding paragraphs, a description is given of the constraints selected, and the steps taken to transform these constraints into a dimensional space representing the perturbations from an equilibrium condition. Nonetheless, most of the constraints remain nonlinear, the exceptions being the two velocity limitations. Because the aircraft response analysis involves linear models, it is believed appropriate to have the constraint envelope defined by linearized representations of the nonlinear constraint boundaries.

Figure C-2 illustrates a hypothetical arrangement of the transformed nonlinear constraint boundaries discussed previously. They are shown by the dashed lines in the figure. The following concept is employed in the linearization process. Some point on each constraint boundary is in nearest proximity to the equilibrium condition (origin of the $\bar{\alpha}$ - v axis system). Through each such point, construct a straight line with the same slope as that of the nonlinear boundary at this point. The resulting set of straight lines intersect one another to form a constraint envelope whose perimeter consists of straight line segments.

An examination of the equations presented earlier shows that the constraint envelope, such as that shown in Figure C-2, is uniquely defined by the aircraft and flight condition parameters M, h, and W/S. It was known that constraint envelopes would need to be established for a possible large number of different conditions involving these three parameters. Thus, a computerized method of defining the envelopes was developed. This development is discussed in the remainder of this Appendix.

Identifying Proximity Points

In any computer approach to envelope definitions, the first obvious step would be to compute the coefficients K_1, K_2, K_3, . . . K_8, as given by Equations (C-22) through (C-29). With these available, the constraint boundary Equations, (C-16) through (C-21), would be defined. The next task would be to define the four nearest proximity points of positive and negative lift buffet boundaries, and the two load factor boundaries. The method developed for accomplishing this is described for each of the boundaries.

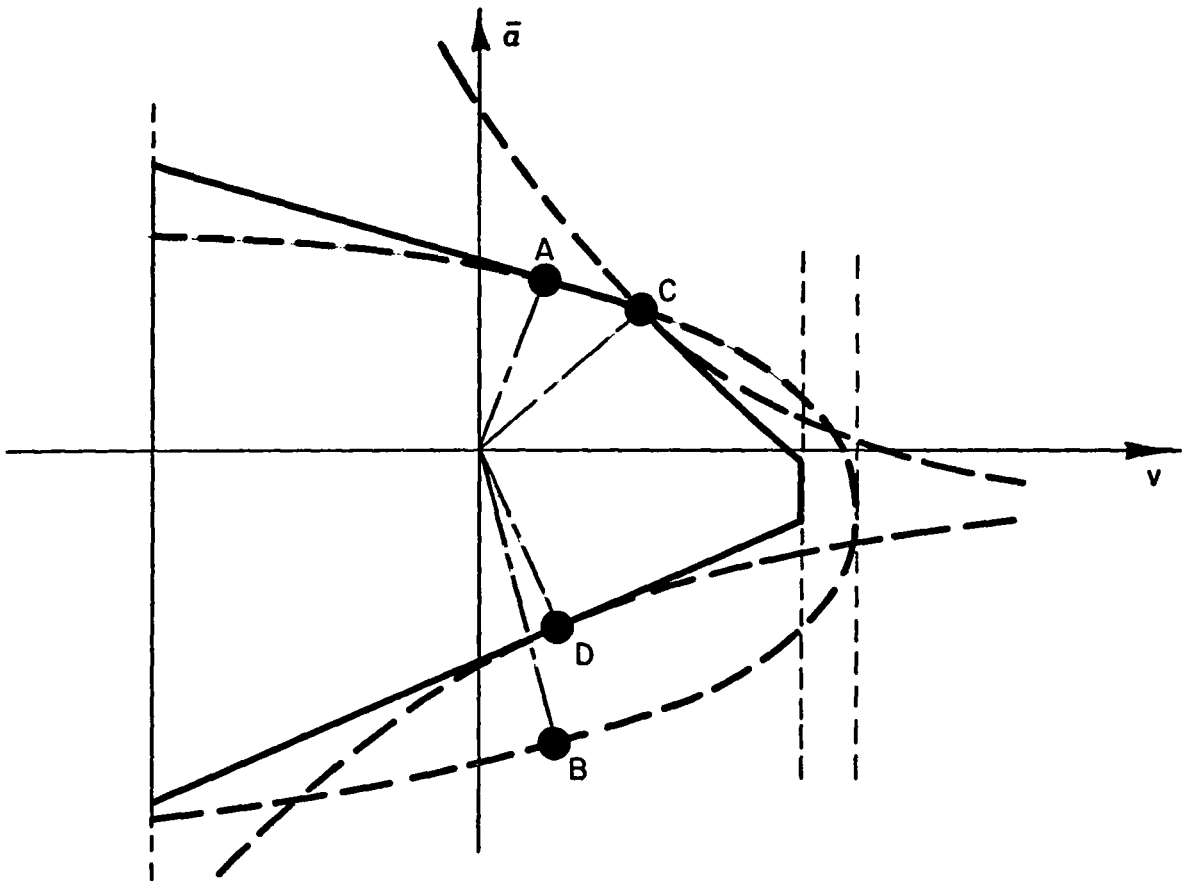

FIGURE C-2. DEVELOPMENT OF THE LINEARIZED CONSTRAINT ENVELOPE.

Buffet Boundary

The following approach is used to identify the nearest promixity points of interest.

(1) Develop an expression giving the distance r from the origin to any point ($\bar{\alpha}$ - v) on the boundary.

(2) Find the values of v at which r is an extremum (minimum or maximum).

(3) Discriminate among these roots to identify those for which r is a minimum.

(4) Find the appropriate value of $\bar{\alpha}$ corresponding to each v-root for which r is a minimum.

The buffet voundary is defined in Equation (C-16) as

$$\bar{\alpha} = \pm K_1 \left[1 - K_2 (v + 1)^2\right]^{1/2} - K_3$$

The distance r, mentioned above, is given by

$$r = \left[\bar{\alpha}^2 + v^2\right]^{1/2} \qquad \text{(C-30)}$$

Combining these two equations to eliminate $\bar{\alpha}$, and solving for r gives

$$r = \left\{K_1^2 \left[1 - K_2(v + 1)^2\right] - 2K_1K_3\left[1 - K_2(v + 1)^2\right]^{1/2} + K_3^2 + v^2\right\}^{1/2} \qquad \text{(C-31)}$$

The partial derivative of r with respect to v is

$$\frac{\partial r}{\partial V} = \frac{-2K_1^2K_2(v + 1) + \left\{2K_1K_2K_3(v + 1)/\left[1 - K_2(v + 1)^2\right]^{1/2}\right\} + 2v}{2r} \qquad \text{(C-32)}$$

Setting the expression for $\partial r/\partial v$ equal to zero, and rearranging gives a polynomial of the following form

$$A_0 v^4 + A_1 v^3 + A_2 v^2 + A_3 v + A_4 = 0 \qquad \text{(C-33)}$$

where

$$A_0 = - K_2 + 2K_1^2 K_2^2 - K_1^4 K_2^3 \qquad \text{(C-34)}$$

$$A_1 = - 2K_2 + 6K_1^2 K_2^2 - 4K_1^4 K_2^3 \qquad \text{(C-35)}$$

$$A_2 = 1 - 2K_1^2 K_2 + K_1^4 K_2^2 - K_2 + 6K_1^2 K_2^2 - 6K_1^4 K_2^3 - K_1^2 K_2^2 K_3^2 \qquad \text{(C-36)}$$

$$A_3 = - 2K_1^2 K_2 + 2K_1^4 K_2^2 + 2K_1^2 K_2^2 - 4K_1^4 K_2^3 - 2K_1^2 K_2^2 K_3^2 \qquad \text{(C-37)}$$

$$A_4 = K_1^4 K_2^2 - K_1^4 K_2^3 - K_1^2 K_2^2 K_3^2 \qquad \text{(C-38)}$$

Figure C-3 illustrates the four points whose v coordinates are given by the four roots of Equation (C-33). Because of the nature of the buffet boundary, it is clear that the minus v root can always be discarded, leaving three roots to be examined further. Of these, the two for which r is a minimum can be identified by examining the sign of the second derivative of r with respect to v. It is given by

$$\frac{\partial^2 r}{\partial v^2} = \frac{-2K_1^2 K_2 + 2K_1 K_2 K_3 \left\{[1-K_2(v+1)^2]^{-1/2} + K_2(v+1)^2[1-K_2(v+1)^2]^{-3/2}\right\} + 2}{r} \qquad \text{(C-39)}$$

That v-root whose second derivative is negative is discarded. This finally leaves the two roots for which r is a minimum.

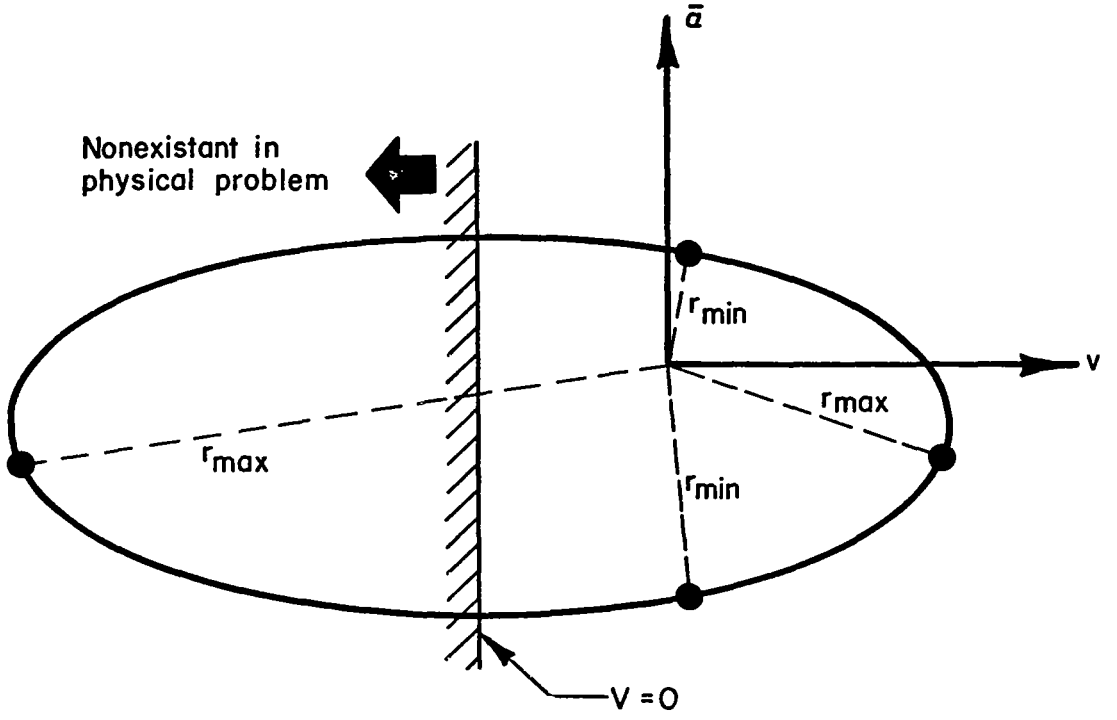

FIGURE C-3. TYPICAL EXTREME VALUES OF r FOR THE BUFFET BOUNDARY

Having found the v coordinates of the two nearest proximity points, it is necessary to find their respective $\bar{\alpha}$ coordinates. Equation (C-16) illustrates that two possible $\bar{\alpha}$ values exist for each v value. Namely,

Option 1: $$\bar{\alpha} = K_1 \left[1 - K_2(v + 1)^2\right]^{1/2} - K_3$$

Option 2: $$\bar{\alpha} = - K_1 \left[1 - K_2(v + 1)^2\right]^{1/2} - K_3$$

The desirable $\bar{\alpha}$ value is that which, together with the v value in question, meets the test that $\partial r/\partial v$ equals zero. Differentiating Equation (C-30) with respect to v provides an expression for testing this requirement. The form of this expression differs for the two options involved. Namely,

$$\text{Option 1:} \quad \frac{\partial r}{\partial v} = \frac{v}{\left[\bar{\alpha}^2 + v^2\right]^{1/2}} - \frac{\bar{\alpha}}{\left[\bar{\alpha}^2 + v^2\right]^{1/2}} \cdot \frac{K_1 K_2 (v + 1)}{\left[1 - K_2 (v + 1)^2\right]^{1/2}} \tag{C-40}$$

$$\text{Option 2:} \quad \frac{\partial r}{\partial v} = \frac{v}{\left[\bar{\alpha}^2 + v^2\right]^{1/2}} + \frac{\bar{\alpha}}{\left[\bar{\alpha}^2 + v^2\right]^{1/2}} \cdot \frac{K_1 K_2 (v + 1)}{\left[1 - K_2 (v + 1)^2\right]^{1/2}} \tag{C-41}$$

The steps above allow for explicit determination of the proximity points on the buffet boundary. The slope of the buffet boundary at each nearest proximity point, $\partial\bar{\alpha}/\partial v$, would be given by the expression obtained in differentiating Equation (C-16) with respect to v and is used to establish the linearlized envelope segment. The form differs for the two options.

$$\text{Option 1:} \quad \frac{\partial \bar{\alpha}}{\partial v} = - \frac{K_1 K_2 (v + 1)}{\left[1 - K_2 (v + 1)^2\right]^{1/2}} \tag{C-42}$$

$$\text{Option 2:} \quad \frac{\partial \bar{\alpha}}{\partial v} = + \frac{K_1 K_2 (v + 1)}{\left[1 - K_2 (v + 1)^2\right]^{1/2}} \tag{C-43}$$

Positive Load Factor Boundary

Using much the same procedure as was used with the buffet boundary, Equations (C-17) and (C-30) can be combined to yield an expression for r in terms of v.

$$r = \left[\frac{K_4^2}{(v+1)^4} - \frac{2K_3K_4}{(v+1)^2} + K_3^2 + v^2 \right]^{1/2} \qquad \text{(C-44)}$$

Its derivative with respect to v is

$$\frac{\partial r}{\partial v} = \frac{-\frac{2K_4^2}{(v+1)^5} + \frac{2K_3K_4}{(v+1)^3} + v}{r} \qquad \text{(C-45)}$$

Setting this equal to zero and rearranging terms yields a polynomial of the following form,

$$B_0v^6 + B_1v^5 + B_2v^4 + B_3v^3 + B_4v^2 + B_5v + B_6 = 0 \qquad \text{(C-46)}$$

where

$$B_0 = 1$$

$$B_1 = 5$$

$$B_2 = 10$$

$$B_3 = 10$$

$$B_4 = 2K_3K_4 + 5$$

$$B_5 = 4K_3K_4 + 1$$

$$B_6 = -2K_4^2 + 2K_3K_4$$

Figure C-4 shows the nature of the boundary given by Equation (C-17). This equation allows for the existance of a boundary in a nonexistant physical region (negative velocities). It can be observed that Equation (C-46) can only have two real roots which have physical significance and that only one of these, a positive v, is the v-coordinate of the nearest proximity point. Thus, the six roots of (C-46) can be examined and all imagainary and negative real roots can be discarded.

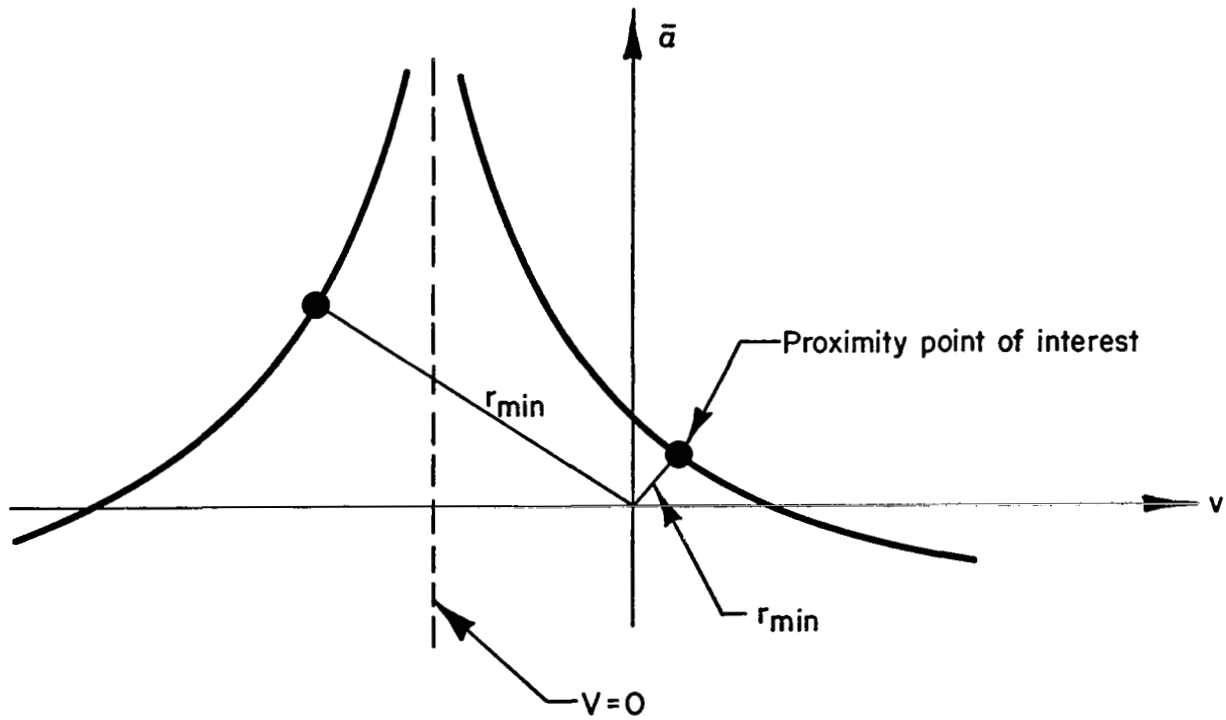

FIGURE C-4. TYPICAL EXTREME VALUES OF r FOR THE POSITIVE LOAD FACTOR BOUNDARY.

When the single v-root of interest is found, the associated $\bar{\alpha}$ coordinate can be obtained from Equation (C-17). That is,

$$\bar{\alpha} = \frac{K_4}{(v+1)^2} - K_3 \qquad \text{(C-47)}$$

The derivative of (C-47) with respect to v provides an equation for the slope of the positive load factor boundary, at the nearest proximity point and, hence, the slope of a segment of the linearized constraint envelope. It is

$$\frac{\partial \bar{\alpha}}{\partial v} = - \frac{2K_4}{(v + 1)^3} \tag{C-48}$$

Negative Load Factor Boundary

Using the same procedure as was used for the positive load factor boundary, the resulting polynomial is

$$C_0 v^6 + C_1 v^5 + C_2 v^4 + C_3 v^3 + C_4 v^2 + C_5 v + C_6 = 0 \tag{C-49}$$

where

$$C_0 = 1$$

$$C_1 = 5$$

$$C_2 = 10$$

$$C_3 = 10$$

$$C_4 = - 2K_3K_5 + 5$$

$$C_5 = - 4K_3K_5 + 1$$

$$C_6 = - 2K_5^2 - 2K_3K_5$$

As before, four of the six roots of (C-49) are imaginary and can be discarded. Of the two real roots, only the one greater than zero is of interest. The $\bar{\alpha}$ coordinate and the boundary slope at the nearest proximity point are given by the following two equations.

$$\bar{\alpha} = - \frac{K_5}{(v + 1)^2} - K_3 \tag{C-50}$$

$$\frac{\partial \bar{\alpha}}{\partial v} = \frac{2K_5}{(v+1)^3} \tag{C-51}$$

Linear Boundary Definitions

Including the two velocity limitations, the linearized constraint boundaries are six in number. This includes a boundary for both the upper and lower surfaces of the nonlinear buffet boundary. These linear boundaries can be expressed by an equation of the following form:

$$D_i \bar{\alpha} + E_i v = F_i \qquad (i = 1, 2, \ldots, 6) \tag{C-52}$$

The following equation assignments are made.

$$D_1 \bar{\alpha} + E_1 v = F_1 \quad , \qquad \text{minimum speed boundary} \tag{C-53}$$

$$D_2 \bar{\alpha} + E_2 v = F_2 \quad , \qquad \text{maximum speed boundary} \tag{C-54}$$

$$D_3 \bar{\alpha} + E_3 v = F_3 \quad , \qquad \text{upper buffet boundary} \tag{C-55}$$

$$D_4 \bar{\alpha} + E_4 v = F_4 \quad , \qquad \text{lower buffet boundary} \tag{C-56}$$

$$D_5 \bar{\alpha} + E_5 v = F_5 \quad , \qquad \text{positive load factor boundary} \tag{C-57}$$

$$D_6 \bar{\alpha} + E_6 v = F_6 \quad , \qquad \text{negative load factor boundary} \tag{C-58}$$

In computing the values of D_i, E_i, and F_i for these equations, it can be shown that

$$D_1 = D_2 = 0 \tag{C-59}$$

$$D_i = 1, \quad i = 3,4,5,6 \qquad \text{(arbitrary)} \tag{C-60}$$

$$E_1 = E_2 = 1 \qquad \text{(arbitrary)} \tag{C-61}$$

$$E_i = - \left(\frac{\partial \bar{\alpha}}{\partial v}\right)_i, \qquad i = 3,4,5,6 \tag{C-62}$$

$$F_i = D_i \bar{\alpha}_i + E_i v_i, \qquad i = 1, 2, \ldots, 6 \tag{C-63}$$

where $\bar{\alpha}_i$ and v_i are the nearest proximity point coordinates, and $\left(\frac{\partial \bar{\alpha}}{\partial v}\right)_i$ is the boundary slope at the nearest proximity point. For the minimum and maximum speed boundaries,

$$v_1 = K_6 \tag{C-64}$$

$$v_2 = \begin{cases} K_7, \text{ for } K_7 \leq K_8 \\ K_8, \text{ for } K_8 < K_7 \end{cases} \tag{C-65}$$

Constraint Envelope Definition

Figure C-5 depicts a hypothetical case for which the six linearized constraint boundaries are defined in the $\bar{\alpha}$ - v plane. With the exception of the two speed constraint boundaries which are parallel, every boundary intersects all other boundaries to form a total of 14 intersection points designated P_{ij}. The symbols i and j represent the two boundaries whose intersection is being considered.

Clearly, the constraint envelope of interest is not defined by all 14 intersect points. In Figure C-5, for example, the constraint envelope is defined by the points P_{13}, P_{35}, P_{25}, P_{26}, P_{46}, and P_{14}. It is, therefore, necessary to develop a routine by which these unique points can be identified.

Every point P_{ij} has the coordinates $\bar{\alpha}_{ij}$ and v_{ij}. The equations of the two lines involved would be

$$\left.\begin{aligned} D_i \bar{\alpha} + E_i v &= F_i \\ D_j \bar{\alpha} + E_j v &= F_j \end{aligned}\right\} \text{ where } i \neq j \tag{C-66}$$

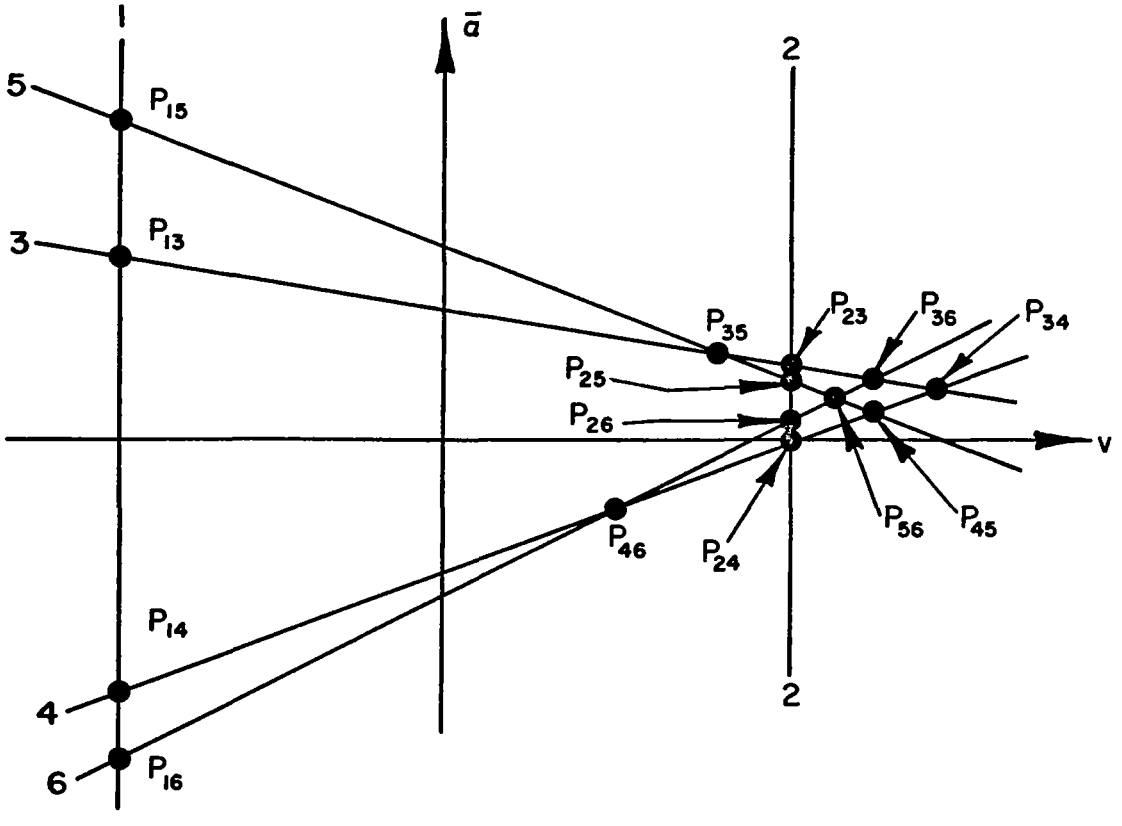

FIGURE C-5. CONSTRAINT SEGMENT INTERSECTIONS WHICH ARE THE BASIS OF THE CONSTRAINT ENVELOPE DEFINITION.

These two equations can be solved simultaneously to yield expressions for the $\bar{\alpha}$ and v coordinates. They are

$$\bar{\alpha}_{ij} = \frac{F_i E_j - E_i F_j}{D_i E_j - E_i D_j} \tag{C-67}$$

$$v_{ij} = \frac{D_i F_j - F_i D_j}{D_i E_j - E_i D_j} \tag{C-68}$$

Now, Equations (C-53) through (C-58) define the constraint-boundary lines. However, being constraints, these boundaries exclude portions of the $\bar{\alpha}$ - v domain from consideration. Therefore, for any point P_{ij} to qualify as a point which uniquely defines the constraint envelope, it must satisfy the following six inequalities.

$$D_1\bar{\alpha}_{ij} + E_1 v_{ij} \geq F_1 \tag{C-69}$$

$$D_2\bar{\alpha}_{ij} + E_2 v_{ij} \leq F_2 \tag{C-70}$$

$$D_3\bar{\alpha}_{ij} + E_3 v_{ij} \leq F_3 \tag{C-71}$$

$$D_4\bar{\alpha}_{ij} + E_4 v_{ij} \geq F_4 \tag{C-72}$$

$$D_5\bar{\alpha}_{ij} + E_5 v_{ij} \leq F_5 \tag{C-73}$$

$$D_6\bar{\alpha}_{ij} + E_6 v_{ij} \geq F_6 \tag{C-74}$$

The procedure above provided a straightforward process for identifying those points which uniquely define the constraint envelope.

Appendix D

Statistical Response Analysis Model

Table of Contents

List of Figures

Appendix D

Statistical Response Analysis Model

Introduction

The material herein deals with the development of an analytical model for examining the response of a linearized aircraft to random turbulence, and assessing the aircraft's performance as given by two criteria. The aircraft's response is viewed in a two-dimensional space defined by two state variables of interest. The basic performance criterion is taken to be the probability that the response will exceed a constraint envelope defined in the state space of interest. An alternate performance measure deals with the frequency of crossing the bounds of the constraint envelope. The analytical developments for these two criterion are given in the following paragraphs.

Nomenclature

d = distance from origin to a given line

E = expectation operator

$f(\ )$ = probability density function

I_1, I_2, I_3 = moment integrals

N_d = number of crossings of the level d per unit time

$R_e\{\ \}$ = real part of $\{\ \}$

t = time

u,v = transformed coordinates

x,y = components of a two-dimensional Gaussian random process

z = projection of a two-dimensional Gaussian random process onto a given line

θ = angle of rotation of coordinate system

ρ = covariance between x and y

σ^2 = variance

τ = time delay

Φ_{ii} = power spectral density

Φ_{ij} = cross spectral density

ψ = direction of the normal to a given line

ω = frequency

Probability of Envelope Exceedance

The probability density function of a zero-mean, bivariate Gaussian distribution in the variables x and y is given[D-1] by

$$f(x,y) = \frac{1}{2\pi\sigma_x\sigma_y\left[1 - \rho^2\right]^{1/2}} \exp\left\{-\frac{1}{2(1-\rho^2)}\left[\frac{x^2}{\sigma_x^2} - \frac{2\rho xy}{\sigma_x\sigma_y} + \frac{y^2}{\sigma_y^2}\right]\right\} \qquad \text{(D-1)}$$

where

$$\sigma_x^2 = E\left\{x^2\right\} \qquad \text{(D-2)}$$

$$\sigma_y^2 = E\left\{y^2\right\} \qquad \text{(D-3)}$$

$$\rho = \frac{E\left\{xy\right\}}{\sigma_x\sigma_y} \qquad \text{(D-4)}$$

It is easily shown that $|\rho| \leq 1$. The case where $\rho = 1$ (i.e., the two variables are linearly related) will not arise in the intended application. Accordingly, it is assumed that $|\rho| < 1$ so that f (x,y) is always well defined.

Now consider a convex polygon (constraint envelope) in the x-y plane defined by the vertices x_i, y_i, where i = 1, 2, . . . N. Given the vertices x_i, y_i, and the parameters σ_x, σ_y, and ρ, the problem is to determine the probability of being outside the polygon, or to find the numerical value of the integral

$$I = \iint_A f(x,y)\, dxdy \qquad \text{(D-5)}$$

where A is the region outside the polygon.

The computational approach taken is to rotate the coordinate system until the cross-product term in Equation (D-1) disappears, then to perform the two quadratures in sequence. This will eliminate the need for a general two-dimensional integration process.

Rotation of Coordinates

Figure D-1 shows a new coordinate system u-v, rotated by an angle θ from the x-y axes. The x-y coordinates of an arbitrary vector may be expressed in terms of the u-v coordinates of the same vector as follows:

$$x = u \cos \theta - v \sin \theta \qquad \text{(D-6)}$$

$$y = u \sin \theta + v \cos \theta \qquad \text{(D-7)}$$

Using these equations to eliminate x and y from Equation (D-1) gives

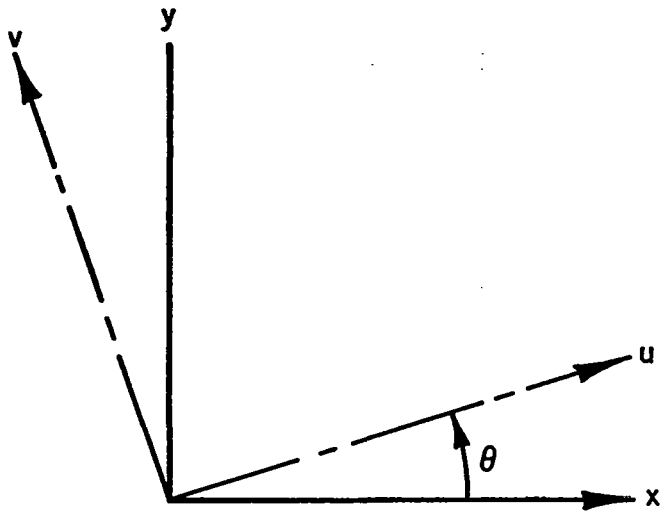

FIGURE D-I. NOMENCLATURE OF AXIS SYSTEM ROTATION

$$f(u,v) = \frac{1}{2\pi\sigma_x\sigma_y\left[1 - \rho^2\right]^{1/2}} \exp\left\{-\frac{1}{2(1-\rho^2)}\left[u^2\left(\frac{\cos^2\theta}{\sigma_x^2} - \frac{2\rho}{\sigma_x\sigma_y}\sin\theta\cos\theta\right.\right.\right.$$

$$\left. + \frac{\sin^2\theta}{\sigma_y^2}\right) + uv\left(\frac{2\rho}{\sigma_x\sigma_y}(\sin^2\theta - \cos^2\theta) + \left(\frac{2}{\sigma_y^2} - \frac{2}{\sigma_x^2}\right)\sin\theta\cos\theta\right) \qquad \text{(D-8)}$$

$$\left.\left. + v^2\left(\frac{\sin^2\theta}{\sigma_x^2} + \frac{2\rho}{\sigma_x\sigma_y}\sin\theta\cos\theta + \frac{\cos^2\theta}{\sigma_y^2}\right)\right]\right\}$$

Now suppose that θ is selected in such a way that the coefficient of the uv term in Equation (D-8) vanishes. It is easily shown that this will occur if and only if

$$\sin 2\theta = \pm \frac{2\rho\sigma_x\sigma_y}{\left[\left(\sigma_x^2 - \sigma_y^2\right)^2 + 4\rho^2\sigma_x^2\sigma_y^2\right]^{1/2}} \tag{D-9}$$

and

$$\cos 2\theta = \mp \frac{\sigma_y^2 - \sigma_x^2}{\left[\left(\sigma_x^2 - \sigma_y^2\right)^2 + 4\rho^2\sigma_x^2\sigma_y^2\right]^{1/2}} \tag{D-10}$$

Using these two expressions, the coefficient of the u^2 term in Equation (D-8) becomes

$$\frac{1}{2\sigma_x^2\sigma_y^2}\left\{\sigma_x^2 + \sigma_y^2 \mp \left[\left(\sigma_x^2 - \sigma_y^2\right)^2 + 4\rho^2\sigma_x^2\sigma_y^2\right]^{1/2}\right\} \tag{D-11}$$

While the coefficient of the v^2 term in (D-8) becomes

$$\frac{1}{2\sigma_x^2\sigma_y^2}\left\{\sigma_x^2 + \sigma_y^2 \pm \left[\left(\sigma_x^2 - \sigma_y^2\right)^2 + 4\rho^2\sigma_x^2\sigma_y^2\right]^{1/2}\right\} \tag{D-12}$$

If it is required that the u axis be the major axis of the probability ellipse, the u^2 coefficient must be smaller than the v^2 coefficient. This means that the upper algebraic signs should be used in (D-11) and (D-12).

The desired values of Sin θ and Cos θ will now be

$$\text{Sin } \theta = \text{sgn } \rho \left\{ \frac{1}{2}\left[1 - \frac{\left(\sigma_x^2 - \sigma_y^2\right)}{\left[\left(\sigma_x^2 - \sigma_y^2\right)^2 + 4\rho^2\sigma_x^2\sigma_y^2\right]^{1/2}}\right]\right\}^{1/2} \tag{D-13}$$

$$\text{Cos } \theta = \text{sgn } \rho \left\{ \frac{1}{2}\left[1 + \frac{\left(\sigma_x^2 - \sigma_y^2\right)}{\left[\left(\sigma_x^2 - \sigma_y^2\right)^2 + 4\rho^2\sigma_x^2\sigma_y^2\right]^{1/2}}\right]\right\}^{1/2} \tag{D-14}$$

$$\text{sgn } \rho = \begin{cases} +1, & \rho \geq 0 \\ -1, & \rho < 0 \end{cases} \tag{D-15}$$

Now, if the following definitions are made,

$$\sigma_u^2 = \frac{2\left(1 - \rho^2\right)\sigma_x^2\sigma_y^2}{\sigma_x^2 + \sigma_y^2 - \left[\left(\sigma_x^2 - \sigma_y^2\right)^2 + 4\rho^2\sigma_x^2\sigma_y^2\right]^{1/2}} \tag{D-16}$$

$$\sigma_v^2 = \frac{2\left(1 - \rho^2\right)\sigma_x^2\sigma_y^2}{\sigma_x^2 + \sigma_y^2 + \left[\left(\sigma_x^2 - \sigma_y^2\right)^2 + 4\rho^2\sigma_x^2\sigma_y^2\right]^{1/2}} \tag{D-17}$$

then the transformed density function becomes

$$f_\theta(u,v) = \frac{1}{2\pi\sigma_u\sigma_v} \exp\left\{ -\frac{1}{2}\left[\frac{u^2}{\sigma_u^2} + \frac{v^2}{\sigma_v^2}\right]\right\} \tag{D-18}$$

The original ordered list of vertices x_i, y_i, may be transformed into a new ordered list u_i, v_i, by using Equations (D-6) and (D-7) with sin θ and cos θ as given by Equations (D-13) and (D-14). The problem is then to integrate Equation (D-18) over the region exterior to the convex polygon defined by the vertices u_i, v_i.

The Gaussian Quadrature

The probability of exceeding the constraint envelope may now be written as the numerical value of the integral

$$I = \iint_A f_\theta(u,v)\, dudv \qquad \text{(D-19)}$$

where A is again the region outside the polygon.

Figure D-2 shows a hypothetical convex polygon which lies in the u,v plane and contains the origin. The symbols u^- and u^+ represent the smallest and largest values of the u_i, respectively. The symbols v^- and v^+ are the v values of the lower and higher intersections of a line of constant u with the polygon. Using these notations, Equation (D-19) can be written as

$$I = \int_{-\infty}^{u-} du \int_{-\infty}^{+\infty} f_\theta(u,v)\, dudv + \int_{u-}^{u+} du \left\{ \int_{-\infty}^{v-} f_\theta(u,v)\, dv + \int_{v+}^{+\infty} f_\theta(u,v)dv \right\}$$

$$+ \int_{u+}^{+\infty} du \int_{-\infty}^{+\infty} f_\theta(u,v)dv \qquad \text{(D-20)}$$

The first and last of the three integrals in Equation (D-20) can be written, respectively, as

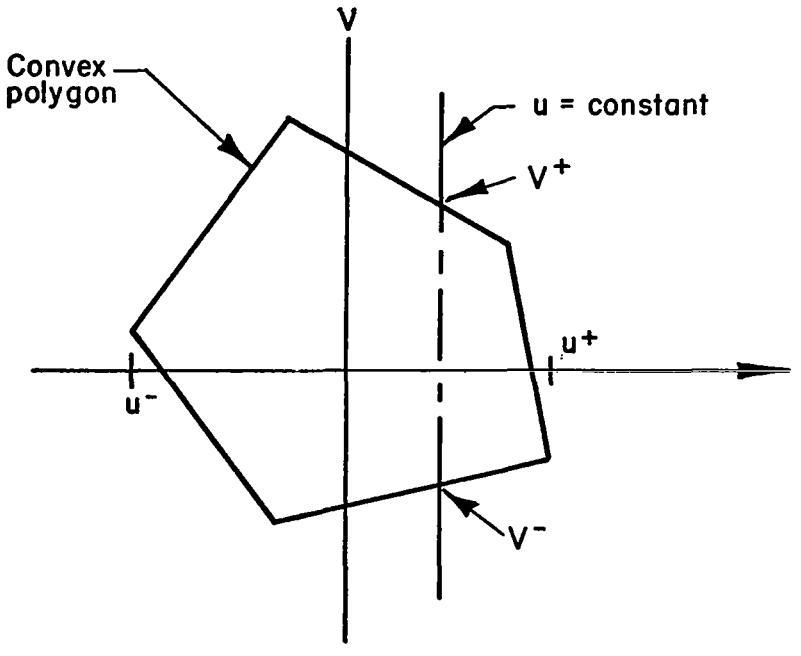

FIGURE D-2. NOMENCLATURE PERTAINING TO THE EVALUATION OF THE PROBABILITY INTEGRAL

$$\int_{-\infty}^{u-} du \int_{-\infty}^{+\infty} f_\theta(u,v)\, dv = 1 - \frac{1}{2}\,\mathrm{erfc}\left(\frac{u-}{\sqrt{2}\,\sigma_u}\right) \tag{D-21}$$

and

$$\int_{u+}^{+\infty} du \int_{-\infty}^{+\infty} f_\theta(u,v)\, dv = \frac{1}{2}\,\mathrm{erfc}\left(\frac{u+}{\sqrt{2}\,\sigma_u}\right) \tag{D-22}$$

where erfc is the error-function complement:

$$\text{erfc}\ (z) = \frac{2}{\sqrt{\pi}} \int_{z}^{+\infty} e^{-t^2} dt \qquad \text{(D-23)}$$

Next, consider the first term of the second integral of Equation (D-20). It can be rewritten as

$$\int_{u-}^{u+} du \int_{-\infty}^{v-} f_\theta(u,v)\ dv = \frac{1}{2\pi\sigma_u\sigma_v} \int_{u-}^{u+} \exp\left(-\frac{u^2}{2\sigma_u^2}\right) du \left\{ \int_{-\infty}^{v-} \exp\left(-\frac{v^2}{2\sigma_v^2}\right) dv \right\} \qquad \text{(D-24)}$$

the inner integral of which is, in turn, expressible in terms of erfc; thus,

$$\int_{-\infty}^{v-} \exp\left(-\frac{v^2}{2\sigma_v^2}\right) dv = \sqrt{\frac{\pi}{2}}\ \sigma_v \left[2 - \text{erfc}\left(\frac{v-}{\sqrt{2}\ \sigma_v}\right)\right] \qquad \text{(D-25)}$$

so that (D-24) may be rewritten as

$$\int_{u-}^{u+} du \int_{-\infty}^{v-} f_\theta(u,v)\ dv = \frac{1}{2\sqrt{2\pi}\ \sigma_u} \int_{u-}^{u+} \exp\left(-\frac{u^2}{2\sigma_u^2}\right) \left[2 - \text{erfc}\left(\frac{v-}{\sqrt{2}\ \sigma_v}\right)\right] du \qquad \text{(D-26)}$$

Proceeding along similar lines with the second term of the second integral of Equation (D-20), one obtains

$$\int_{u-}^{u+} du \int_{v+}^{+\infty} f_\theta(u,v)\ dv = \frac{1}{2\sqrt{2\pi}\ \sigma_u} \int_{u-}^{u+} \exp\left(-\frac{u^2}{2\sigma_u^2}\right) \text{erfc}\left(\frac{v+}{\sqrt{2}\ \sigma_v}\right) du \qquad \text{(D-27)}$$

Combining all results, the desired probability is given by

$$I = 1 - \frac{1}{2}\,\mathrm{erfc}\left(\frac{u-}{\sqrt{2}\,\sigma_u}\right) + \frac{1}{2}\,\mathrm{erfc}\left(\frac{u+}{\sqrt{2}\,\sigma_u}\right) + \frac{1}{2\sqrt{2\pi}\,\sigma_u}\int_{u-}^{u+} \exp\left(-\frac{u^2}{2\sigma_u^2}\right)$$

$$\left[2 - \mathrm{erfc}\left(\frac{v-}{\sqrt{2}\,\sigma_v}\right) + \mathrm{erfc}\left(\frac{v+}{\sqrt{2}\,\sigma_v}\right)\right] du \qquad \text{(D-28)}$$

The integral in Equation (D-28) may be evaluated by a one-dimensional Gaussian quadrature. It is necessary only to be able to evaluate the integrand for any given value of u. To do this, it is necessary to be able to compute v- and v+ for any given value of u. This can be readily accomplished since the straight-line faces of the polygon are defined by the known vertices, u_i, v_i.

Frequency of Crossing

Consider two random processes x(t) and y(t) which are jointly Gaussian, wide-sense stationary with continuous spectra and zero means. Assume that the following two moments exist

$$\int_0^\infty \omega^2 \Phi_{xx}(\omega)\,d\omega \qquad \text{(D-29)}$$

$$\int_0^\infty \omega^2 \Phi_{yy}(\omega)\,d\omega \qquad \text{(D-30)}$$

where Φ_{xx} and Φ_{yy} are the power spectra of the two processes. This process may be viewed as the motion of a point in the x-y plane.

Suppose that a line is given in the x-y plane and that it divides the plane into two half-planes, one of which contains the origin. If the line goes through the origin there is some ambiguity; this case is excluded. The problem is to find the average number of crossings of the point x,y from the half-plane containing the origin into the other half-plane, per unit of time.

The analogous one-dimensional problem was solved by Rice[D-2] a number of years ago. Actually, the problem posed above may be reduced to Rice's and his results can be applied. No well developed procedure was found for

considering the frequency of crossing the multiple boundaries which make up the constraint envelope. Thus, attention was confined to the crossing of individual boundaries.

Establishing a Reference

Figure D-3 depicts an x-y domain and a given line in it defined by two noncoincident points, x_1, y_1, and x_2y_2. It is desired to establish a reference line normal to the given line and which also passes through the origin. This line is assumed to be of length d, and to be displaced from the x-axis by the angle ψ.

It is of importance to define d and θ in terms of the coordinates of the given points. Thus,

$$d = \frac{|x_1y_2 - x_2y_1|}{\left[(x_2 - x_1)^2 + (y_2 - y_1)^2\right]^{1/2}} \tag{D-31}$$

$$\sin \psi = \frac{(x_1 - x_2)\ \mathrm{sgn}\ (x_1y_2 - y\,x_2)}{\left[(x_2 - x_1)^2 + (y_2 - y_1)^2\right]^{1/2}} \tag{D-32}$$

$$\cos \psi = \frac{(y_2 - y_1)\ \mathrm{sgn}\ (x_1y_2 - y_1x_2)}{\left[(x_2 - x_1)^2 + (y_2 - y_1)^2\right]^{1/2}} \tag{D-33}$$

Applying the Level-Crossing Formula

If the random process is at some point x,y, then the projection of this point onto the normal is given by

$$z = x \cos \psi + y \sin \psi \tag{D-34}$$

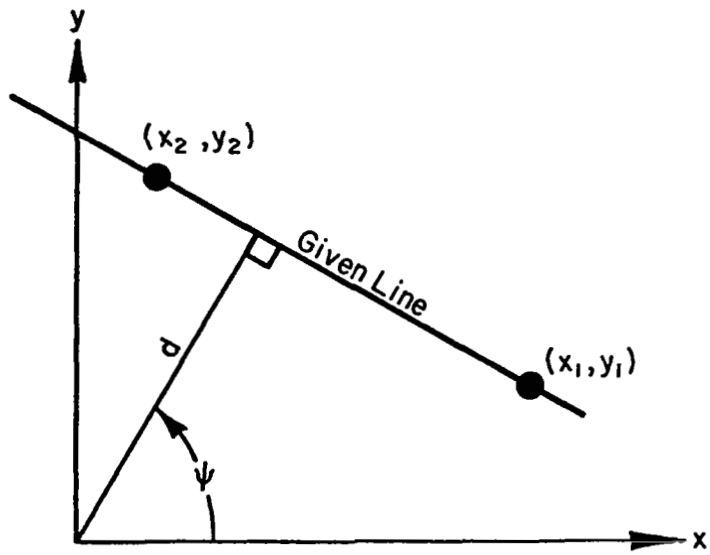

FIGURE D-3. DEFINING A DESIRED NORMAL TO A GIVEN LINE

If $z > d$, the random process is in the half-plane not containing the origin. If $z < d$, it is in the half-plane containing the origin. Accordingly, it is sufficient to determine the frequency with which the random process

$$z(t) = x(t) \cos \psi + y(t) \sin \psi \qquad \text{(D-35)}$$

crosses the level, z = d. This is the one-dimensional problem studied by Rice. The desired frequency of crossing is given by Bendat[D-3] and is

$$N_d = \frac{1}{\pi}\left[\frac{\int_0^\infty \omega^2 \Phi_{zz}(\omega)d\omega}{\sigma_z^2}\right]^{1/2} e^{-\frac{d^2}{2\sigma_z^2}} \qquad \text{(D-36)}$$

where σ_z^2 is the variance of z and $\Phi_{zz}(\omega)$ is its spectral density. It is necessary to determine these quantities.

Since x(t) and y(t) are zero-mean stationary random processes, z(t) will also be stationary, with zero mean. The autocorrelation of z(t) will be:

$$\varphi_{zz}(\tau) = E\left\{z(t)\ z(t+\tau)\right\} \qquad \text{(D-37)}$$

or

$$\varphi_{zz}(\tau) = \cos^2\psi\ E\left\{x(t)\ x\ (t+\tau)\right\} + \sin\psi\cos\psi\left[E\left\{x(t)\ y(t+\tau)\right\}\right. \qquad \text{(D-38)}$$
$$\left. + E\left\{y(t)\ x(t+\tau)\right\}\right] + \sin^2\psi\ E\left\{y(t)\ y(t+\tau)\right\}$$

It is observed that (D-38) can be rewritten as

$$\varphi_{zz}(\tau) = \cos^2\psi\ \varphi_{xx}(\tau) + \sin\psi\cos\psi\left[\varphi_{xy}(\tau) + \varphi_{yx}(\tau)\right] + \sin^2\psi\ \varphi_{yy}(\tau) \qquad \text{(D-39)}$$

where $\varphi_{xx}(\tau)$ and $\varphi_{yy}(\tau)$ are the autocorrelations of the processes x(t) and y(t) and $\varphi_{xy}(\tau)$ and $\varphi_{yx}(\tau)$ are the covariances. Multiplying this Equation by $\frac{e^{-j\omega\tau}}{\pi}$ and integrating from $\omega = -\infty$ to $\omega = +\infty$ (Fourier transformation) gives:

$$\Phi_{zz}(\omega) = \cos^2\psi\ \Phi_{xx}(\omega) + \sin\psi\cos\psi\left[\Phi_{xy}(\omega) + \Phi_{yx}(\omega)\right] + \sin^2\psi\ \Phi_{yy}(\omega) \qquad \text{(D-40)}$$

It is easily shown that $\Phi_{yx}(\omega)$ is the complex conjugate of $\Phi_{xy}(\omega)$ so that

$$\left[\Phi_{xy}(\omega) + \Phi_{yx}(\omega)\right] = 2\ R_e\left\{\Phi_{xy}(\omega)\right\} \tag{D-41}$$

where $R_e\{\ \}$ means the real part of $\{\ \}$. Therefore, Equation (D-40) can be rewritten as

$$\Phi_{zz}(\omega) = \cos^2\psi\ \Phi_{xx}(\omega) + 2\sin\psi\cos\psi\ R_e\left\{\Phi_{xy}(\omega)\right\} + \sin^2\psi\ \Phi_{yy}(\omega) \tag{D-42}$$

The variance of z may now be found. It is given by

$$\sigma_z^2 = \int_0^\infty \Phi_{zz}(\omega)d\omega \tag{D-43}$$

or, from Equation (D-42), it can be expanded to

$$\sigma_z^2 = \cos^2\psi \int_0^\infty \Phi_{xx}(\omega)d\omega + 2\sin\psi\cos\psi \int_0^\infty R_e\left\{\Phi_{xy}(\omega)\right\}d\omega + \sin^2\psi \int_0^\infty \Phi_{yy}(\omega)d\omega \tag{D-44}$$

By definition, this is seen to be

$$\sigma_z^2 = \sigma_x^2\cos^2\psi + 2\sigma_x\sigma_y\,\rho\sin\psi\cos\psi + \sigma_y^2\sin^2\psi \tag{D-45}$$

Now, the following can also be written:

$$\int_0^\infty \omega^2\,\Phi_{zz}(\omega)d\omega = I_1\cos^2\psi + 2I_2\sin\psi\cos\psi + I_3\sin^2\psi \tag{D-46}$$

where

$$I_1 = \int_0^\infty \omega^2 \Phi_{xx}(\omega) d\omega \ , \tag{D-47}$$

$$I_2 = \int_0^\infty \omega^2 R_e\left\{\Phi_{xy}(\omega)\right\} d\omega \ , \tag{D-48}$$

$$I_3 = \int_0^\infty \omega^2 \Phi_{yy}(\omega) d\omega \tag{D-49}$$

Finally, using Equation (D-46), the desired frequency of crossing given by Equation (D-36) can be expressed as

$$N_d = \frac{1}{\pi\sigma_z}\left[I_1 \cos^2\psi + 2I_2 \sin\psi \cos\psi + I_3 \sin^2\psi\right]^{1/2} \exp\left\{-\frac{d^2}{2\sigma_z^2}\right\} \tag{D-50}$$

References

D-1. Burington, R. S., and May, D. C., Handbook of Probability and Statistics, Handbook Publishers, Inc., Sandusky, Ohio, 1953.

D-2. Rice, S. O., Mathematical Analysis of Random Noise, Bell System Technical Journal, Volume 23, pp 282-332, July, 1944.

D-3. Bendat, Julius, Principles and Applications of Random Noise Theory, p 127, John Wiley and Sons, Inc., New York City, 1958.